

AN INVESTIGATION OF PERIPHERAL FACTORS
AFFECTING THE SPATIAL PERCEPTION OF TACTILE
POINT STIMULI

AN INVESTIGATION OF PERIPHERAL FACTORS
AFFECTING THE SPATIAL PERCEPTION OF TACTILE
POINT STIMULI

By Jonathan Tong, B.Sc.

A thesis submitted to the School of Graduate studies in
Partial Fulfillment of the requirements for the Degree Doctor
of Philosophy

McMaster University © Copyright by Jonathan Tong
July 2014

McMaster University

DOCTOR OF PHILOSOPHY (2014)

Hamilton, Ontario

(Psychology, Neuroscience and Behaviour)

TITLE: AN INVESTIGATION OF PERIPHERAL FACTORS
AFFECTING THE SPATIAL PERCEPTION OF TACTILE POINT
STIMULI

AUTHOR: Jonathan Tong, B.Sc. (McMaster University)

SUPERVISOR: Dr. Daniel Goldreich

NUMBER OF PAGES:

Abstract

The earliest measures of tactile spatial acuity reflect the ability of human observers to localize and discriminate the simplest of stimuli: single or double point (punctate) indentations. Because punctate stimuli cover an extremely small area, they typically only activate a few peripheral afferents at a time. Therefore, many researchers have used single-point localization and two-point discrimination thresholds to probe the density of innervation at different body sites.

This thesis explores the relationship between peripheral properties and the spatial perception of tactile point stimuli. In chapter 2, we simulate the neural responses of primary afferents to single and double points, capturing many realistic properties of the periphery: innervation density, the shape and size of receptive fields, and interactions between two-point stimuli. Furthermore, we model optimal performance in localization and discrimination tasks given these afferent responses, and compare it to human performance. We find that human performance is well below optimal, suggesting that humans do not make use of all the information present at the level of the primary afferents. Nevertheless, many human performance trends, resulting from peripheral properties, are predicted by our computational analysis. Using empirical methods, in Chapter 3, we further investigate one of these trends: surround suppression (the

suppression of two-point responses relative to that of a single point) is thought to provide a magnitude cue during two-point discrimination (2PD), resulting in elevated performance even at zero separation between two points. We demonstrate that human observers do indeed show elevated 2PD performance at zero separation on a variety of tested body-sites; an alternative task involving orientation discrimination, however, does not show this same trend and is therefore unlikely to be contaminated by the same magnitude cue. In Chapter 4 we review and test a Bayesian model of two-point trajectory estimation that replicates a famous perceptual length contraction illusion. We provide evidence in support of the model: stimuli that give rise to poor spatial acuity also give rise to a stronger length contraction illusion.

Overall, the three studies covered in this thesis elucidate many of the peripheral and stimulus properties that shape our perception of tactile point stimuli.

Preface

There are a total of five chapters in this thesis. Chapter 1 gives a brief introduction and review of the background literature in the topic of tactile point stimuli. Chapters 2-4 describe studies that were carried out to further investigate the relationship between peripheral properties and the perception of tactile points. Chapter 2 is a computational study, and chapters 3 and 4 are empirical studies. Chapter 3 has been published in the journal *Frontiers in Human Neuroscience*¹ as an open-access article, included in this thesis under the terms of the Creative Commons Attribution License. Chapter 5 discusses the findings and implications of these studies (chapters 2-4).

The work detailed in this thesis was supported by a Natural Sciences and Engineering Research Council of Canada (NSERC) Discovery Grant awarded to Dr. Daniel Goldreich. I received further support through an Ontario Graduate Scholarship (2008) and annual funding by McMaster University (graduate stipended).

¹ Tong J, Mao O, Goldreich D (2013) Two-point orientation discrimination versus the traditional two-point test for tactile spatial acuity assessment. *Front Hum Neurosci* 7: 579. doi: 10.3389/fnhum.2013.00579.

Declaration of Academic Achievement

Chapter 2

I was involved in all aspects of the modeling: programming, simulations, statistical analysis and writing. Dr. Daniel Goldreich also made major contributions to programming, analysis and editing of the manuscript.

Chapter 3

I was involved in all aspects of the research: experimental design, programming, statistical analysis, and writing. An undergraduate student, Oliver Mao, assisted in collecting a major portion of the data, and editing of the manuscript. Dr. Daniel Goldreich also made major contributions to experimental design, programming, statistical analysis and editing of the manuscript.

Chapter 4

I was involved in all aspects of the research: experimental design, programming, statistical analysis, and writing. An undergraduate student, Vy Ngo, assisted in data collection. Dr. Daniel Goldreich also made major contributions to experimental design, programming, statistical analysis and editing of the manuscript.

Acknowledgments

I would like to express my sincerest gratitude to Dr. Daniel Goldreich, my supervisor and mentor throughout my graduate studies. His guidance has helped me through the process of developing and honing my research, analytical, critical thinking, organizational, writing and communication skills. I am also indebted to my graduate committee members, Dr. Deda Gillespie and Dr. Patrick Bennett, for their guidance and helpful feedback throughout the years.

I would like to thank my fellow graduate students, and lab-mates, Dr. Michael Wong, Dr. Ryan Peters, Dr. Andy Bhattacharjee, and Luxi Li for their support and friendship. You have helped make graduate school and attending conferences fun and interesting experiences. Thank you to my undergraduate students, Oliver Mao and Vy Ngo, who helped with data collection and giving me the opportunity to be a mentor.

Finally, I am greatly indebted to my family (Richard, Ruth, Julian and Ryan Tong) for your continued support in whatever I do in life. Thank you to my fiancé, Natasha Crighton, for being a supportive and loving life-partner and to her family for their kind support.

Table of Contents

Chapter 1	1
<hr/>	
General Introduction	
1.1 The importance of touch	1
1.2 Cutaneous point stimuli and their applications	2
1.3 Basic measures of tactile spatial acuity	3
1.4 Peripheral factors and their relation to spatial acuity	5
1.5 Overview of studies	9
1.6 References	13
Chapter 2	16
<hr/>	
2.1 Preface	16
2.2 Abstract	17
2.3 Introduction	17
2.4 Methods	28
2.5 Results	49
2.6 Discussion	54
2.7 Tables	64

2.8	Figures	66
2.9	References	80
Chapter 3		84
3.1	Preface	84
3.2	Abstract	86
3.3	Introduction	86
3.4	Materials and Methods	87
3.5	Results	89
3.6	Discussion	90
3.7	References	95
Chapter 4		97
4.1	Preface	97
4.2	Abstract	97
4.3	Introduction	98
4.4	Methods	106
4.5	Results	117

4.6	Discussion	120
4.7	Figures	130
4.8	References	146

Chapter 5 **148**

5.1	Summary of studies	148
5.2	Other Channels involved in the processing of tactile information	151
5.3	Central mechanisms of tactile spatial acuity	153
5.4	Future directions	158
5.5	Conclusion	158
5.6	References	160

List of Tables and Figures

CHAPTER 2

Table 1. Parameters defining the modeled body sites	64
Table 2. A summary of simulation results for microstim.	65
Table 3. A summary of simulation results for single-point localization	65
Figure 1. General modeling of a receptive field	66
Figure 2. Modeling a patch of skin (afferent RFs)	67
Figure 3. Single-point localization with afferent-like responses	69
Figure 4. Single-point localization with cortical-like responses	70
Figure 5. A comparison of model and human performance on single-point localization	71
Figure 6. Sequential vs. simultaneous two-point discrimination	72
Figure 7. Comparison of thresholds for sequential and simultaneous two-point discrimination	73
Figure 8. Elliptical receptive field	74

Figure 9. Differences in two-point discrimination between stimuli oriented longitudinally and transversely	75
Figure 10. Summary of anisotropy results	76
Figure 11. Modeling surround suppression as a function of two-point separation	77
Figure 12. Surround suppression results in a two-point discrimination magnitude cue	78
Figure 13. Two-point orientation discrimination is unaffected by surround suppression	79
 CHAPTER 3	
Figure 1. Calipers	87
Figure 2. Two-interval forced-choice perceptual tasks	88
Figure 3. Bayesian adaptive testing procedure	89
Figure 4. Mean performance by task and body site	89
Figure 5. Mean γ -parameters by task and body site	90
Figure 6. Mean 95%-correct thresholds by task and body site	90
Figure 7. 95%-correct thresholds versus receptor spacing	91

Figure 8. Neural response magnitude cues in the 2PD task 91

Figure 9. Advantage of 2POD over 2PD for tactile spatial acuity
assessment 94

CHAPTER 4

Figure 1. The low-velocity prior 130

Figure 2. Prediction 1 131

Figure 3. Prediction 2 133

Figure 4. Measuring spatial uncertainty 134

Figure 5. Length contraction experiment 136

Figure 6. Performance on length comparison 137

Figure 7. Predicted behavior in length contraction experiments 139

Figure 8. Mean σ_s 140

Figure 9. Length comparison PSEs as a function of comparison time
141

Figure 10. Forearm best-fit τ 143

Figure 11. Finger best-fit τ 144

Figure 12. Predicted behavior for a constant σ_v 145

List of abbreviations and symbols

Abbreviations

RF	Receptive Field
2PD	Two-Point Discrimination
2POD	Two-Point Orientation Discrimination
2-IFC	Two-interval Forced Choice
SA	Slowly-Adapting
RA	Rapidly-Adapting
S1	Primary Somatosensory Cortex
S2	Secondary Somatosensory Cortex
BF	Bayes Factor
PDF	Probability Distribution Function

Symbols

λ	expected firing rate
r	firing rate
ψ	Psychometric Function
a	X-position of the Psychometric Function
b	Slope of the Psychometric Function
δ	Participant Lapse Rate

γ	performance (percent correct) at zero separation
σ	standard deviation
τ	tau-parameter

Chapter 1

General Introduction

1.1 The importance of touch

Our sense of touch is often overlooked and taken for granted, as vision and hearing are widely seen as the dominant senses: we rely on vision to give us a clear spatial depiction of the world so that we may effectively navigate our environment, identify faces, read text, and enjoy art; our hearing gives us a fine temporal account of the millisecond-by-millisecond changes around us so that we may communicate with ease, quickly focus our attention to unseen sound sources, and enjoy music. It is clear that our efficiency in carrying out daily tasks would be severely diminished in the absence of vision or hearing; however, without the sense of touch, life would be exceptionally difficult and the chances of bodily harm or death would be greatly increased. Our ability to move safely throughout the world relies on constant feedback provided by our sense of touch and body positioning (proprioception) while our sense of temperature and pain (both branches of our somatosensory system) allows us to detect and quickly avoid harmful stimuli. The skin, which receives a majority of touch stimuli, covers the entire body surface and is therefore the largest sensory organ. Besides detecting the presence of objects contacting the skin, our sense of touch also allows us to localize these points of contact with varying degrees of accuracy. The fingertips are so proficient at transmitting spatial information, that we can

identify objects based on fine texture alone (e.g. identifying a coin in your pocket or fabric types by rubbing it between your fingertips). Here we will explore the perception of fine details contacting the skin, specifically the perception of points, and various factors of the nervous system that affect this process.

1.2 Cutaneous point stimuli and their applications

A single punctate (point) indentation is the most basic type of stimulus on the skin; with minimal spatial complexity, it is confined to a single, isolated region on the body surface. Additionally, several small systematically placed points can conceivably approximate any spatial pattern of higher complexity, as demonstrated by the sensory substitution device known as the Optacon: an array of probes that transforms high-resolution optical information (e.g. text or symbols) into a tactile equivalent (Goldish and Taylor, 1974; Heller et. al. 1990, Arezzo and Schaumburg, 1980). Furthermore, punctate patterns have been successfully applied as a means of communication in the writing system known as Braille: groups of simple raised dot patterns, consisting of up to six points per character, are capable of conveying language through the sense of touch alone. Therefore, the study of how punctate stimuli are perceived and how various factors may affect their perception is not only important for understanding the fundamentals of touch, but also in the design of effective tactile displays and Braille interfaces (Myles and Binseel, 2007; Nolan and Kederis, 1969).

Because of their geometrical simplicity, and fundamentality, point stimuli have been used for more than a century to map the basic functions of detection and spatial discrimination throughout the body surface (Weber, 1834; Weinstein, 1968, 1993). Single points of contact have been used to stimulate the skin with controlled contact forces; when the tip of a Von Frey hair (or Semmes-Weinstein monofilament) is applied to the skin surface, the bending of its thin shaft ensures stimulation with an upper limit on contact force (Weinstein, 1993). Extremely thin Von Frey hairs can achieve forces on the order of a few thousandths of a Newton, allowing investigators to measure the minimal force with which a single point can be detected or for which a single afferent reaches spiking threshold (Bell-Krotoski et al., 1995; Johansson et al., 1980).

1.3 Basic measures of tactile spatial acuity

Punctate stimuli have also been used to measure tactile spatial acuity. The most basic test of spatial acuity is the localization of a single point. Schady and Torebjork (1983) stimulated the arms and hands of participants with a Von Frey hair, with a force above their detection threshold, and subsequently had them mark down where they felt the stimulus. They found that the fingertip and finger base were the most accurate at localizing points, with mean errors of 2.6 mm and 9.9 mm, while the palm and forearm were much less accurate, with mean errors of 17.6 and 23.4 mm. A variation of this single point localization test, first

documented by Weinstein (1968), which we will refer to as sequential two-point discrimination, entails stimulating at a reference location and again at the same or a different site (varying distances away); participants subsequently report whether they were stimulated in the same or different locations. Weinstein (1968) measured the mean distance the probe must be moved away from the reference location for participants to perform at 50% accuracy: the fingertips are once again shown to have superior localization ability (threshold $\sim 1.6\text{mm}$) compared to other sites like the palm (threshold $\sim 5\text{mm}$) and arm (threshold $\sim 10\text{mm}$).

A less simple, but better-known, spatial acuity task is the “two-point test” (also known as two-point discrimination). Reportedly first conceived of more than a century ago by Weber (1834), two-point testing was carried out by the simultaneous application of a pair of compass points to the skin. The observer’s task is to report whether two points or one are felt (To distinguish this test from the sequential two-point test, we will refer to it as simultaneous two-point test.). When the points are far enough apart, the observer almost always reports feeling two points; however, as the compass tips approach one-another, the observer begins to report feeling only one point. The separation at which half of the responses indicate two points is known as the two-point limen or threshold. Measuring the threshold on different body sites, Weber discovered that spatial acuity varied greatly across the body surface, with the lips and finger tips having

exceptionally high resolution (on the order of a mm) and other areas such as the back and forearm having much poorer resolution (on the order of a few cm). These findings have been replicated in other studies, since Weber (Weinstein, 1968, 1993; Vallbo and Johansson, 1978), and investigators have generally interpreted these results to reflect the underlying innervation densities of touch sensitive nerve fibers on different body sites.

Weinstein (1968), in addition to measuring sequential two-point thresholds, used the simultaneous two-point discrimination task across most of the body surface. The study demonstrated a wide variability of two-point discrimination thresholds across the body, with values comparable to those measured by Weber (1834), as well as the absence of any threshold differences based on laterality (homologous sites on opposite sides of the body had roughly the same thresholds). His study also demonstrated a marked difference between sequential and simultaneous two-point thresholds: sequential thresholds were consistently lower than simultaneous thresholds (the difference between thresholds is larger on areas of poorer acuity).

1.4 Peripheral factors and their relation to spatial acuity

A modern study by Vallbo and Johansson (1978) identified the density of innervation and the surface area(s) over which single nerve fibers can detect

contact forces (receptive field) throughout the palmar side of the human hand. These values were compared to simultaneous two-point discrimination thresholds, throughout the hand, of the same individuals in which the neural recordings were made. What the authors found was a clear monotonic trend relating the mean receptive field area of nerve fibers, their densities, and two-point thresholds; body sites with large receptive fields and low innervation density had poor spatial resolution. This seminal study, which successfully combined neurophysiological and psychophysical techniques, provided a strong confirmation of the relationship between innervation and spatial resolution on the skin, and seemed to justify the use of the two-point threshold as a proxy for innervation density and receptive field size. Indeed, many clinicians have taken to using the classic two-point discrimination task to assess the functionality or pathology of neural pathways affecting touch sensation.

The interpretation of the two-point threshold as a proxy for innervation density and receptive field size is based on a simple assumption: when two closely spaced points fall within a single afferent receptive field, the resulting profile of activity in the population of afferents is indistinguishable from that of a single point stimulus; both configurations (one point or two closely spaced points) presumably result in an identical, single locus of neural activity. However, the findings of one study challenge this simple assumption: Johnson and Phillips

(1981) carried out a more rigorous version of the two-point test in which participants were given both a single point stimulus and a two-point stimulus, of varying separation, on each trial; their task was to identify which was the two-point stimulus. Surprisingly, participants were consistently able to identify the two-point stimulus well above chance, even when the two points were in direct contact with one another. Because the mean size and spacing of receptive fields could not account for this apparent “hyperacuity” (the mean RF spacing on the fingertips is 1.2mm) (Johansson and Vallbo, 1979), the authors concluded that some non-spatial cue must have aided the participants in the task (Craig and Johnson, 2000). The most likely scenario was that each of the two closely spaced points had mutually suppressed the neural response of the other, a surround suppression phenomenon characterized by Vega-Bermudez and Johnson (1989). This interaction between the two points, in turn, markedly lowers the mean response relative to that of a single point, such that the task of identifying the two-point stimulus becomes a task of magnitude, rather than spatial, discrimination. In other words, although two apposed points may result in a single locus of activity in the population response, the magnitude of this peak is markedly less than that of a single point.

Another peculiar trait of the two-point limen is that it differs based on the orientation of the two points. In Weber’s (1834) original two-point discrimination

studies, he found that by placing the two points along the longitudinal axis of the arm, higher thresholds are measured compared to when the points were placed transversely. Receptive field size and density alone cannot explain this anisotropy; one must also consider the shape of the receptive fields: Johansson and Vallbo (1980) found that three quarters of receptive fields on the hand are elliptical in shape and two-thirds of these elongated fields are longitudinally oriented. Since, with a majority of these receptive fields, two transversely oriented points must be brought closer together to fall within the same receptive field than longitudinally oriented points, the two-point discrimination threshold is smaller in the transvers direction than in the longitudinal direction.

Although two-point thresholds correlate with receptive field size and density, it is clear from the above examples that other peripheral factors must be taken into consideration to fully explain the limits of spatial acuity. By incorporating information about the exact shape and orientation of receptive fields, one might be able to further investigate the neural underpinnings of anisotropy in two-point thresholds; furthermore, by considering the phenomenon of surround suppression one might be able to address an apparent flaw in the interpretation of two-point discrimination thresholds as a pure measure of spatial acuity. It is the goal of this thesis to explore these specific examples, and others,

of peripheral and stimulus factors that affect the limits of acuity in the perception of point stimuli.

1.4 Overview of studies

The goal of this thesis is to investigate the factors affecting the perception of statically applied tactile punctate stimuli, at the level of both the stimulus and the neural input conveyed by primary afferents. Using empirical methods, we examine factors ranging from the location of a single stimulus to the spatial and temporal intervals between two stimuli; we further explore how the characteristics of primary inputs affect perception by implementing a computational model of underlying touch receptors (afferents) and the optimal decoding of their responses.

The second chapter of this thesis takes a computational approach to investigate the relationship between spatial resolution, as measured by a variety of tasks, and the anatomical and physiological characteristics of the first order (peripheral) neurons, namely the Slowly Adapting type 1 (SA1) afferents. Although 3 other tactile channels, or afferent types, have been identified (Bolanowski et al., 1988), only the SA1s have been demonstrated to be capable of encoding spatial details on the skin with sufficient resolution to underlie human perceptual performance (Johnson and Lamb, 1981). In addition to receptive field

sizes and densities of SA1s, characterized by Vallbo and Johansson (1978), we incorporate other known characteristics into our modeling, such as receptive field shape, inter-stimulus interactions (namely, surround suppression) and response variability. Our aim is to investigate how these factors affect the ability of an “ideal observer” to localize a single indentation, resolve two points and identify the orientation of a two-point stimulus (all typical tasks used to measure spatial acuity). We show that human performance is typically quite far from optimal, given the information provided by primary afferents, even when considering the addition of noise encountered in cortical neurons. Nevertheless, we demonstrate that our perceptual model can account for specific performance trends such as the correlation between receptive field size and density with spatial acuity, differences between sequential and simultaneous two-point thresholds, anisotropy due to receptive field orientation and shape, and elevated two-point thresholds due to a surround suppression magnitude cue.

The third chapter revisits the major criticism of two-point discrimination: that it may be contaminated by a non-spatial cue, namely a magnitude cue resulting from surround suppression. This point is addressed theoretically in the second chapter, and is predicted by our ideal observer analysis; in Chapter 3 we test this prediction by implementing a two-interval forced-choice version of two-point discrimination and compare performance against a proposed alternative

task involving two point orientation discrimination (2POD). Our aim was to identify whether there is evidence for a magnitude cue in a handheld two-point discrimination (2PD) task, similar to how a clinician would administer it, and to evaluate an alternative task that we predict would not be contaminated by magnitude cues. Our findings confirm the elevated 2PD performance at zero separation on the fingertip, found by Johnson and Phillips (1981), as well as on the finger base, palm and forearm (as predicted in the ideal observer analysis of Chapter 2); additionally, we demonstrate that the 2POD task does not suffer from this shortcoming (also predicted in Chapter 2). The data suggest that two-point discrimination, but not 2POD, is contaminated by a magnitude cue. We conclude that clinicians should switch to the 2POD task when assessing somatosensory nerve function.

The fourth chapter explores the case of sequential two-point stimulation, with varying temporal separations, and the resulting phenomenon of perceptual length contraction when the intervening time between stimuli is sufficiently short. This illusion, termed the tau effect, reflects the spatiotemporal nature of inferring traversed distances (Helson and King, 1931). We briefly introduce a model that views perception of trajectories as a probabilistic (Bayesian) inference that takes into account the prior probability of trajectories based on experience (Goldreich, 2007; Goldreich and Tong, 2013). According to the model, a combination of

spatial uncertainty and a strong prior expectation for slowly moving stimuli give rise to the tau effect. Following our introduction of the model, we detail an empirical study that we have carried out to test the model's prediction that spatial uncertainty largely determines the extent of perceptual length contraction. Our results support the model's prediction that greater spatial uncertainty results in a larger tau effect.

1.5 References

- Arezzo, J. C., & Schaumburg, H. H. (1980). The use of the Optacon as a screening device: a new technique for detecting sensory loss in individuals exposed to neurotoxins. *Journal of Occupational and Environmental Medicine*, 22(7), 461-464.
- Bell-Krotoski, J. A., Fess, E. E., Figarola, J. H., & Hiltz, D. (1995). Threshold detection and Semmes-Weinstein monofilaments. *Journal of Hand Therapy*, 8(2), 155-162.
- Bolanowski Jr, S. J., Gescheider, G. A., Verrillo, R. T., & Checkosky, C. M. (1988). Four channels mediate the mechanical aspects of touch. *The Journal of the Acoustical society of America*, 84(5), 1680-1694.
- Craig JC & Johnson KO (2000). The two-point threshold: Not a measure of tactile spatial resolution. *Current Directions in Psychological Science*. 9(1): 29–32.
- Goldish, L. H., & Taylor, H. E. (1974). The Optacon: A Valuable Device for Blind Persons. *New Outlook for the Blind*, 68(2), 49-56.
- Goldreich, D. (2007). A Bayesian perceptual model replicates the cutaneous rabbit and other tactile spatiotemporal illusions. *PLoS One*, 2(3), e333.
- Goldreich, D., & Tong, J. (2013). Prediction, postdiction, and perceptual length contraction: a Bayesian low-speed prior captures the cutaneous rabbit and related illusions. *Frontiers in psychology*, 4.
- Heller, M. A., Rogers, G. J., & Perry, C. L. (1990). Tactile pattern recognition with the Optacon: Superior performance with active touch and the left hand. *Neuropsychologia*, 28(9), 1003-1006.
- Helson, H., & King, S. M. (1931). The tau effect: an example of psychological relativity. *Journal of Experimental Psychology*, 14(3), 202.

- Johansson RS & Vallbo ÅB (1979). Tactile sensibility in the human hand: relative and absolute densities of the four types of mechanoreceptive units in glabrous skin. *Journal of Physiology*. 286: 283–300.
- Johansson RS, Vallbo ÅB & Westling G (1980). Thresholds of mechanosensitive afferents in the human hand as measured with Von Frey hairs. *Brain Research*. 184: 343–351.
- Johnson, K. O., & Lamb, G. D. (1981). Neural mechanisms of spatial tactile discrimination: neural patterns evoked by braille-like dot patterns in the monkey. *The Journal of physiology*, 310(1), 117-144.
- Johnson KO & Phillips JR (1981). Tactile spatial resolution. I. Two-point discrimination, gap detection, grating resolution, and letter recognition. *Journal of Neurophysiology*. 46: 1177–1191.
- Johansson, R. S., & Vallbo, Å. B. (1983). Tactile sensory coding in the glabrous skin of the human hand. *Trends in Neurosciences*, 6, 27-32.
- Myles, K., & Binseel, M. S. (2007). *The tactile modality: a review of tactile sensitivity and human tactile interfaces* (No. ARL-TR-4115). ARMY RESEARCH LAB ABERDEEN PROVING GROUND MD HUMAN RESEARCH AND ENGINEERING DIRECTORATE.
- Nolan, C. Y., & Kederis, C. J. (1969). Perceptual Factors in Braille Word Recognition. (American Foundation for the Blind. Research Series No. 20).
- Schady, W. J. L., Torebjörk, H. E., & Ochoa, J. L. (1983). Cerebral localisation function from the input of single mechanoreceptive units in man. *Acta physiologica scandinavica*, 119(3), 277-285.
- Weber, E. H. (1834). *De tactu*. Koehler, Leipzig.
- Weinstein, S. (1968). Intensive and extensive aspects of tactile sensitivity as a function of body part, sex and laterality. In *the First Int'l symp. on the Skin Senses, 1968*.
- Weinstein, S. (1993). Fifty years of somatosensory research: from the Semmes-Weinstein monofilaments to the Weinstein Enhanced Sensory Test. *Journal of Hand therapy*, 6(1), 11-22.

- Vega-Bermudez, F., and Johnson, K. O. (1999). Surround suppression in the responses of primate SA1 and RA mechanoreceptive afferents mapped with a probe array. *J. Neurophysiol.* 81, 2711–2719.

Chapter 2

2.1 Preface

Point stimuli are frequently used to probe the sensitivity and spatial acuity of sensory systems. Single and two-point stimuli are simple to apply and have very local effects on the skin, often only activating a few afferents (this is true for two-point stimuli separated by extremely small distances). By having observers localize a single indentation or discriminate two points on the skin, investigators have found that performance on these tasks is related to innervation density, much like how pixel density determines image resolution on a display. In this chapter, we explore this relationship in greater detail by using a technique known as ideal observer analysis. In addition to innervation density, we explore other properties of the peripheral afferents, such as the size, shape, and response properties of their receptive fields (the area of skin for which they detect point stimuli). We demonstrate that human performance is far from optimal, as reflected by an ideal observer's performance on various localization and discrimination tasks. Nevertheless, the ideal observer is able to predict (or replicate) many interesting human performance trends in these very tasks.

2.2 Abstract

Comparing human performance to what is considered ideal or optimal allows investigators to probe how effectively the brain uses information to accomplish a task. Ideal observer analysis, thus, characterizes the optimal level of performance given the information available at a specific level of the processing hierarchy. In this chapter we apply ideal observer analysis on the information available in the responses of peripheral tactile afferents to characterize optimal performance on single-point localization and variations of two-point discrimination. We apply noise that is either consistent with what is measured at the level of these afferents or in cortical neurons. We demonstrate that human observers perform tactile localization and discrimination tasks well below what is revealed to be optimal by our ideal observer analysis. Furthermore, by incorporating realistic receptive field properties such as size, spacing, shape and surround suppression, our ideal observer analysis predicts many trends found in human performance including anisotropy, differences between sequential and simultaneous two-point discrimination, and elevated performance of two-point discrimination attributed to a magnitude cue.

2.3 Introduction

The most basic definition of tactile spatial acuity is the accuracy with which a single indented point can be localized on the skin. A second, more common,

definition is the minimal required separation between two points that elicits the perception of distinct points of contact. Weber first conceived of these definitions over a century ago when investigating the limits of spatial acuity in humans (Weber, 1996). Researchers have since developed other, more sophisticated, means of measuring spatial acuity and have theorized about the underlying anatomical and physiological determinants of acuity (Weber, 1996; Vallbo and Johansson 1978; Stevens and Patterson, 1995; Craig and Johnson 2000). In particular, Johansson and Vallbo (1978) investigated the correlation between classic two-point acuity, as defined by Weber, and innervation density on various regions of the human hand. The correlation and similarities between these two measures at various body sites led the authors to conclude that it was the density of nerve fibres relaying spatial information that determined the limits of spatial acuity. What other input properties of the peripheral nervous system are important for determining the limits of acuity? The computational study expounded here aims to elucidate some of the characteristics of the peripheral nervous system that may largely determine performance trends in tactile spatial discrimination: receptive field spacing, size, shape and orientation as well as the variability in firing rates. We explore these effects by analyzing simulated neural data in which parameters have been informed by the anatomy and physiology of afferents that transmit fine-touch information.

Consider the simple task of localizing a single point: when a point makes contact with the body surface, the skin is locally compressed and deformed, causing underlying stretch-sensitive nerve fibers to send impulses towards the brain. Distributed throughout the entire skin surface, these nerve fibers independently detect contact-force within their immediate vicinity. Altogether, they provide a differential profile of activity that the brain can use to infer the most likely position of contact (roughly where the peak of activity occurs). Thus, the greater the number of independent nerve fibers (detectors) in a patch of skin, the better the theoretical limit of spatial resolution in that region. In the case of two-point stimulation, the resulting profile of activity would likely consist of two peaks of activity, rather than just one, assuming that there are a sufficient number of silent fibers between the sites of stimulation. When the two-point separation falls below the spacing between receptors, only a single peak of activity will result, an activity profile consistent with a single point stimulus. Thus, a simple way the brain could discriminate two points is to identify whether the activity profile was more consistent with single or double point stimulation. This chapter will explore how the information contained in the complete activity profile could be used to probabilistically infer stimulus properties, such as the location of a single indented point or the discrimination of two simultaneously or sequentially indented points.

Several early studies investigated single neuron responses to point-stimuli, measured in impulse frequency, of afferents innervating the skin (Vega-Bermuez and Johnson, 1999a,b; Vallbo and Johanson, 1978; Johansson and Westling, 1980; Knibestol, 1975b; Schady et. al., 1983; Schady and Torebjork, 1983). These pioneering experiments characterized hand and forearm receptive fields: skin areas that, when stimulated by a probe, elicit bursts of activity in a corresponding nerve fiber. Further studies of these cutaneous receptive fields produced estimates of their mean density and surface area in different body sites (Johansson and Vallbo, 1979; Olausson 2000). With such rich physiological and anatomical data, the stimulus-evoked firing rates of a hypothetical population of sensory neurons can be computationally modeled. However, the formulation of such a forward (or generative) model, is only a first step towards understanding tactile spatial perception, as the nervous system must decode the afferent information to infer the stimulus. The task of the nervous system, then, is to solve the “inverse problem,” inferring stimulus structure from the afferent fiber discharge pattern.

Here we implement a generative model that is informed by realistic receptive field properties to yield stimulus-evoked firing rates of simulated SA1 afferents. Furthermore, we construct an ideal observer that interprets the stimulus-evoked firing rates to infer stimulus point location, indentation depth, and

two-point discrimination. We investigate how a number of modeled receptive-field characteristics (density, size, surround suppression, shape and orientation) may contribute to performance in point localization and two-point discrimination tasks. We find trends in the ideal observer's performance that reflect many of the trends found in the human psychophysics and microstimulation literature; this lends credence to the idea that the model may not only capture many of the important characteristics of peripheral neural responses, but also that the nervous system may perform Bayesian-like inferences in simple tactile perception. As far as we know, this is the first study to use an ideal Bayesian observer analysis of neural responses to tactile point stimuli.

Ideal observer theory applies Bayesian statistics to determine the optimal performance in a task, given the physical stimulus properties and biological constraints (Geisler, 1984, 1989). The analysis may be applied to different stages of the sensory and perceptual process. For example, the analysis may be applied at the level of the stimulus itself, where in the case of tactile stimulation, the information under investigation may be the stretch or strain profiles of the skin. In the present study we investigate the information present at the level of afferent firing rates, specifically those of the SA1 afferents. SA1s are known to carry information crucial for the discrimination of textures and the detection of statically indented stimuli (Bolanowski et. al., 1988; Johnson, 2001). Therefore,

we chose to model this particular afferent channel since it is presumably the principal one involved in point localization and discrimination tasks.

In our “population-coding” approach, the entire ideal observer model may be broken down into a two-step process of encoding and decoding. Encoding involves the transformation of physical stimulus characteristics (ie. indentation depth and location) into neural data (ie. firing rates, spike counts) in what is known as a forward or generative model. Decoding involves inferring the most likely stimulus to have given rise to the neural data. The challenge in decoding arises from the fact that neural data tend to be variable: given a consistent stimulus, the resulting firing rates of any neuron will vary. If a decoder knows the statistical structure of the stimulus-evoked firing rate noise (or variability), however, it can calculate the probability of the neural data given each possible stimulus (the likelihood function). By joining this likelihood function with a prior probability distribution over stimulus values, according to Bayes’ theorem, the observer can then infer the most probable stimulus. In this study we only model uniform prior distributions such that each considered stimulus value is a priori equally likely to occur.

Bayesian ideal observer models have been proposed to describe visual, auditory and multi-modal perception, many of them demonstrating that humans

perform in a near optimal manner (Ma et al. 2006; Stocker and Simoncelli 2006; Geisler and Kersten 2002; Knill and Pouget, 2004). However, to our knowledge, no study has yet put forth a Bayesian ideal observer model of tactile perception. Thus, the current study is the first of its kind to carry out an ideal observer analysis of simple point localization and discrimination on the skin and to demonstrate the parallels between probabilistic inference on population codes and human performance in tasks of tactile acuity.

Part 1: Single point stimulation

Modeling microneural stimulation: projected fields and pressure sensation

We start our ideal observer analysis by investigating a single afferent's ability to encode stimulus position. Schady et al. (1983) first explored this in human observers by using the technique of intraneural microstimulation, in which a single afferent was isolated and stimulated with injected current. The observers reported feeling a single, extremely light tap, which they were able to localize with limited accuracy. In our current study, we model microstimulation of a single SA1 afferent by initially silencing all but one afferent, to which we assign an expected response that corresponds to a point stimulus on the RF center with a fixed indentation depth. After adding spontaneous activity and realistic noise to these responses, we then decode the inferred position of stimulation and calculate its

distance from the location of the RF center. We find that the reported localization repeatedly falls within the RF of the stimulated SA1, with extremely small error. We also find that indentation depth or stimulus intensity is consistently judged to be lower than the stimulus intensity corresponding to the level of microstimulation.

Modeling single-point localization (locognosia)

We then carry out an ideal observer analysis of the simplest of physical stimuli, a single indented point, and have the model localize the point on a simulated patch of skin. We report the mean localization error (locognosia) for different modeled skin sites (fingertip, finger base, palm and forearm). The same analysis is repeated for different neural response characteristics: afferent-like responses have zero spontaneous activity and Gaussian noise with a low standard deviation, while cortical-like responses have a 10 Hz spontaneous rate and Poisson noise (standard deviation equal to the square root of expected firing rate). We show that decoding of noisy, cortical-like responses results in less accurate localization than decoding less noisy, afferent-like responses. Additionally, our simulations agree with the well-accepted principle that the density of afferents in a region of skin plays a primary role in determining the accuracy of localization.

Part 2: Dual point stimulation

Modeling simultaneous and sequential two-point discrimination tasks

We next turn our attention to the more complex case of two-point stimulation, investigating first the discrimination of sequential points and then of simultaneous points. In sequential two-point discrimination, a modeled patch of skin is first stimulated in one location and then once again at a different location. As the separation between two taps decreases, the probability of the model answering “two locations” rather than “one” decreases. We report the separation at which the model performs at chance as the standard threshold, the same threshold measure commonly used in studies of human perception.

In simultaneous two-point discrimination, the two points of stimulation are applied synchronously and the model is asked to discriminate between two possibilities, that either one point or two points were presented. Once again, we report the separation at which the model performs at chance as the standard threshold.

Our simulations demonstrate that sequential two-point thresholds are consistently smaller than simultaneous two-point thresholds, a finding that has

been commonly reported, but without explanation, in the tactile spatial acuity literature.

Modeling the effect of elliptical receptive fields on two-point discrimination (the anisotropy effect)

Early pioneering studies, which characterized the response properties of tactile afferents (in monkey and human), showed that receptive fields are not simply circular in shape, as previously assumed. Instead, it has been found that most receptive fields (roughly three-quarters) have slightly elongated, elliptical areas, with two-thirds of them oriented parallel to the longitudinal axis of the arm (Johansson and Vallbo, 1980). Many have theorized on the implications such receptive field shape and orientation would have on spatial acuity; specifically, it is thought that these properties would yield an anisotropy in tactile spatial acuity. That is, 2PD thresholds would be lower when the two points are transversely oriented compared to when they are longitudinally oriented. The reason for this presumed effect would be that two separate receptive fields could be activated with a smaller point separation in the transverse direction than in the longitudinal direction, due to the tendency of receptive field elongation in the longitudinal direction (see fig. 8). By modeling a hypothetical situation, in which all receptive fields are elongated with the same aspect ratio (the mean value found in humans) and oriented longitudinally, we used the ideal observer model to investigate the

theoretical implication of an anisotropy effect. We found that the ideal observer consistently performs better (smaller thresholds) in the transverse orientation compared to the longitudinal orientation. This anisotropy effect grows with increasing receptive field size and spacing (with the arm having the strongest effect out of the four simulated body sites).

Modeling the effect of surround suppression on two-point discrimination (the magnitude cue)

It is thought that two-point discrimination is affected by non-spatial magnitude cues, brought upon by surround suppression: underlying receptors tend to discharge a greater number of spikes in response to a single point than to two closely-spaced points of equal indentation. As a result of this surround suppression, two-points can theoretically be discriminated from one (in a two-interval discrimination task) with extremely high accuracy even when the two points are in contact and between adjacent receptors. We use the ideal observer analysis to test this idea by modeling surround suppression (as characterized by Vega-Bermudez and Johnson, 1999b) in a population of receptors and decoding their responses to simulated two-point stimuli (see “The two-point stimulus response” under the methods section). We then ask the ideal observer whether one or two-points were given and track its responses with or without surround suppression. Our simulations agree with previous speculation (Craig and

Johnson, 2000; Johnson and Phillips, 1981) that surround suppression provides a magnitude cue that the brain could use to perform the 2PD task at extremely small separations (without spatial modulation of firing rates).

2.4 Methods

The complete model is comprised of two parts. The first part is the generative model, in which the response of a population of SA1 neurons to a point stimulus is simulated. Noise is added to these firing rates to replicate the response variability found in either the periphery (low-variance) or cortex (high-variance, Poisson-like). The second part is the decoder or ideal observer, which calculates the most likely stimulus (two-points or one, location of point(s), indentation depth) to have given rise to the simulated population activity.

The Generative Model

The goal of the generative model is to, as realistically as possible, simulate the firing rates of SA1 neurons innervating a patch of skin. Therefore we chose to model skin regions that were well characterized in terms of density of innervation and SA1 receptive field structure (Vega-Bermuez and Johnson, 1999a,b; Vallbo and Johanson, 1978; Johansson and Vallbo, 1980; Knibestol, 1975b; Schady & Torebjork, 1983; Johansson, Vallbo, 1979; Olausson 2000), namely: the index finger-tip (distal pad), the index finger base (proximal pad), the palm, and the

forearm. The receptive field of an SA1 can be defined simply as the area of the skin surface that, when stimulated, elicits a response in that SA1. The density of SA1 innervation is defined here as the number of SA1 receptive fields per square mm of skin. For convenience of interpretation, in the present study we report not density but rather the linear spacing between receptive field centers. For a full list of parameters used in the simulation of various skin regions see table 1.

Modeling a patch of skin

We modeled a patch of skin by placing SA1 receptive fields within a square area. The density of innervation for a given patch of skin determines the number of SA1 receptive fields and the mean spacing between them. The actual position of each receptive field center was determined by first setting them on the points of a square grid equal to the density of innervation, then allowing each one to deviate from its initial position by a value drawn from a Gaussian distribution (centered on zero with a standard deviation of $\frac{1}{2}$ of the mean spacing) (see fig 2). This “jittering” of RF positions ensured that the point stimuli did not consistently land on the center of RFs for particular separations. We chose to define the x-axis as the longitudinal axis of the body part (this convention is important when considering elliptical fields with particular orientations).

Modeling the stimulus

A modeled stimulus is characterized by an indentation depth (amplitude) and the position of the stimulus center. Additional characteristics describe the double-point stimulus: the separation between points, the orientation of the stimulus (either longitudinal or transverse), and whether the two taps occurred simultaneously or sequentially. We apply all modeled stimuli so that the center point of the stimuli always falls on the center of the patch of skin.

Generating the response to point stimuli (general)

In order to determine the expected firing rate, λ , of each SA1 neuron in response to the modeled stimulus, we interpolated it from a characteristic SA1 stimulus-response function obtained in monkeys (rhesus) (Vega-Bermudez and Johnson, 1999a). The stimulus response function plots the expected firing rate of an SA1 as a function of the point indentation depth and distance from the spot of maximal activity (taken to be the receptive field center). For each SA1 receptive field, the expected firing rate is interpolated from the stimulus-response function at the calculated Euclidean distance between the stimulus point and the receptive field center. Interpolating in this way, regardless of the direction of the point stimulus relative to the RF center, is equivalent to assuming a completely circular RF. We can further scale the stimulus-response function according to both the size and

shape of the receptive field we wish to model (see section titled “size scaling of RF and shape scaling of RF”).

The interpolation described above results in an expected or mean SA1 firing rate in response to a point stimulus. However, neural responses are typically noisy: given constant stimulus parameters, different number of spikes may result during each stimulus presentation. Additionally, there is a baseline of spontaneous activity that is independent of stimulation (0 Hz for SA1, and 10Hz for cortical neurons) that is added to the response of every afferent. Therefore, to model a response with noise characteristic similar to those observed in peripheral and central neurons, we apply the following methods:

We simulate SA1 noise by drawing from a Gaussian distribution centered on the expected spike count for the k^{th} neuron, λ_k , and with a standard deviation of

$\sigma = 0.45 \lambda_k^{0.21}$. This is the standard deviation for the distribution of the spike counts to repeated trials, of 200ms stimulation, measured by Vega-Bermudez and Johnson (1999). The Gaussian distribution can be written as:

$$p(r_k | \lambda_k) = \frac{1}{\sqrt{2\pi\sigma^2}} e^{-\frac{(r_k - \lambda_k)^2}{2\sigma^2}}$$

We simulate cortical neuronal noise by sampling from a Poisson distribution (Knuth (1998) defined by the expected spike count, λ . The following expression gives the probability of the k^{th} neuron spike count of r_k , when λ is expected:

$$p(r_k | \lambda) = \frac{\lambda^{r_k} e^{-\lambda}}{r_k!}$$

The two expressions above determine the probability of drawing a given spike count r_k when expecting λ spikes. We assume that all SA1 responses are independent of one another, and are independent of previous stimulus presentations.

Size scaling of the receptive field

Vega Bermudez and Johnson's (1999a) characteristic SA1 stimulus response curve was measured in the index fingertip of monkeys; here we assume the same general receptive field response properties in our model of human skin. For the fingertip we do not scale the receptive field size, since we assume the same fingertip receptive field sizes between human and monkey. However, to model receptive fields with surface areas differing from those of the fingertips (i.e. the finger base, palm and forearm) we simply scale the x-axis of the stimulus response function from Vega-Bermudez and Johnson (1999a)[see figure 1]. The

scaling factor we use is the square-root of the ratio between the surface area of the RF being modeled and that of the mean fingertip RF area (10.8mm²). This scaling factor is, therefore, equivalent to the ratio of the radii of different RF sizes (assuming circular RFs). The sizes of all receptive fields for a given body part were set as a constant (reliable values of variability were not found in the reviewed literature). See table 1 for a summary of the RF scaling factors used on each body site.

The two-point stimulus response

When stimulating with two points simultaneously, the potential interaction between the two points must be taken into consideration. Studies have shown that the neural response to two simultaneously indented points, of equal depth, is not equal to the sum of responses to the two points presented separately. Vega Bermudez, and Johnson (1999b) report that two-point stimuli separated by a mm, on average, trigger only ~88.5% the number of spikes generated by a single point near the SA1 afferent's RF centre. This is due to surround suppression when multiple, simultaneous indentations occur, likely caused by skin mechanics. According to Sripati et al (2006) and Phillips and Johnson (1981), all two-point interactions cease when the separation between points is 3mm or greater.

To implement the above characteristics in the generative model, we approximate the response to two simultaneous points as: $(p_1 + p_2)/A$; where p_1 and p_2 are the responses to either of the points alone, and A is a free parameter. When $A = 2$, the response to two points equidistant from the center of the RF is equivalent to the response to just one of them alone (perfectly controlling for magnitude differences). When $A = 2.25$ the ratio of the single point response to the dual response is ~89% (the mean value reported by Vega Bermudez and Johnson, 1999b). When $A = 1$ the response to two points is simply the sum of the two individual responses. Therefore, in simulations where two-point interactions are informed by Vega Bermudez and Johnson (1999b) and Sripathi et al (2006), we use the following values for A :

Modeling surround suppression:

If $\Delta x > 3\text{mm}$, $A = 1$

If $2\text{mm} < \Delta x < 3\text{mm}$, $A = 4 - (\Delta x/\text{mm})$

If $1\text{mm} < \Delta x < 2\text{mm}$, $A = 2.5 - 0.25(\Delta x/\text{mm})$

If $0\text{mm} < \Delta x < 1\text{mm}$, $A = 2.25$

Figure 11 shows a graphical representation of A as a function of the two-point separation, Δx .

In situations for which we intend to model perfect magnitude control (i.e. in the complete absence of interstimulus effects) we assign the A parameter a value of 2.

Shape scaling of receptive field (modeling an elliptical RF)

Vega-Bermudez and Johnson's stimulus-response function (1999a) gives the expected impulse rate as a function of the distance between the probe and the receptive field hotspot. Interpolating from this function, in the methods described above, assumes a perfectly circular receptive field. However, this method of interpolation does not account for elliptical receptive field shapes, which have been observed in both primate and human subjects (Johansson and Vallbo, 1978; Vega-Bermudez and Johnson 1999a). In order to model the response to a stimulus distance, d , from the RF hotspot that is consistent with an elliptical receptive field, we scale the stimulus-response function according to the aspect ratio of the ellipse (the ratio of the major radius to the minor radius). This amounts to "compressing" (or deforming) a circular RF for the neuron (as described in Vega-Bermudez and Johnson, 1999a) into an equivalent elliptical receptive field.

We start with the Euclidean distance of the stimulus from the RF center, d . Along with the x-component of this distance, Δx , we can solve for the angle, θ , between

d and Δx . Knowing θ , we can now define an ellipse (constrained by the aspect ratio, asp) on which the stimulus falls. The ellipse is defined by the parameters a and b , the major radius and the minor radius, which we solve for using the following equation:

$$d = \frac{ab}{\sqrt{(b \cos \theta)^2 + (a \sin \theta)^2}}$$

The above expression can be rearranged in terms of the ratio between a and b (equivalent to the aspect ratio). $a = (asp)b$

$$b = d \sqrt{\left(\frac{\cos \theta}{asp}\right)^2 + (\sin \theta)^2}$$

For our modeling purposes, the aspect ratio takes on values ≥ 1 ; the receptive field is circular when the aspect ratio is 1 and elliptical when it is greater than 1 (we use the specific value of 1.68, the mean aspect ratio of SA1 receptive fields derived from Vega-Bermudez and Johnson 1999a).

Knowing the parameters a and b of the ellipse, we can now define a circle with the same area using the following expressions relating the area of a circle to that of an ellipse:

$$A = \pi r^2 = \pi ab$$

$$r = \sqrt{ab}$$

r is then taken as the distance from the receptive field hotspot, at which we interpolate an expected firing-rate from Vega-Bermudez and Johnson's stimulus-response function (1999a).

All of the above steps, taken together, are equivalent to finding a circular iso-firing rate curve that corresponds (gives an equivalent firing rate) to an elliptical iso-firing rate curve, defined by the aspect ratio and distance of the stimulus from the RF hot-spot.

The aspect ratio of elliptical fields is based on measurements done by Vega-Bermudez and Johnson (1999a), who report a mean aspect ratio of 1.68. Vallbo and Johansson (1980) also report that about 3/4 of receptive fields are elliptical in shape, the remaining quarter are roughly circular; of the fields that are elliptical, 2/3 have their long-axes aligned with the longitudinal direction of the

hand and the rest are intermediately oriented. For simulations concerning RF shape we assign every elliptical field an aspect ratio of 1.68 and align their long axes in the longitudinal direction (exactly 180 degrees). We use this particular configuration to address the question of whether elongated RFs, oriented in a particular direction, will result in a performance anisotropy.

The Bayesian Decoder

Once the firing rate, with variability, for each simulated SA1 has been generated, the ideal observer now has the task of decoding the population response, thereby inferring the most probable model for the stimulus that occurred (one point or two points, same or different location) or estimating the most likely location of a single point, given the population activity profile.

Single point localization

Localization of a single point in two dimensions is a simple parameter estimation problem: the ideal observer considers a discrete set of possible x- and y-positions, x_i , y_i , on a grid (with intervals of 0.5mm, or 0.25mm for finer resolution in microstimulation) spanning the entire area of skin, where stimulation may occur (all body sites were modeled as a patch of skin 10mm by 10mm in area) as well as different possible indentation depths (d). Using the full form of Bayes theorem

the probability of any given location, x_i , y_i , and depth combination given the population activity, R , may be computed:

$$P(x_i, y_j, d_l | R) = \frac{P(R | x_i, y_j, d_l) P(x_i, y_j, d_l)}{\sum_{i,j,l} P(R | x_i, y_j, d_l) P(x_i, y_j, d_l)}$$

The above expression can be marginalized across indentation depths, to give a probability distribution over positions alone:

$$P(x_i, y_j | R) = \sum_l P(x_i, y_j, d_l | R)$$

Conversely, marginalizing over positions gives a distribution over indentation depths:

$$P(d_l | R) = \sum_{i,j} P(x_i, y_j, d_l | R)$$

The above marginal posteriors are used to find the most probable value (for either position or depth) given the population response. In other words, the modes of the marginal posterior distributions are taken to be the optimal estimates for the location of stimulation and its indentation depth.

Recall that $P(x_i, y_j, d_l)$ is uniform, any position and depth is equally likely to be stimulated a priori, and $P(R | x_i, y_j, d_l)$ depends on the type of noise in the firing rates. For example, the likelihood for the position x_i , y_j and indentation depth, d_l , given the population firing rates, R , assuming Poisson noise is:

$$P(R | x_i, y_j, d_l) = \prod_k P(r_k | x_i, y_j, d_l : \lambda) = \prod_k \frac{\lambda^{r_k} e^{-\lambda}}{r_k!}$$

Assuming Gaussian noise, the expression becomes:

$$P(R | x_i, y_j, d_l) = \prod_k p(r_k | x_i, y_j, d_l : \lambda) = \prod_k \frac{1}{\sqrt{2\pi\sigma^2}} e^{-\frac{(r_k - \lambda)^2}{2\sigma^2}}$$

Running simulations of single afferent microstimulation

A single SA1 fiber in the center of the modeled patch of skin was selected for “stimulation”: its expected firing rate on every trial was equivalent to what would be expected from an indentation directly over its receptive field center, for an indentation depth of 500 microns. We set the expected rate of all other SA1 fibers to the spontaneous rate of discharge (zero for SA1-like responses, and 10 Hz for cortical-like responses). Noise was introduced as previously described: the activity of each fiber was drawn from either a Gaussian distribution (afferent-like response) or Poisson distribution (cortical-like response). Decoding of the responses was identical to the procedure for single-point localization described

above. The best estimate for position was the mode of the marginal distribution: $P(x_i, y_j | R)$. We also found the best estimate for indentation depth in each trial by finding the mode of the marginal distribution: $P(d_i | R)$.

Simulations consisted of 1000 trials of microstimulation of the same centrally placed neuron (the neuron in the center of the grid before jittering RF positions). The resulting position estimates for each trial (projected field) was compared to the position of the center of the stimulated neuron's receptive field; the Euclidean distance between these two positions was calculated for each trial and reported as the inter-field distance (IFD), another measure of localization developed by Schady et al (1983). The mean IFD and standard deviation was calculated for the 1000 trials. Simulations were run on the four modeled body-sites: fingertip, finger base, palm and arm.

Running simulations of single point localization

The mid-point on the modeled patch of skin was "stimulated" (position [5mm, 5mm]) for 1000 trials on each modeled body site. The resulting mode of the marginal posterior distribution over stimulus position was recorded for all 1000 trials and the mean and standard deviation were calculated. Additionally, the mean error of localization was calculated by averaging over the Euclidean distance between the mode and the actual position of stimulation (distance from

the mid-point) on each trial. This mean error of localization is the measure commonly reported in human single point localization studies, also referred to as the measurement of “locognosia”.

The Classic Two-Point Task (simultaneous points)

In the classic two-point task, when the stimulus is longitudinally oriented, the model is only uncertain about the x position of the stimulus point(s) (the y-position is the same for both taps in the two-point case). With the two points oriented transversely, only the y-positions of the stimulus points are unknown. For the point of simplicity in illustration, we will only consider the longitudinal stimulation case here. The decoder considers two models, that either one point or two points were applied to the patch of skin. Each model consists of a set of sub-hypotheses: The one-point model considers a discrete set of possible x-positions, x_i , on a grid (with intervals of $1/40^{\text{th}}$ of the body site’s length) spanning the entire area of skin; the two-point model considers possible pairs of x-positions, x_i and x_j (where $x_j \neq x_i$) that two points can occupy. In the classic two-point task, stimuli are occurring simultaneously, so we only count each possible pair of locations once.

The probability of any given pair of points, assuming 2-points, is known as a prior for 2-point model sub-hypotheses, $P(x_i, x_j | 2pts)$. The prior is assumed to

be uniform for all possible pairs of two-point locations. The probability of the population response for SA1 afferents, R , given a pair of points, is known as the likelihood, $P(R | x_i, x_j)$.

The probability of any point, assuming the 1-point model, is known as the prior for the one-point model sub-hypotheses. The prior is assumed to be uniform for all possible locations of the point. The probability of the population response for SA1 afferents, R , given a point location, is known as the likelihood, $P(R | x_i)$.

The following rules about priors and likelihoods apply to all tasks/model comparison examples in this study (i.e. Classic two-point, sequential two-point and single point localization):

Assuming a uniform probability for the sub-hypotheses within a given model, the priors are equal to the reciprocal of the number of sub-hypotheses in that model.

The likelihood for any particular sub-hypothesis depends on the type of noise added during the encoding stage; it is simply equal to the product of the probabilities for observing r_k spikes when λ_k spikes are expected under that sub-hypothesis, for each of the neurons in the population.

For example, the likelihood for the positions of two points, x_i, x_j , given the population firing rates, R , is:

$$P(R | x_i, x_j) = \prod_k p(r_k | x_i, x_j : \lambda_k) = \prod_k \frac{\lambda_k^{r_k} e^{-\lambda_k}}{r_k!}$$

Assuming Gaussian noise, the expression becomes

$$P(R | x_i, x_j) = \prod_k p(r_k | x_i, x_j : \lambda_k) = \prod_k \frac{1}{\sqrt{2\pi\sigma^2}} e^{-\frac{(r_k - \lambda_k)^2}{2\sigma^2}}$$

Note that the above expressions assume that each neuron's response is independent of the others'.

Expressed in odds form, Bayes theorem is a ratio of the marginal likelihoods for each model. The marginal likelihood for a given model is the sum of the product of subhypothesis likelihoods and priors. Since our model assumes a uniform prior over subhypotheses, the priors are simply the reciprocal of the number of subhypotheses in each model.

$$BF = \frac{P(R | 2pts)}{P(R | 1pt)}$$

Bayes Factor for simultaneous two-point task:

$$= \frac{\sum_{i,j} P(x_i, x_j | 2pts) P(R | x_i, x_j)}{\sum_i P(x_i | 1pt) P(R | x_i)}$$

where $x_j \neq x_i$.

With an unbiased and optimal decision criterion, when the Bayes Factor ratio is greater than 1, the two-point model is favored and the ideal observer reports two-points. On the contrary, when the Bayes Factor ratio is less than one, the one-point model is favored and the ideal observer reports one point.

Two-point orientation discrimination

An additional task we model is orientation discrimination of two points. The two-point stimuli could either land longitudinally (along the x-axis) or transversely (along the y-axis). The model's task is to discriminate which of the two possible orientations was presented, given the population response.

Decoding the stimulus is, once again, a matter of Bayesian model selection as described above, in which the models correspond to two-points oriented either transversely or longitudinally:

$$BF = \frac{P(R|long)}{P(R|trans)}$$

$$= \frac{\sum_{i,j} P(x_i, x_j | long) P(R | x_i, x_j)}{\sum_{i,j} P(y_i, y_j | trans) P(R | y_i, y_j)}$$

where $x_j \neq x_i$ and where $y_j \neq y_i$.

All sub-hypothesis likelihoods and priors are calculated as described for the two-point model in the section “The classic two-point task (simultaneous)”, above.

Running simulations of simultaneous two-point discrimination

In simulating the single-interval version of the task, the two-point stimulus is always given, with the stimulus mid-point falling directly on the mid-point on the patch of skin (position [5mm, 5mm] on the finger tip and base and [15mm, 15mm] on the palm and arm). This is repeated 100 times for each separation (0.125 to 2.375 in steps of 0.125) for a total of 10 blocks. For each separation in a block, the proportion of correct trials: number of times the Bayes Factor was greater than 1 (two-point model wins) was calculated and, from these values, the separation that would result in 50% correct was interpolated. The mean interpolated 50%-threshold, and the standard deviation, was then calculated for all 10 blocks.

In addition to the single-interval version of simultaneous two-point discrimination, we also simulated the two-interval forced-choice (2IFC) version for addressing the issues of anisotropy and surround suppression. In 2IFC two-point discrimination, each trial consisted of two intervals of stimulation: in the first interval, the model was presented with a two-point stimulus of a given separation and in the second interval, the model was presented with the single point. Each stimulus was placed such that its center-point fell on the center-point of the modeled patch of skin. Following each stimulation interval, the model would calculate the corresponding Bayes Factor for each interval: if the first interval resulted in a larger Bayes Factor than for the second interval, the outcome would be a correct response by the model (the 1st interval is identified correctly as being more likely to contain the two-point stimulus). Conversely, if the second interval's Bayes Factor were greater than the first, the model would have an "incorrect" response for that trial. This is repeated 100 times for each two-point separation (0.125 to 2.375 in steps of 0.125) for a total of 10 blocks. For each separation in a block, the proportion of correct trials was calculated and, from these values, the separation that would result in 75% correct was interpolated. The mean interpolated 75%-threshold, and the standard deviation, was then calculated for all 10 blocks. Additionally, another measurement of interest was the performance level that was approached (asymptote) as the two-point separation approached zero.

Sequential two-point task

In the sequential two-point task, a subject must identify whether two sequential taps occurred at the same location or different locations. The same-location model consists of subhypotheses for the position of the two taps, x_j . The different-location model consists of subhypotheses for every pair of possible position of two consecutive taps, x_j and x_i (where $x_j \neq x_i$). Since each sequential tap results in a unique population activity profile (R_1 and R_2), the Bayes Factor calculation for “same” or “different” locations is more complex than that of the one or simultaneous two-points task.

Likelihoods and priors are calculated in the same way as described above (in the classic two-point task).

Bayes Factor for sequential two-point task:

$$BF = \frac{P(R_1, R_2 \mid \text{different})}{P(R_1, R_2 \mid \text{same})} \quad \text{where } x_j \neq x_i$$

$$= \frac{\sum_{i,j} P(x_i, x_j \mid \text{different}) P(R_1, R_2 \mid x_i, x_j)}{\sum_i P(x_i \mid \text{same}) P(R_1, R_2 \mid x_i)} = \frac{\sum_{i,j} P(x_i, x_j \mid \text{different}) P(R_1, x_i, x_j) P(R_2 \mid x_i, x_j)}{\sum_i P(x_i \mid \text{same}) P(R_1, x_i) P(R_2 \mid x_i)}$$

When the Bayes Factor ratio is greater than one, the “different-locations” model is favored and the ideal observer reports “different locations”. On the contrary, when

the Bayes Factor ratio is less than one, the same-location model is favored and the ideal observer reports “one location”.

Running simulations of sequential two-point discrimination

We simulated the single-interval version of sequential two-point discrimination: the two-point stimulus is always given, with the stimulus mid-point falling directly on the mid-point on the patch of skin (position [5mm, 5mm] on the finger tip and base and [15mm, 15mm] on the palm and arm). This is repeated 100 times for each separation (0.125 to 2.375 in steps of 0.125) for a total of 10 blocks. For each separation in a block, the proportion of correct trials: number of times the Bayes Factor was greater than 1 (two-point model wins) was calculated and, from these values, the separation that would result in 50% correct was interpolated. The mean interpolated 50%-threshold, and the standard deviation, was then calculated for all 10 blocks.

2.5 RESULTS

Microstimulation

We ran simulations of microstimulation to analyze the contribution of a single SA-1 fiber in encoding point location. Much like in Schady et al.’s study of the microstimulation in humans (1983), our measure of a single SA1’s “encoding

fidelity”, when stimulated, is the distance from its receptive field center to the location of where the evoked sensation is perceived to be (the projected field). This distance between projected and receptive fields is termed the inter-field distance (IFD) (Schady et al. 1983).

Our simulation results show that modeled skin sites with larger receptive fields also tend to have greater IFDs, or greater disagreement between the location of the evoked sensation and the RF position. Overall, the locations of the evoked sensations consistently fall within the stimulated receptive field (mean IFDs +/- SD on each body site are smaller than the RF radii) (See table 2).

Given that we set the expected firing rate of a single SA1 fiber to be equivalent to that of an indentation of 500 microns at the center of its RF, the model consistently reported a best estimate of intensity lower than 500 microns. However, this discrepancy gets smaller as we move from modeling the fingertip to the forearm. (See table 2)

Single point localization

In general, our simulations of single-point localization show that there is a direct relationship (nearly linear) between localization accuracy and innervation density. The greater the innervation density, the more accurately a point can be

localized: the error, or difference between the perceived and actual stimulated location, is smallest at the fingertips and increases as we move proximally towards the forearm. (See table 3, and figure 3, 4, 5)

Additionally, the type of noise or variability in neural responses also affects localization accuracy. Overall, greater variability in responses results in greater uncertainty in the decoding process. Therefore, decoding SA1-like responses (drawn from a Gaussian distribution) leads to more accurate localization than decoding cortical-like responses (drawn from a Poisson distribution). With SA1 noise, the model was so accurate at localization on the fingertip and finger base that the error of localization was zero on these body sites (See table 3 and figure 3).

Sequential and simultaneous two-point discrimination

Our simulations show that when two-points, whether sequentially or simultaneously presented, are separated by a greater distance the probability of an ideal observer responding “two points” increases. Furthermore, when comparing between sequential and simultaneous two-point discrimination, it can be easily seen that sequential discrimination thresholds are consistently smaller than that of simultaneous discrimination (see fig. 6 and 7). The absolute difference between sequential to simultaneous thresholds grows from fingertip to

forearm; however, the ratio between these thresholds decreases from fingertip to forearm.

Simultaneous two-point discrimination with longitudinally oriented elliptical receptive fields

To investigate whether longitudinally oriented elliptical receptive fields results in a performance anisotropy for two-point discrimination, 2IFC simulations were run with the two-point stimuli oriented either transversely (perpendicular to the long axis of the RFs) or longitudinally (parallel to the long axis of the RFs). The separation at which 75% performance is achieved by the ideal observer was compared between these two configurations. (see figure 9 and 10)

Performance thresholds (75%) were consistently larger when two-point stimuli were oriented longitudinally compared to when the two points were oriented transversely. This absolute magnitude of this difference grows as we move proximally from fingertip to forearm; however, the ratio between transverse and longitudinal thresholds decreases from fingertip to forearm (see fig 10).

Simultaneous two-point discrimination with surround suppression

To investigate the effects of surround suppression on two-point discrimination we ran simulations using a two-interval forced choice (2IFC) design

so that each trial contained a two-point and then a one-point stimulus and the model was tasked with deciding whether two-points was presented first or second.

Our simulation results show that, with surround suppression parameter settings (see Methods section: The two-point stimulus response), the ideal observer was able to reliably discern between two-point and one-point stimuli even as the two-point separation approached zero. Performance asymptotes to a value above chance (0.5) for each modeled body part (see fig 12 A); this “minimal performance-value” decreases as we go from fingertip to forearm. Simulating a force controlled situation, where two-points equidistant from an RF center have the same response as a single point, effectively removes surround suppression; in this case the ideal observer approaches chance performance as the two-point separation approaches zero (see fig 13 B).

Two-point orientation discrimination with surround suppression

To address whether a novel task, two-point orientation discrimination, would be susceptible to surround suppression, as was shown for classic two-point discrimination, we carried out a 2IFC version of orientation discrimination in the presence of modeled surround suppression. Our simulation results show that, even with surround suppression, orientation discrimination approaches

chance levels as the separation between two points decreases to zero on any given body site (see fig 13).

2.6 Discussion

Our simulations demonstrate ideal performance in single-point localization and two-point discrimination tasks, given the population responses of tactile afferents. The ideal observer consistently outperforms human on these tasks. This is not surprising, since there are likely further sources of noise or uncertainty in the nervous system that we have not considered in our model. We have also made simplifying assumptions, such as the independence of responses between neurons. Despite the model's simplifying assumptions and inclusion of only peripheral activity of SA1 channels, our simulations nevertheless parallel many trends found in human performance of point localization and discrimination. Here, we will focus on these parallels and our model's assumptions.

Microstimulation

Schady and colleagues (1983) studied the role of single fibers in representing point location by using the technique of intraneural microstimulation. They isolated and stimulated a single SA1 afferent with a known receptive field location and had the observers subsequently report where they felt the evoked stimulus. The investigators termed the reported location(s) of sensation the

projected field. They further compared the locations of these projected fields against the locations of the stimulated fiber's RF, and found much agreement between these locations on areas of high acuity (i.e. the fingertip). There was much greater disagreement in less acute areas, such as the palm and forearm. The distance between the projected field and the fiber's RF, is known as the inter-field difference (IFD) and is found to be greater on skin sites where RF sizes are larger (2.6mm on fingertip, 9.9mm on finger base, 17.6mm on palm, 23.4mm on forearm). Our ideal observer simulations also show a larger disagreement between projected fields (the most probable position estimates) and RF-centers as we move from fingertip to forearm. This finding agrees with Shady et al.'s (1983) speculation that innervation density is not the only peripheral factor that determines localization accuracy but an individual fiber's response properties (RF size, shape and response variability) must also be considered.

Schady et al (1983) also report that microstimulation in humans consistently yields sensations of taps of extremely weak intensity, so weak that participants were required to concentrate intently to localize the sensations. Similarly, another study by Vallbo et al. (1984) reports that stimulating an SA1 fiber with 20-100Hz pulses evoked a sensation equivalent to an indentation of ~8mN; however, when the fiber was activated by skin stimulation with an external 8mN Von-Frey hair, the resulting impulse rate was only 1-3Hz. Our model

qualitatively replicates this phenomenon in that its best estimates for stimulus intensity are consistently lower than the intensity that is expected, given the stimulated fiber's mean response (corresponding to a 500 μm tap in the RF center). This can be explained by the fact that a real point indentation of a given depth will likely cause co-activation of more than one surrounding nerve fiber, specifically where receptive fields overlap. During microstimulation, however, the brain is likely to interpret the relative silence of neighboring RFs as the result of an extremely light tap on the skin. This would suggest that not only the magnitude of activity in fibers, but also the overall number of fibers activated, contains information about the stimulus magnitude. This is likely true for regions where there is much RF overlap, where an indentation would often vigorously activate more than one fiber. As our model demonstrates, in areas with sparser innervation and less RF overlap, a single fiber should more accurately translate intensity information during microstimulation since the activation profile more closely matches real stimulation. Future microstimulation studies should further elucidate how injected current to one or more fibers relates to perceived intensity.

Single point-localization

The simplest tactile spatial acuity task involves localizing a single point of contact on the body surface. Many investigators have measured the ability of human participants to perform this task (Schady et. al. 1983; Hamburger, 1980;

Craig and Rhodes, 1992; Boring, 1977). The primary performance measure they report in single point localization is the mean error between the actual tap location and the perceived tap location reported by an observer. This is known as the measure of locognosia (or the error of localization); the smaller the locognosia value, the more accurate an observer is at localizing a point. Although the definition of this measure is standard among investigators, a large variety of measurement techniques have been developed and implemented, each mainly differing in the way observers report the stimulus location: some studies have the observer mark down or touch their skin at the perceived stimulus location (either with or without vision of the stimulated area), others require the observer to indicate this location without making contact with their skin, sometimes using a photograph (or other visual representation) of the body site (Boring, 1977). These different techniques have resulted in a considerable degree of variability in reported locognosia values. In general, values are smaller (less error) when visual cues are provided (i.e. either the body site or a photograph of the site is viewed during reporting) compared to cases where no visual cues are provided and the observer must rely entirely on their internally generated map of skin space based on kinaesthetic cues.

In general, areas of dense innervation, such as the finger, have small locognosia values (3.3 mm on the tip, 5.7mm on the proximal phalanx); areas of sparser innervation are less accurate, with locognosia values of 7.6mm and

15.85mm on the palm and forearm (averages from Schady et al 1983; Hamburger,1980). Our ideal observer simulations also demonstrate this trend of localization error linearly increasing as we move proximally from the fingertip towards the arm (to areas of sparser innervation), suggesting that peripheral factors such as SA1 density and RF size largely determine the limits of accuracy in point localization.

Our simulations show that decoding cortical-like responses results in less accurate localization than decoding afferent-like responses. Not surprisingly, Poisson noise in cortical-like responses leads to more uncertainty and more variability in the mode of the posterior probability distribution for position. The ideal observer in either noise condition, however, still outperforms humans in this task: the mean error of localization on the finger tip of humans, 3.3mm (Schady et al. 1983; Hamburger,1980), is about 30 times that of the cortical-like decoding model. This suggests that humans are far from optimal when decoding peripheral activity for point localization. However, It is important to note that our model uses RF response properties derived from the macaque fingertip; nevertheless, human innervation density and RF sizes were incorporated. Another assumption or simplification is that we model cortical-like variability by simply drawing firing rates from a Poisson distribution with a mean equal to the expected SA1 firing rate. Real cortical responses however, are far more complex than the way we

have chosen to model them; for example, receptive field size tends to grow as we ascend the processing hierarchy of the central nervous system, indeed certain cortical receptive fields are typically larger than SA1 receptive fields (Sur, 1980).

Sequential and simultaneous two-point discrimination

Weinstein (1968) was the first to compare performance on both simultaneous and sequential versions of the two-point task. He found that thresholds for sequential discrimination were consistently lower than thresholds for simultaneous discrimination on all the body sites he tested. There was ~30% difference between the thresholds of the two tasks on the fingertip, but this difference grew to 45% and ~75% on the palm and arm, respectively. Our model replicates the trend of sequential thresholds being consistently smaller than simultaneous thresholds. However, we did not find a fractional increase in difference between simultaneous and sequential thresholds, but instead an increase in the absolute difference (simultaneous threshold – sequential threshold) between simultaneous and sequential thresholds from fingertip to forearm.

Intuitively, simultaneous thresholds are likely to be higher than sequential thresholds due to the added SA1 activation in the intervening area of

simultaneous taps. With enough activity between simultaneous taps, it becomes more difficult to determine whether the response profile came from two separate points or a single one. On the contrary, sequential taps, separated by enough time, will have completely independent response profiles and lead to a task akin to single point localization of either tap. Indeed, Weinstein described the sequential two-point task as a variant of single-point localization with a reference tap. Thus, one can appreciate that the simultaneous and sequential tasks are quite different qualitatively, further explaining differences in measured thresholds.

Elliptical receptive fields and anisotropy

When Weber (1996) first implemented the classic two-point discrimination task, he noticed that discrimination thresholds tended to be lower when the two points were oriented transversely (perpendicular to the long axis of the arm) compared to when they were oriented longitudinally (along the long axis of the arm). More contemporary studies have also found such an anisotropy for a variety of discrimination thresholds, from grating orientation, to gap detection and orientation discrimination (Essock et al., 1992; Stevens and Patterson, 1995; Gibson and Craig, 2005). Investigators have attributed performance anisotropy to the elongated shape of a majority of receptive fields in the glabrous skin, as well as their tendency to be oriented along the longitudinal axis: the minimum

separation between two points required to activate the same RF is greater on the long-axis than on the short-axis.

Our simulations with modeled elliptical receptive fields (aspect ratio =1.68) aligned in the longitudinal direction show that such an RF configuration gives rise to anisotropy in two-point discrimination. Thresholds are consistently higher when the two-point stimuli are aligned with the long-axes compared to short-axes of the RFs. The anisotropy effect becomes larger moving from fingertip to the forearm, similar to Weber's finding that anisotropy is most readily measured on the forearm, whereas on the most distal region of the fingertip, anisotropy was not found (Weber, 1996).

The effect of surround suppression in simultaneous two-point discrimination

The simultaneous two-point discrimination task has been widely criticized for its unexplained, high performance variability, both between and within observers. When asked whether a stimulus feels like two points or one, observers must base their decision on a criterion for whether the stimulus feels more like two points rather than one. Because this criterion can differ from observer to observer, or change unexpectedly during the course of an experiment, it is likely

to be a major source of inconsistency in two-point discrimination performance. To mitigate criterion effects, investigators have proposed a variant of the task in which both one and two-points are given so that the observer may directly compare between the two alternatives and respond with which one they thought was two points (the first or second). This 2-interval forced choice (2IFC) version of the task, however, presents another issue: when the two-point stimulus has a separation of zero, observers are still able to distinguish between the one and two-point stimuli (with an accuracy of ~80% on the fingertip) (Johnson and Phillips, 1981). Given that the average spacing between adjacent RFs on the fingertip is 1.2mm, it is highly unlikely that the brain is using the spatial activity profile of SA1s to identify the two-point stimulus of zero separation. It is more likely that the brain is taking advantage of the surround suppression inherent in two-point responses. Because of this issue, two-point discrimination is not a pure measure of spatial acuity.

A comparison between the ideal observer's behavior with and without surround suppression clearly demonstrates that surround suppression introduces a magnitude cue at small separations, allowing the model to discern between one and two-points based on magnitude differences rather than differences in spatial activity profiles. When realistic surround suppression is implemented, performance asymptotes to levels above chance (50%) as two-point separation

approaches zero. This is true for each modeled body site. However, when surround suppression is not implemented in our model, performance asymptotes to chance levels at small separations, regardless of body-site. Therefore, in realistic settings, where it is highly implausible to control for surround suppression, the model predicts that performance on 2IFC two-point discrimination will be above chance at a two-point separation of zero.

The theoretical implication of a magnitude cue in two-point discrimination led us to propose a new task in which the spatial properties of the stimulus must be taken into consideration, regardless of surround suppression. We reasoned that in orientation discrimination of two-point stimuli, surround suppression would not present a magnitude cue for two reasons: 1) a two-point stimulus is always given and 2) task performance relies upon the ability to discern orthogonal orientations for a given separation and would not receive any benefit from magnitude differences. Presumably when the two-point separation falls well below the spacing of neighboring receptive fields, it should not be possible to discern between orientations, and thus chance performance would result; this is especially true if receptive fields are roughly symmetrical and circular in shape.

In the next chapter, we will address whether two-point orientation discrimination is indeed a more pure spatial acuity measure than classic two-point

discrimination by comparing human performance in both tasks. We expect that human classic two-point discrimination will show similar magnitude cue effects as our ideal observer for all tested body sites, and that two-point orientation discrimination will not.

2.7 Tables

Body site	RF area	RF radius	RF scaling factor (relative to fingertip)	Mean Receptor spacing	Body-site length and width
Fingertip	10.8 mm ²	1.85 mm	1.00	1.20 mm	10 mm
Finger base	18.4 mm ²	2.42 mm	1.31	1.77 mm	10 mm
Palm	17.8 mm ²	2.38 mm	1.51	3.53 mm	30 mm for doub point simulation: 10mm for single point simulation:
Forearm*	28.7 mm ²	3.02 mm	1.91	5 mm	30 mm for doub point simulation: 10mm for single point simulation:

Table 1: Parameters defining the modeled body sites. Receptive field areas in all skin regions were taken from Schady & Torebjork (1983); receptive field densities in galoborous skin regions were taken from Johansson and Vallbo (1979) and forearm receptive field density was taken from Olausson* (2000)

Body -Site	Receptive field radius	Inter-field distance (\pm SD)	Human Inter-field distance (Schady et. al 1983)	Intensity estima (\pm SD)
Fingertip	1.85 mm	0.01 \pm 0.03 mm	2.6 \pm 1.7 mm	185.05 \pm 16.06
Finger base	2.42 mm	0.02 \pm 0.05 mm	9.9 \pm 11 mm	207.15 \pm 30.10
Palm	2.38 mm	0.14 \pm 0.15 mm	17.6 \pm 9.9 mm	429.30 \pm 84.70
Forearm	3.02 mm	0.11 \pm 0.23 mm	23.4 \pm 19.7 mm	458.15 \pm 69.57

Table 2: A summary of simulation results for microstimulation. Inter-field distances (3rd column) were consistently less than the receptive field radius (2nd column), indicating that the evoked sensations regularly fell within the stimulated receptive field. Human inter-field distance values (Schady et. al., 1983) are reported for reference. Intensity estimates deviated from 500 microns with decreasing magnitude as we move from fingertip to forearm.

Body -Site	Mean spacing between RF centers	Localization error with SA1 noise (\pm SD)	Localization error with cortical noise (\pm SD)
Fingertip	1.20 mm	0.00 \pm 0.00 mm	0.08 \pm 0.19 mm
Finger base	1.77 mm	0.00 \pm 0.00 mm	0.20 \pm 0.28 mm
Palm	3.53 mm	0.33 \pm 0.57 mm	1.22 \pm 1.34 mm
Forearm	5.00 mm	0.69 \pm 0.99 mm	1.85 \pm 1.65 mm

Table 3: A summary of the simulation results for single point localization. Mean spacing values between RF centers were derived from density values taken from Vallbo and Johanson (1979). A clear relationship can be seen between receptive field spacing and localization error.

2.8 Figures

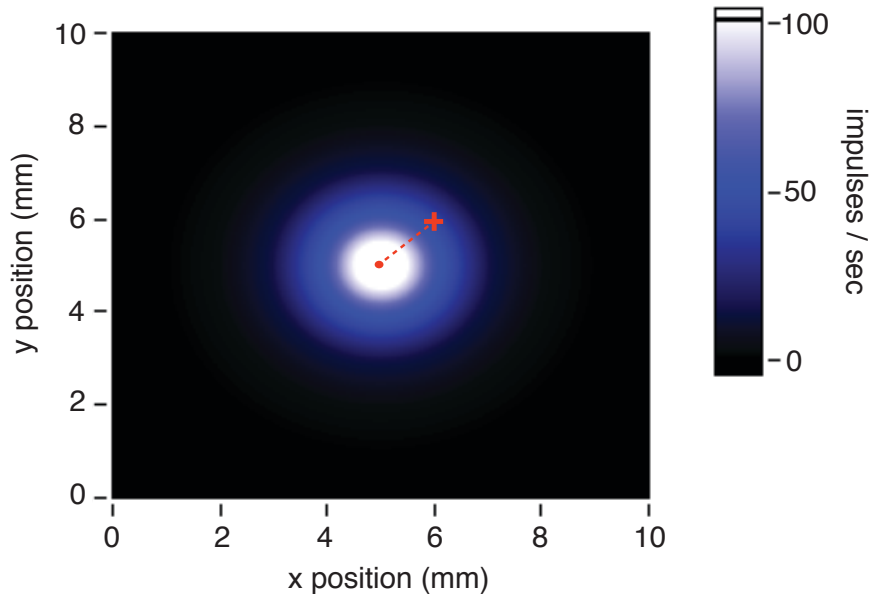


Figure 1: General modeling of a receptive field. An idealized two-dimensional representation of a fingertip receptive field, derived from Vega-Bermudez and Johnosn’s (1999) mean stimulus response function measured in the fingertip of the macaque monkey for an indentation depth of 500 μ m. The same general RF is scaled in size to model the larger receptive fields of other body sites. During microstimulation of such an afferent (with an expected rate corresponding to an indentation in the RF center), the model produces a percept (cross-hair). The distance between the RF center (red dot) and the the position of the percept (cross-hair) is taken as the inter-field distance (IFD, red dotted-line).

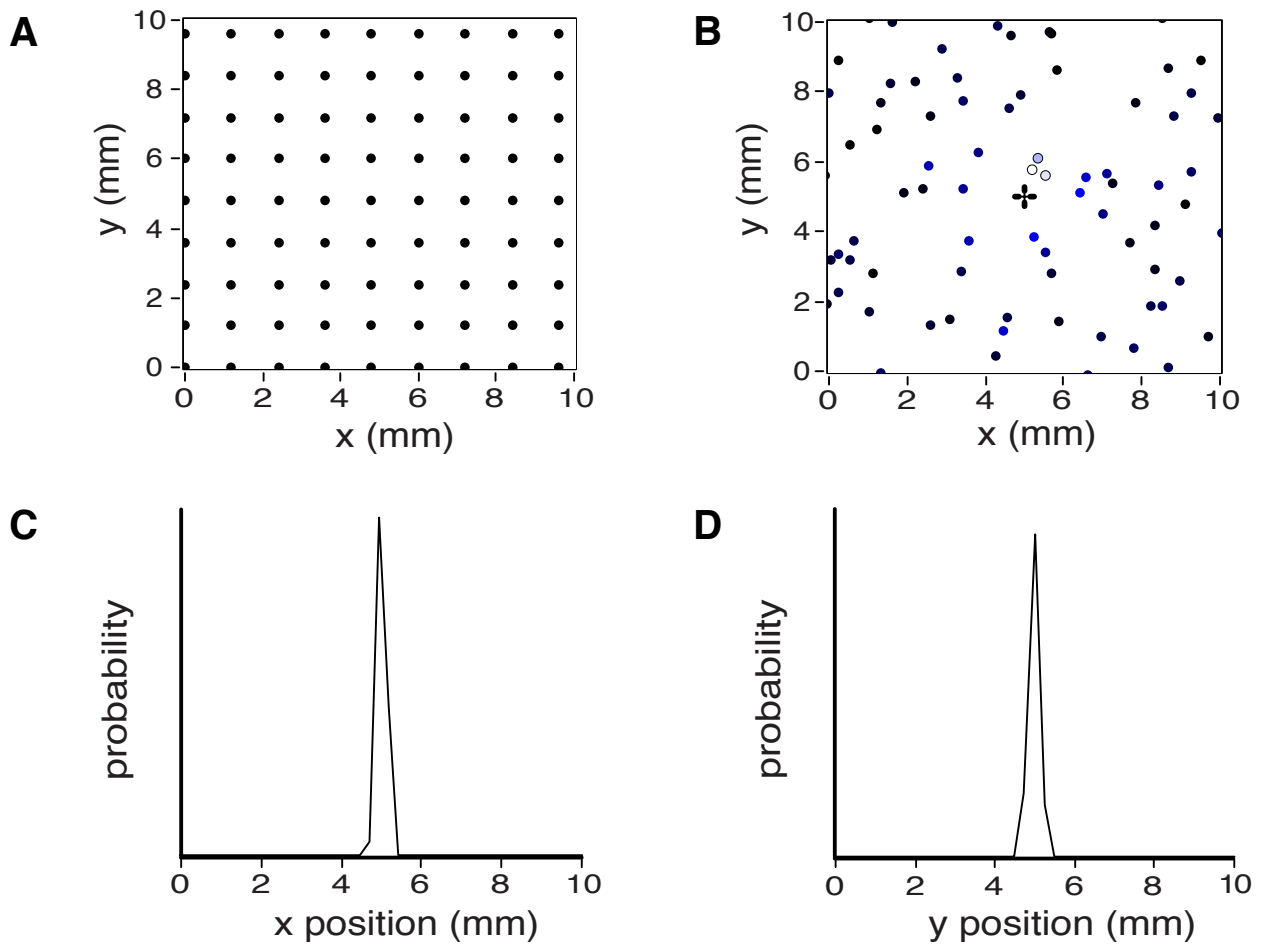


Figure 2: Modeling a patch of skin (afferent receptive fields): A 1 cm² patch of skin on the fingertip is modeled by starting with A: a regular square grid of receptors spaced 1.2 mm apart (the mean spacing on the modeled body site). B: The x and y positions of each receptor are then allowed to deviate from their initial position by a value drawn from a gaussian centered on zero (a standard deviation of ½ the mean spacing). The cross-hair corresponds to the position of a single point stimulation, which results in afferent responses (the brightness levels are proportional to the

intensity of the response: the darkest corresponds to 2 spikes, intermediate light-blue corresponds to 10 spikes and white corresponds to 20 spikes). Expected firing rates are determined by interpolation from Vega-Bermudez and Johnson (1999) stimulus response functions (see figure 1). Trial-to-trial variability in responses are modeled by drawing from a distribution (Gaussian or Poisson for SA1 or cortical-like responses) centered on the expected firing rate. C: The marginal posterior probability function for the y position of the stimulus; the mode of the posterior is 5mm. D: The marginal posterior probability function for the y position of the stimulus; the mode of the posterior is 5mm.

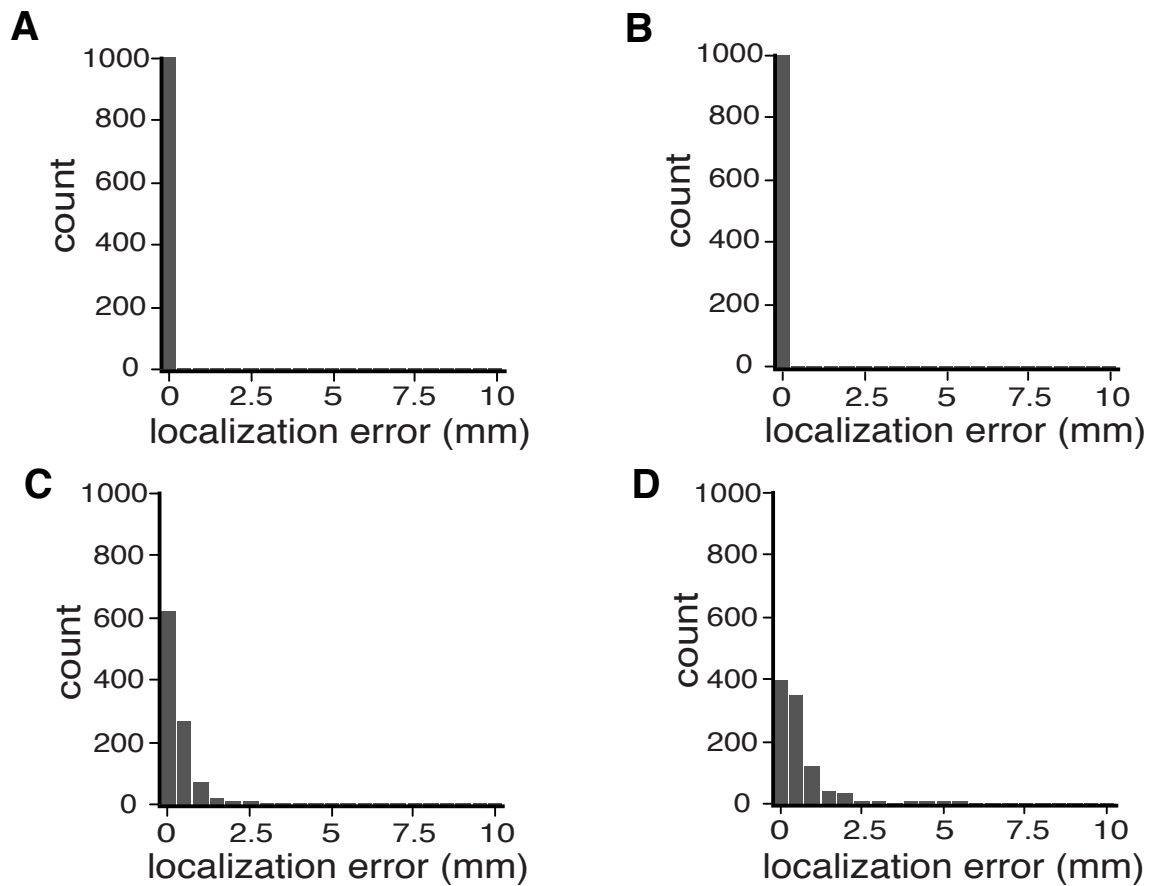


Figure 3: Single-point localization with afferent-like responses. Histograms showing the frequency of localization error values (out of 1000 trials) on A: fingertip, B: finger base, C: palm, and D: forearm; bins correspond to error values of 0 to 10mm in 0.5 mm steps.

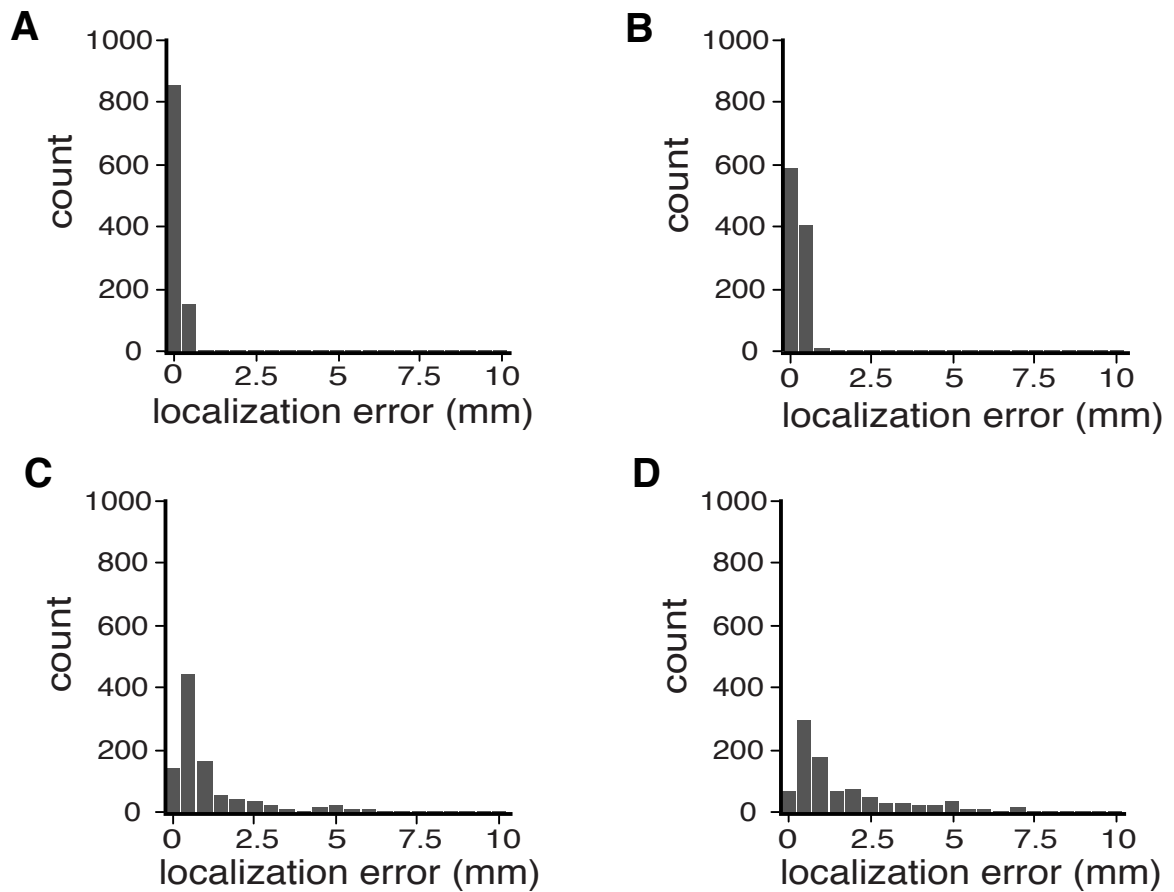


Figure 4: Single-point localization with cortical-like responses. Histograms showing the frequency of localization error values on A: fingertip, B: finger base, C: palm, and D: forearm; bins correspond to error values of 0 to 10mm in 0.5 mm steps.

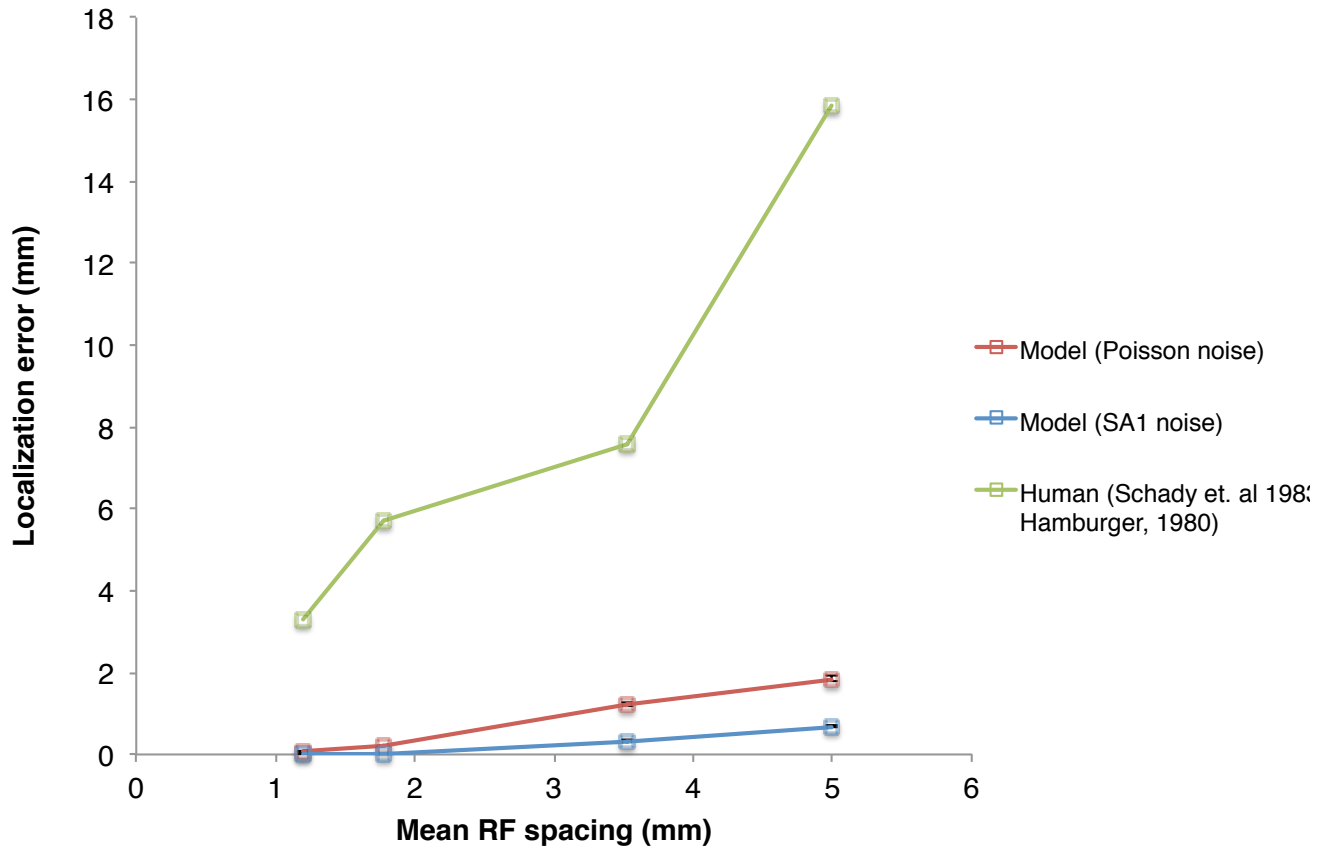


Figure 5: A comparison of model and human performance on single-point localization. Mean localization error is plotted against mean receptive field spacing from Johansson and Vallbo (1979) and Olhaussen (2000). Model performance, with SA1 noise, is plotted in blue; model performance with cortical-like Poisson noise is plotted in red; human performance is plotted in green. Human localization errors are averages of values taken from Schady et. al. 1983 and Hamburger, 1980.

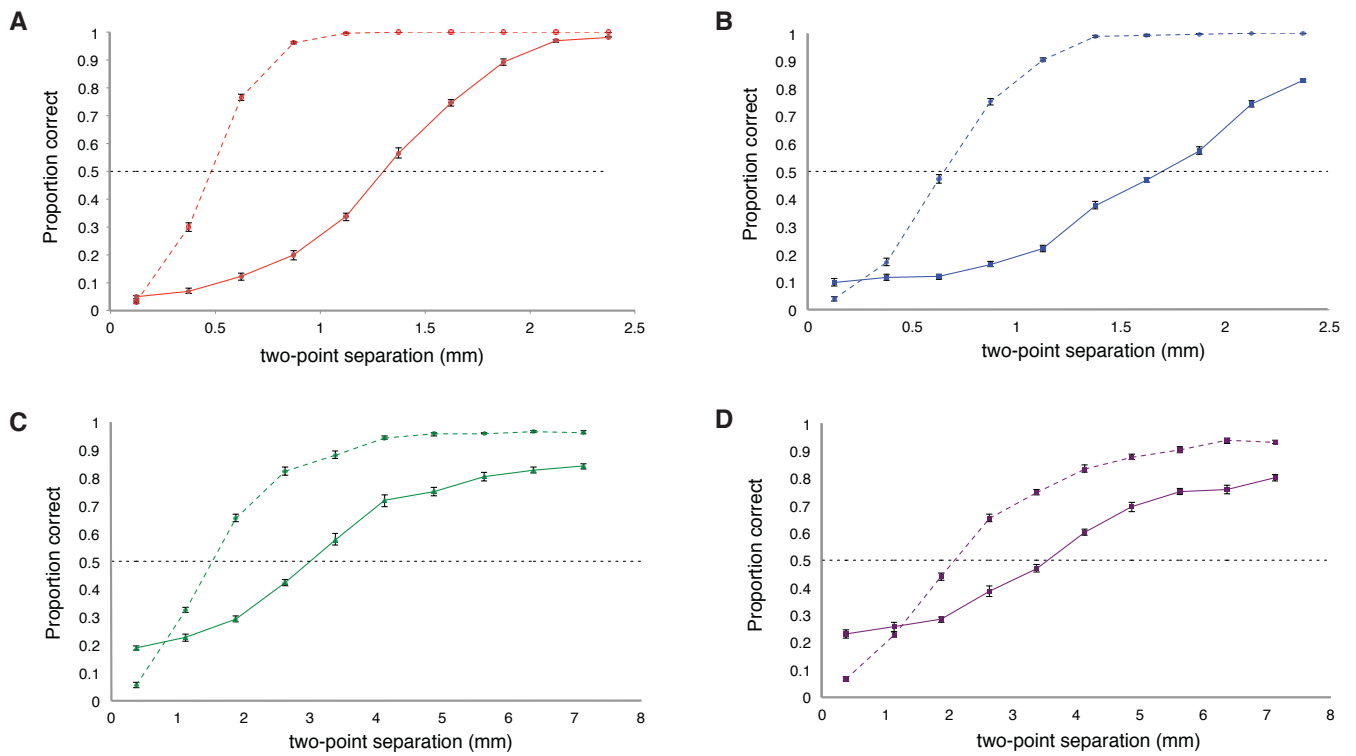


Figure 6: sequential vs. simultaneous two-point discrimination: Ideal
 observer performance on sequential (dashed lines) and standard (solid lines)
 two-point discrimination A: fingertip, B: finger base, C: palm and D: forearm. 50%
 performance is indicated by the black dashed line on each graph.

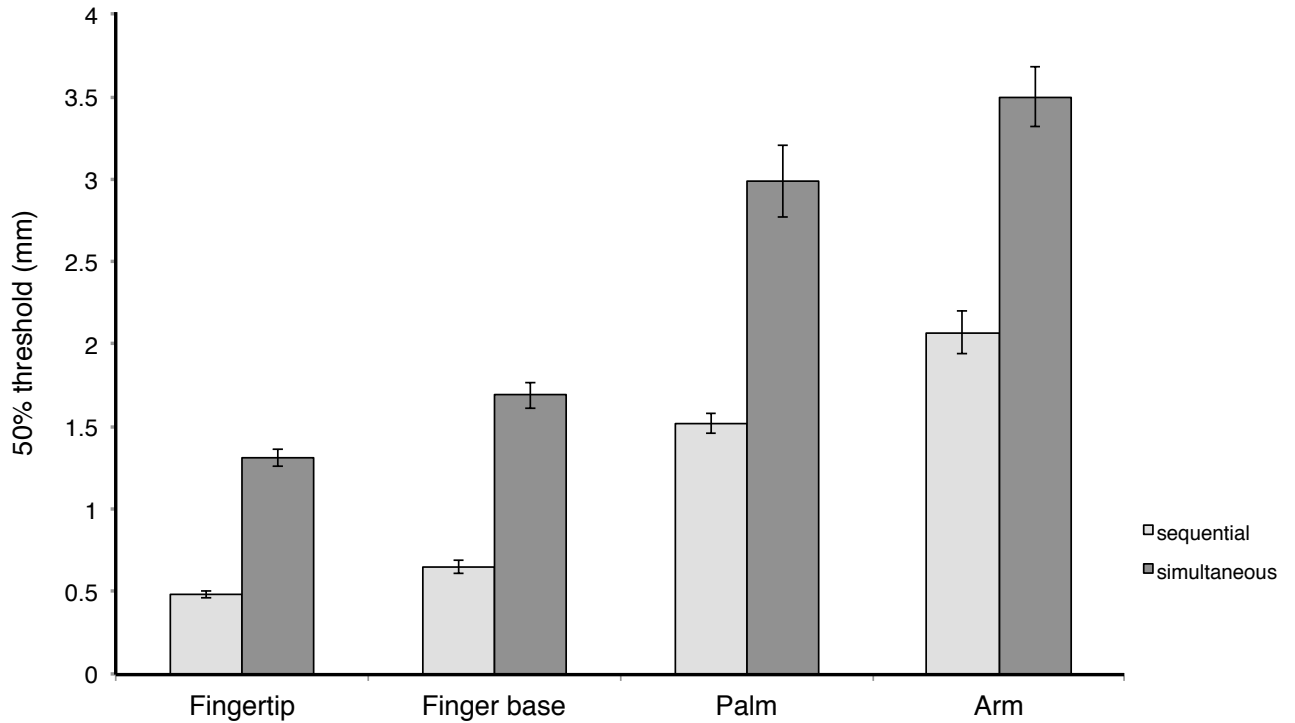


Figure 7: Comparison of thresholds for sequential and simultaneous two-point discrimination. Sequential two-point discrimination thresholds are consistently lower than simultaneous two-point discrimination thresholds. Error bars depict \pm standard deviation.

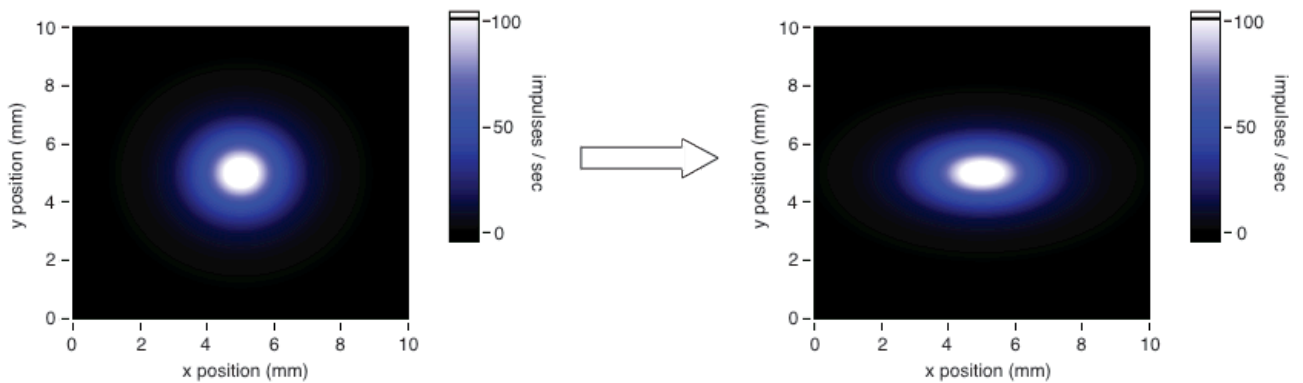


Figure 8: Elliptical receptive field. For simulations involving elliptical receptive fields, initially circular fields (above, left) are rescaled on their x and y-axes, while retaining the same area, to achieve an aspect ratio of 1.68 (the mean measured aspect ratio in human glabrous skin). These elliptical receptive fields are also oriented longitudinally (parallel to the x-axis), as shown above (right), to match the orientation of a majority of the fields in human glabrous skin (Vallbo and Johansson, 1980).

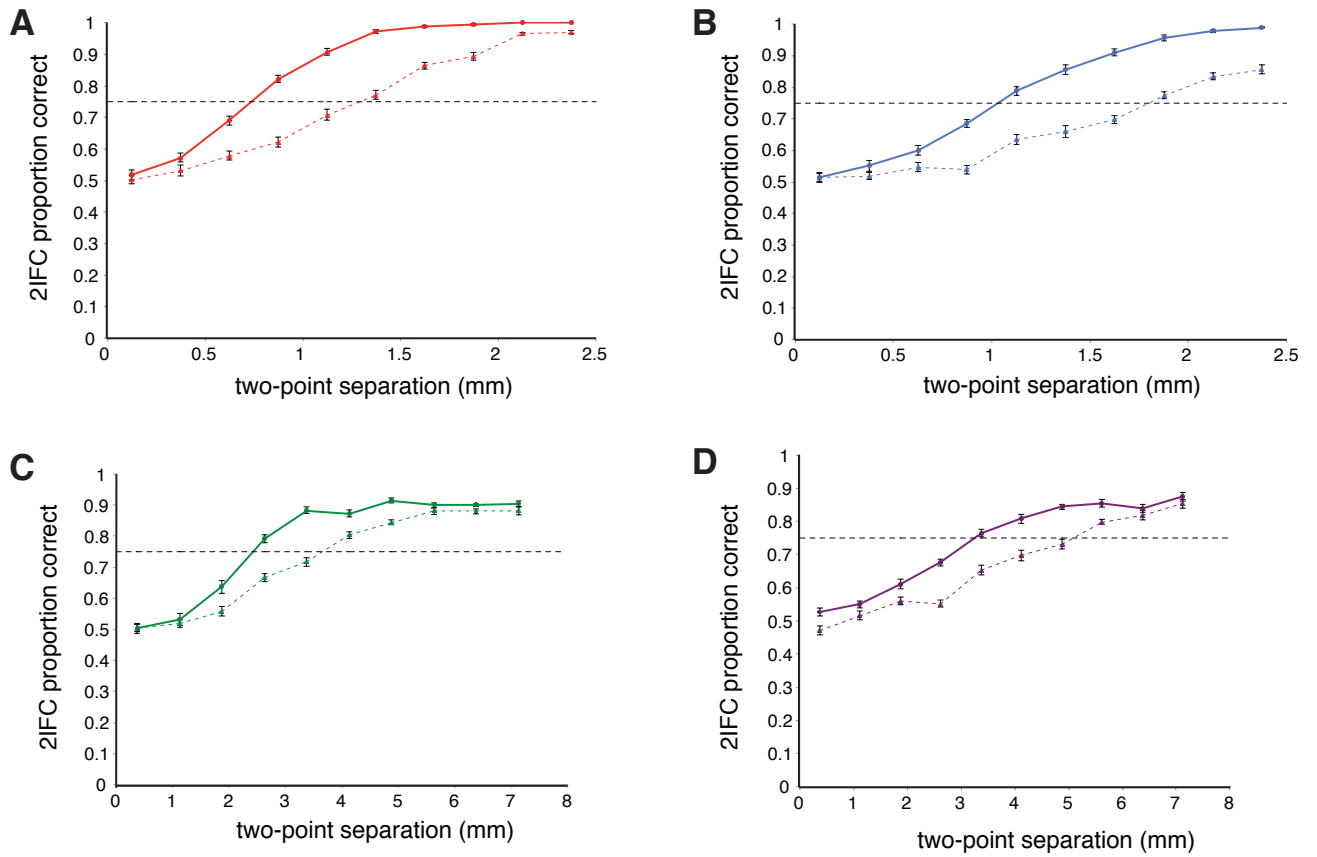


Figure 9: Differences in two-point discrimination between stimuli oriented longitudinally (along the RF long-axis) and transversely (perpendicular to the RF long-axis). Ideal observer performance on 2IFC two-point discrimination for A: fingertip, B: finger base, C: palm and D: forearm, when stimuli are oriented transversely (solid line) versus longitudinally (dashed line). 75% performance is marked off by a black dotted line on each graph.

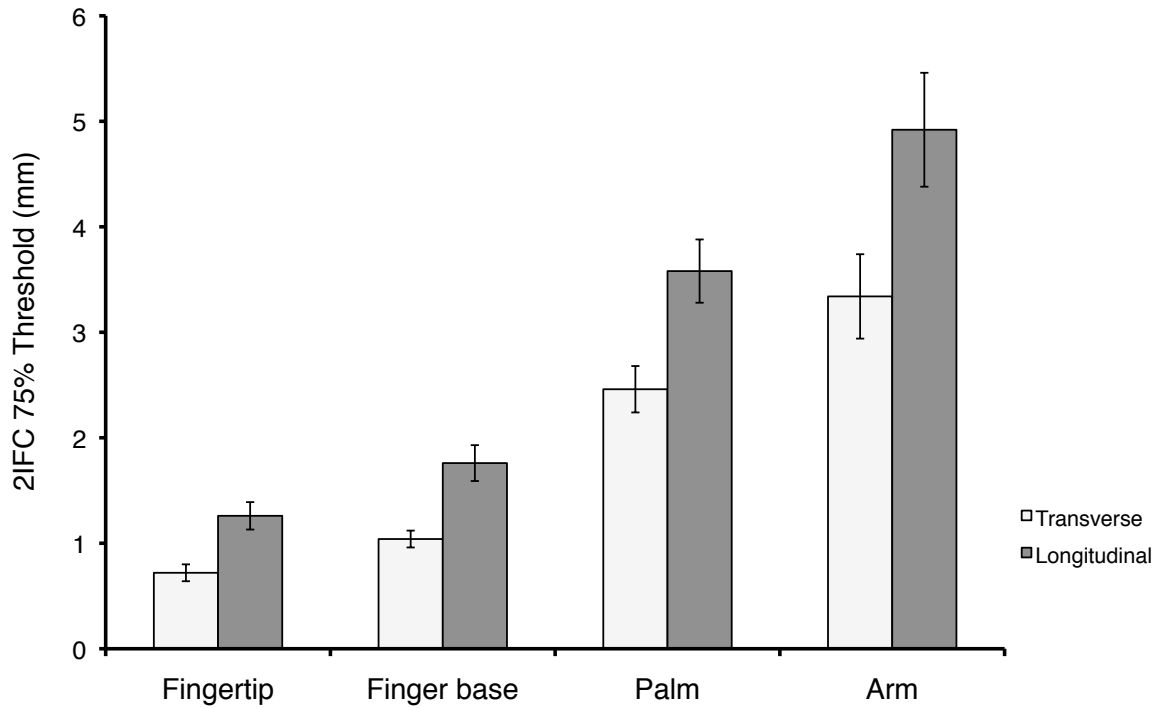


Figure 10: Summary of anisotropy results. A comparison between two-point discrimination thresholds for longitudinal and transverse stimuli demonstrates a clear performance anisotropy. Longitudinal thresholds are consistently higher than transverse thresholds on modeled body sites. Error bars depict \pm standard deviation

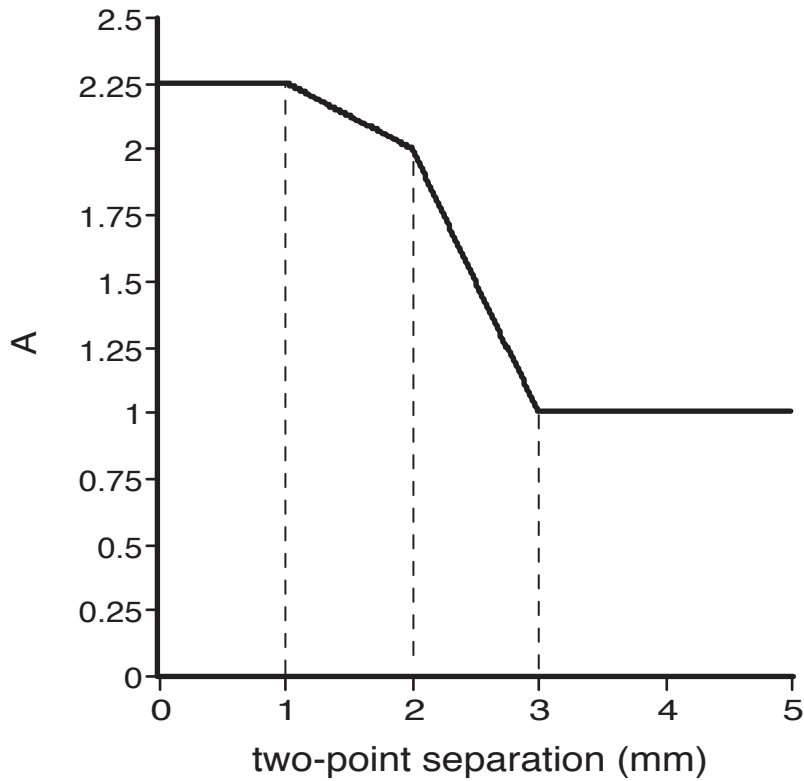


Figure 11: Modeling surround suppression as a function of two-point separation. The expected firing rate of a neuron between two points of stimulation is determined by the expression: $(p_1 + p_2)/A$, the summed response of each point alone, divided by the surround suppression factor, A. The figure above shows A as a function of two-point separation.

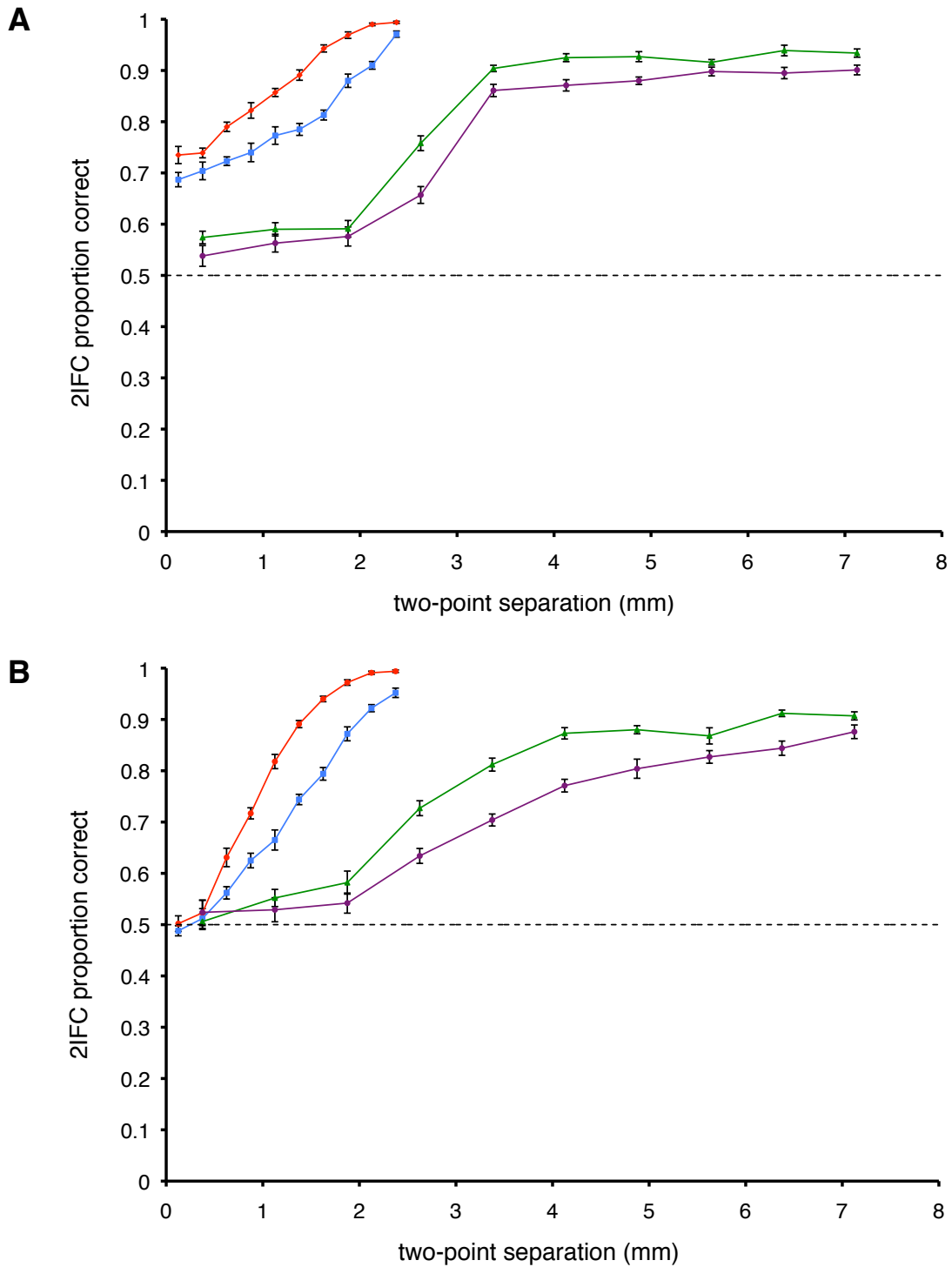


Figure 12: Surround suppression results in a two-point discrimination

magnitude cue. Two-point discrimination performance on fingertip (red), finger

base (blue), palm (green), and forearm (purple) is shown for a range of two-point separations with A: modeled surround suppression and B: without surround suppression. As two-point separation approaches zero, the model is still able to distinguish two-points from one in the presence of surround suppression; in its absence, model performance approaches chance as two-point separation decreases.

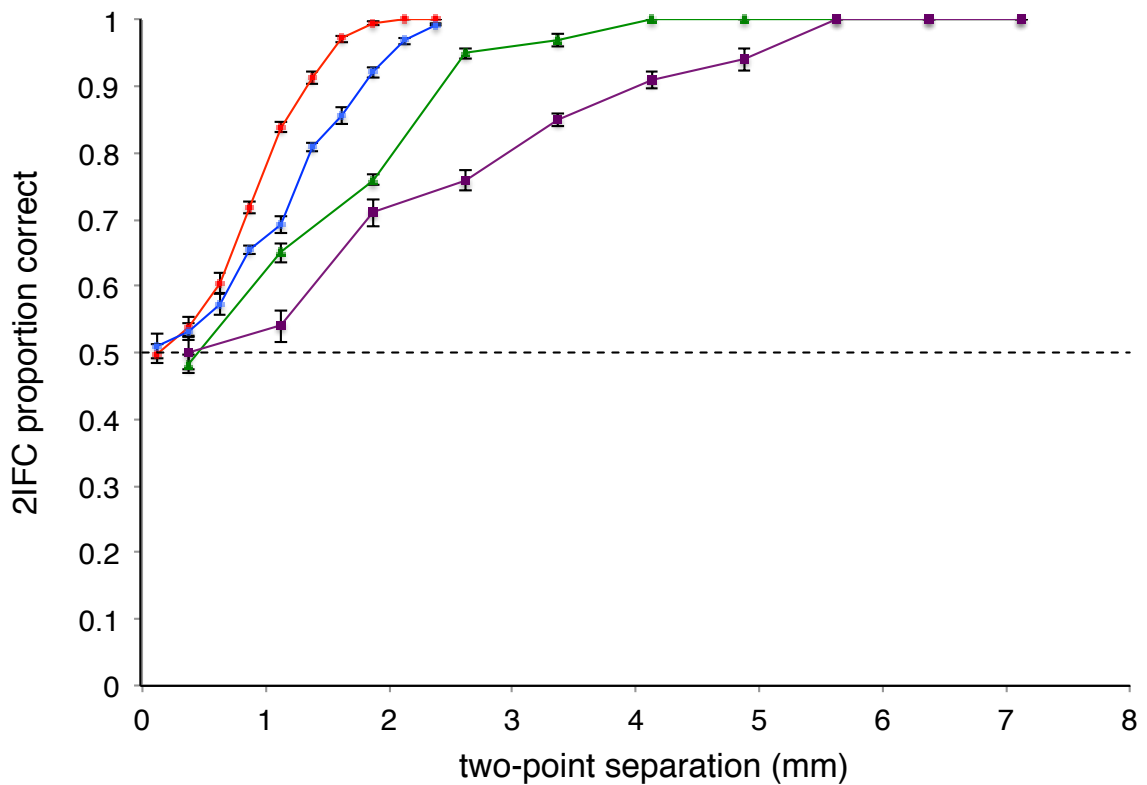


Figure 13: Two-point orientation discrimination is unaffected by surround suppression. Two-point orientation discrimination performance on fingertip (red), finger base (blue), palm (green), and forearm (purple) is shown for a range of two-

point separations with modeled surround suppression. Even in the presence of surround suppression, performance on the 2POD task approaches chance levels as separation approaches zero.

2.9 References

- Bolanowski Jr, S. J., Gescheider, G. A., Verrillo, R. T., & Checkosky, C. M. (1988). Four channels mediate the mechanical aspects of touch. *The Journal of the Acoustical society of America*, 84(5), 1680-1694.
- Boring, E.G. (1942). *Sensation and perception in the history of experimental psychology* (pp.463-522). New York: Appleton-Century-Crofts
- Craig JC & Johnson KO (2000). The two-point threshold: Not a measure of tactile spatial resolution. *Current Directions in Psychological Science*. 9(1): 29–32.
- Craig, J. C., & Rhodes, R. P. (1992). Measuring the error of localization. *Behavior Research Methods, Instruments, & Computers*, 24(4), 511-514.
- Essock, E. A., Krebs, W. K., and Prather, J. R. (1992). An anisotropy of human tactile sensitivity and its relation to the visual oblique effect. *Exp. Brain Res.* 91, 520–524. doi:10.1007/ BF00227848
- Geisler, W. S. (1984). Physical limits of acuity and hyperacuity. *JOSA A*, 1(7), 775-782.
- Geisler, W. S. (1989). Sequential ideal-observer analysis of visual discriminations. *Psychological review*, 96(2), 267.
- Geisler, W. S., & Kersten, D. (2002). Illusions, perception and Bayes. *nature neuroscience*, 5(6), 508-510.
- Gibson, G. O., and Craig, J. C. (2006). The effect of force and

conformance on tactile intensive and spatial sensitivity. *Exp. Brain Res.* 170, 172–181. doi:10.1007/s00221-005-0200-1

- Johansson RS & Vallbo ÅB (1979). Tactile sensibility in the human hand: relative and absolute densities of the four types of mechanoreceptive units in glabrous skin. *Journal of Physiology.* 286: 283–300.
- Johansson, R. S., & Vallbo, Å. B. (1980). Spatial properties of the population of mechanoreceptive units in the glabrous skin of the human hand. *Brain research*, 184(2), 353-366.
- Johansson RS, Vallbo ÅB & Westling G (1980). Thresholds of mechanosensitive afferents in the human hand as measured with Von Frey hairs. *Brain Research.* 184: 343–351.
- Johansson, R. S., & Vallbo, Å. B. (1983). Tactile sensory coding in the glabrous skin of the human hand. *Trends in Neurosciences*, 6, 27-32.
- Johnson, K. O., & Lamb, G. D. (1981). Neural mechanisms of spatial tactile discrimination: neural patterns evoked by braille-like dot patterns in the monkey. *The Journal of physiology*, 310(1), 117-144.
- Johnson KO & Phillips JR (1981). Tactile spatial resolution. I. Two-point discrimination, gap detection, grating resolution, and letter recognition. *Journal of Neurophysiology.* 46: 1177–1191.
- Johnson, K. O. (2001). The roles and functions of cutaneous mechanoreceptors. *Current opinion in neurobiology*, 11(4), 455-461.
- Knibestöl, M. (1975). Stimulus-response functions of slowly adapting mechanoreceptors in the human glabrous skin area. *the Journal of Physiology*, 245(1), 63-80.
- Knill, D. C., & Pouget, A. (2004). The Bayesian brain: the role of uncertainty in neural coding and computation. *TRENDS in Neurosciences*, 27(12), 712-719.

- Ma, W. J., Beck, J. M., Latham, P. E., & Pouget, A. (2006). Bayesian inference with probabilistic population codes. *Nature neuroscience*, 9(11), 1432-1438.
- Olausson, H., Wessberg, J., and Kakuda, N. (2000). Tactile directional sensibility: peripheral neural mechanisms in man. *Brain Res.* 866, 178–187. doi:10.1016/S0006- 8993(00)02278- 2
- Phillips, J. R., & Johnson, K. O. (1981). Tactile spatial resolution. III. A continuum mechanics model of skin predicting mechanoreceptor responses to bars, edges, and gratings. *Journal of Neurophysiology*, 46(6), 1204-1225.
- Schady, W. J. L., Torebjörk, H. E., & Ochoa, J. L. (1983). Cerebral localisation function from the input of single mechanoreceptive units in man. *Acta physiologica scandinavica*, 119(3), 277-285.
- Schady, W. J. L., & Torebjörk, H. E. (1983). Projected and receptive fields: a comparison of projected areas of sensations evoked by intraneural stimulation of mechanoreceptive units, and their innervation territories. *Acta physiologica scandinavica*, 119(3), 267-275.
- Sripati, A. P., Bensmaia, S. J., & Johnson, K. O. (2006). A continuum mechanical model of mechanoreceptive afferent responses to indented spatial patterns. *Journal of neurophysiology*, 95(6), 3852-3864.
- Stevens, J. C., & Patterson, M. Q. (1995). Dimensions of spatial acuity in the touch sense: changes over the life span. *Somatosensory & motor research*, 12(1), 29-47.
- Stocker, A. A., & Simoncelli, E. P. (2006). Noise characteristics and prior expectations in human visual speed perception. *Nature neuroscience*, 9(4), 578-585.
- Vallbo, A. B., & Johansson, R. S. (1978). The tactile sensory innervation of the glabrous skin of the human hand. *Active touch*, 2954.

- Vega-Bermudez, F., & Johnson, K. O. (1999). SA1 and RA receptive fields, response variability, and population responses mapped with a probe array. *Journal of Neurophysiology*, 81(6), 2701-2710.
- Vega-Bermudez, F., and Johnson, K. O. (1999). Surround suppression in the responses of primate SA1 and RA mechanoreceptive afferents mapped with a probe array. *J. Neurophysiol.* 81, 2711–2719.
- Weber, E. H. (1996). *E. H. Weber on the Tactile Senses*. Hove: Erlbaum (UK) Taylor & Francis.
- Weinstein, S. (1968). Intensive and extensive aspects of tactile sensitivity as a function of body part, sex and laterality. In the First Int'l symp. on the Skin Senses, 1968.
- Weinstein, S. (1993). Fifty years of somatosensory research: from the Semmes-Weinstein monofilaments to the Weinstein Enhanced Sensory Test. *Journal of Hand therapy*, 6(1), 11-22.

Chapter 3

3.1 Preface

In chapter 2 we demonstrated that surround suppression theoretically provides observers with an intensity cue during simultaneous two-point discrimination (2PD). When two points are close together ($<2\text{mm}$ apart), an afferent's response to both points is suppressed relative to that of a single point. Because of this difference in response magnitude between the two conditions, an ideal observer is able to correctly identify, with high probability, a two-point stimulus from a single point without relying on differences in the spatial profile of activity. Furthermore, we demonstrated theoretically that a newly proposed task, two-point orientation discrimination (2POD), is unaffected by surround suppression. In this chapter, we test whether these theoretical predictions hold true. By having observers perform two-interval versions of 2PD and 2POD on a number of body sites (finger tip, finger base, palm and arm) we show that 2PD performance is elevated (as high as $\sim 80\%$ accuracy) even when two-points are directly apposed. Because two points with zero separation should be indistinguishable from one, given the known density of afferents, a non-spatial cue is likely to explain this elevated performance (hyper acuity). Conversely, 2POD performance at zero separation is at chance levels, which is expected of a 2-interval task that truly reflects spatial acuity, given afferent density. We

therefore propose that clinicians who wish to carry out a more rigorous screening test for nerve damage replace simultaneous two-point testing with the 2POD task.



Two-point orientation discrimination versus the traditional two-point test for tactile spatial acuity assessment

Jonathan Tong, Oliver Mao and Daniel Goldreich*

Department of Psychology, Neuroscience & Behaviour, McMaster University, Hamilton, ON, Canada

Edited by:

Burkhard Pleger, Max Planck Institute for Human Cognitive and Brain Sciences, Germany

Reviewed by:

Hubert R. Dinse, Ruhr-Universität Bochum, Germany
Michael Bach, University Medical Center, Germany

***Correspondence:**

Daniel Goldreich, Department of Psychology, Neuroscience & Behaviour, McMaster University, 1280 Main Street West, Hamilton, L8S 4K1 ON, Canada
e-mail: goldrd@mcmaster.ca

Two-point discrimination is widely used to measure tactile spatial acuity. The validity of the two-point threshold as a spatial acuity measure rests on the assumption that two points can be distinguished from one only when the two points are sufficiently separated to evoke spatially distinguishable foci of neural activity. However, some previous research has challenged this view, suggesting instead that two-point task performance benefits from an unintended non-spatial cue, allowing spuriously good performance at small tip separations. We compared the traditional two-point task to an equally convenient alternative task in which participants attempt to discern the orientation (vertical or horizontal) of two points of contact. We used precision digital readout calipers to administer two-interval forced-choice versions of both tasks to 24 neurologically healthy adults, on the fingertip, finger base, palm, and forearm. We used Bayesian adaptive testing to estimate the participants' psychometric functions on the two tasks. Traditional two-point performance remained significantly above chance levels even at zero point separation. In contrast, two-point orientation discrimination approached chance as point separation approached zero, as expected for a valid measure of tactile spatial acuity. Traditional two-point performance was so inflated at small point separations that 75%-correct thresholds could be determined on all tested sites for fewer than half of participants. The 95%-correct thresholds on the two tasks were similar, and correlated with receptive field spacing. In keeping with previous critiques, we conclude that the traditional two-point task provides an unintended non-spatial cue, resulting in spuriously good performance at small spatial separations. Unlike two-point discrimination, two-point orientation discrimination rigorously measures tactile spatial acuity. We recommend the use of two-point orientation discrimination for neurological assessment.

Keywords: tactile perception, somatosensory discrimination, reliability and validity, neurological examination, psychophysics, sensory testing, spatial acuity

INTRODUCTION

Two-point discrimination (2PD) has been used to measure tactile spatial acuity ever since E. H. Weber published his seminal work on the sense of touch, *De Tactu*, in 1834 (Weber, 1996). The 2PD task is convenient to apply and is widely used to assess cutaneous innervation and central somatosensory function (Dellon, 1981; American Society for Surgery of the Hand, 1983; Van Boven and Johnson, 1994; Lundborg and Rosen, 2004; Jerosch-Herold, 2005; Campbell et al., 2013).

It has been assumed that two points are distinguishable from one only when the two points are sufficiently separated to evoke spatially distinct foci of neural activity (Mountcastle and Bard, 1968; Vallbo and Johansson, 1978). Therefore, in the “textbook view” of the 2PD task, two points that fall closely together, for instance within a single afferent receptive field, will evoke only one locus of neural activity and consequently will be misperceived as a single point (Brodal, 2010; Purves et al., 2012). Accordingly, the threshold separation at which neurologically healthy individuals can correctly identify two points has been assumed by many to reflect the size and spacing of cutaneous receptive fields,

particularly the innervation density of slowly adapting type-I (SA-1) afferents, the tactile axons that convey fine spatial information (Johnson, 2001).

Nevertheless, the 2PD task has faced serious criticism, because the literature relating 2PD threshold to innervation density is contradictory. As expected of a valid test of spatial acuity, 2PD is indeed reportedly worse on skin sites where SA-1 afferents are more sparsely distributed; for instance, the 2PD threshold is much larger on the forearm than on the fingertips (Weinstein, 1968). Paradoxically, however, healthy participants could perform a two-interval forced-choice (2IFC) 2PD task at approximately 80% accuracy on the fingertip, even when the two-point stimulus was delivered at zero separation (Johnson and Phillips, 1981). This apparently extraordinary spatial resolution is difficult to reconcile with the approximately 1.2 mm center-to-center spacing between fingertip SA-1 receptive fields (Johansson and Vallbo, 1979, 1980; Olausson et al., 2000). For this reason, and because of the large unexplained variation in 2PD thresholds across subjects and studies, investigators have questioned the validity of 2PD as a measure of spatial acuity (Johnson and Phillips, 1981; Johnson et al., 1994;

Stevens and Patterson, 1995; Craig and Johnson, 2000; Lundborg and Rosen, 2004).

One plausible explanation for a measured 2PD threshold that falls well under the receptor spacing is that participants are able to exploit a non-spatial cue to perform the 2PD task (Craig and Johnson, 2000). Indeed, two closely spaced points elicit fewer action potentials in the underlying SA-1 afferents than does a single point of equal indentation (Vega-Bermudez and Johnson, 1999). For this reason, perhaps the brain need not discern the spatial profile of the neural activity evoked by a stimulus, but rather only the overall response magnitude (e.g., total number of action potentials in the afferent population), in order to reliably perform the task. If this were the case, participants would be able to infer whether a stimulus consisted of two closely spaced points or one without actually perceiving two distinct points pressing against the skin. As a consequence, the 2PD task would be prone to yield spuriously good spatial acuity measurements, and some sensory deficits would go undetected, underestimated, or inaccurately quantified by 2PD testing, as reported (Van Boven and Johnson, 1994; van Nes et al., 2008).

As others have noted, the continuing popularity of 2PD testing owes largely to the absence of an equally convenient but rigorous alternative task (Lundborg and Rosen, 2004). Here, we investigated one such alternative task, two-point orientation discrimination (2POD), in which the participant must discriminate the orientation (horizontal vs. vertical) of two points of contact. Because the participant is stimulated always with two points, we hypothesized that neural magnitude cues would be absent from this task. The 2POD task would therefore force the participant to rely entirely on the perceived spatial profile of the evoked neural activity, providing a pure measure of spatial acuity. To test our hypothesis, we measured the performance of the same participants on two-interval forced-choice versions of both tasks, on four body sites: fingertip, finger base, palm, and forearm.

MATERIALS AND METHODS

PARTICIPANTS

Twenty-four neurologically healthy participants (18–26 years old, median age 21 years, 14 men, 22 right-handed) were recruited from the McMaster University community. Participants were screened by survey to ensure they did not have conditions that could adversely affect their tactile sensitivity (e.g., diabetes, carpal tunnel syndrome, calluses, or injuries on tested skin areas) or perceptual processing (dyslexia, attention deficit disorder, learning disability, central nervous system disorders) (Grant et al., 1999). Signed, informed consent was obtained from each participant. The McMaster University Research Ethics Board approved all procedures.

SENSORY TESTING

The participant's right hand and forearm rested comfortably on a towel spread over a desktop, with the palm facing upwards. A partially open box with a cutout for the arm obscured the participant's view while leaving the arm visible and accessible to the experimenter. The tactile stimuli were the tip(s) of an Absolute Digimatic calipers (Mitutoyo Corp.) (Figure 1A). The width of each tip was approximately 0.25 mm and the thickness approximately 0.5 mm;

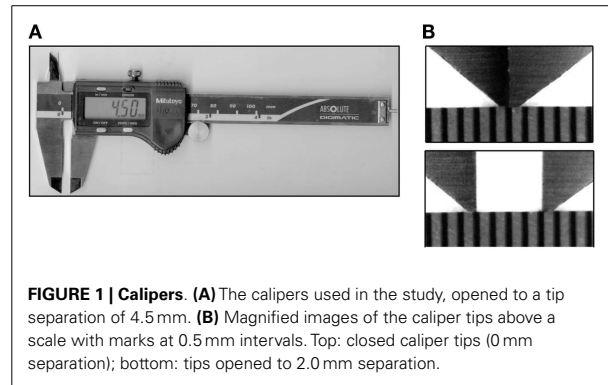


FIGURE 1 | Calipers. (A) The calipers used in the study, opened to a tip separation of 4.5 mm. (B) Magnified images of the caliper tips above a scale with marks at 0.5 mm intervals. Top: closed caliper tips (0 mm separation); bottom: tips opened to 2.0 mm separation.

thus, when fully closed, the caliper tips formed a 0.5 mm by 0.5 mm square contact surface on the skin (Figure 1B). The experimenter lightly pressed the caliper against the skin, ensuring visually that the skin did not indent so much as to contact the edge of the caliper jaw; estimated skin indentation was ≤ 2 mm. The participants did not report any discomfort with the application of stimuli. We purposefully used hand-held calipers, rather than automated equipment, in order to reproduce the manual application typically used in clinics.

We tested the participants on four skin sites on the right hand and arm: index fingertip pad, index finger base pad, palm (thenar eminence), and volar surface of the forearm (Figure 2A). Each participant was tested with both the 2IFC 2PD task (Figure 2B) and the 2IFC 2POD task (Figure 2C) on every skin site (two tasks \times four skin sites = 8 testing blocks of 50-trials each, for a total of 400 trials per participant). One of the 24 possible skin-site orders (four-factorial) was randomly assigned to each of the participants. Following the assigned order, the participant was tested sequentially on the four skin sites, first with one task (testing blocks 1–4), then again in the same order with the other task (testing blocks 5–8). Twelve of the participants were tested first with the 2PD task, and the other 12 first with the 2POD task.

In the 2PD task (Figure 2B), on each trial we indented the calipers approximately 2 mm into the skin surface, once with just one tip (the one-point stimulus) and once with both tips (the two-point stimulus), in randomized order. The two-point stimulus was oriented diagonally (i.e., at ± 45 -degrees relative to the long axis of the arm, with equal probability). Participants indicated whether they perceived the two-point stimulus before or after the one-point stimulus.

In the 2POD task (Figure 2C), on each trial we indented the calipers approximately 2 mm into the skin surface, once with two points oriented parallel (vertical) and once with two points oriented perpendicular (horizontal) to the long axis of the arm, in randomized order. Participants indicated whether they perceived the horizontally oriented points before or after the vertically oriented points.

In all tests, participants registered their responses by pressing one of two buttons on a wireless remote (Kensington, model 33374) held with the left hand. Feedback was not provided. During all tests, pink noise was played over computer speakers (Noise

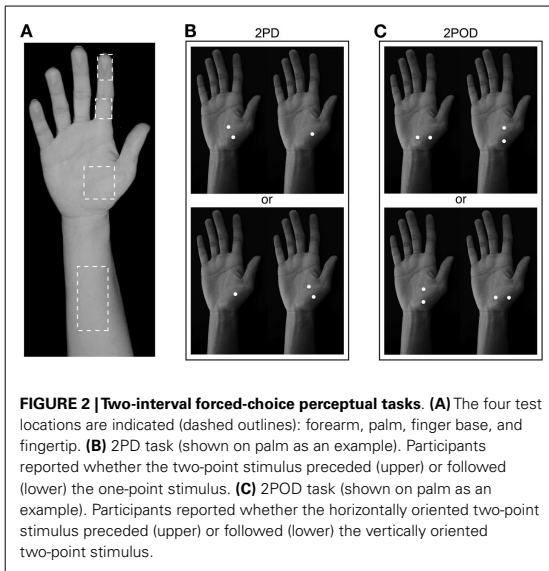


FIGURE 2 | Two-interval forced-choice perceptual tasks. (A) The four test locations are indicated (dashed outlines): forearm, palm, finger base, and fingertip. **(B)** 2PD task (shown on palm as an example). Participants reported whether the two-point stimulus preceded (upper) or followed (lower) the one-point stimulus. **(C)** 2POD task (shown on palm as an example). Participants reported whether the horizontally oriented two-point stimulus preceded (upper) or followed (lower) the vertically oriented two-point stimulus.

ADAPTIVE PSYCHOPHYSICAL PROCEDURE AND BAYESIAN PARAMETER ESTIMATION

To conduct the 2PD and 2POD tasks, we used a Bayesian adaptive algorithm, modified from Kontsevich and Tyler (1999), which we programmed in LabVIEW 9 (National Instruments) for Macintosh. The algorithm efficiently estimated a participant’s psychometric function (proportion of correct responses at each tip separation, x) by choosing on each trial the two-point separation that was predicted to yield the most information in light of the participant’s previous responses (expected entropy minimization). A computer monitor (out of the participant’s view) displayed that tip separation to the investigator, who adjusted the calipers to select the instructed tip separation with a precision of 0.1 mm (Figure 3). For fingertip, finger base, and palm testing, the computer algorithm chose from among 19 tip separations, equally spaced between 0 and 10 mm (i.e., 0, 0.6, 1.1, 1.7, . . . 10.0 mm). For forearm testing, the algorithm chose from among 19 tip separations, equally spaced between 0 and 45 mm (i.e., 0, 2.5, 5.0, 7.5, . . . 45.0 mm).

Our algorithm considered a set of 500,000 possible psychometric functions for the participant’s performance on a given testing block, parameterized as Weibull functions (Klein, 2001; Wichmann and Hill, 2001):

$$\Psi_{a,b,\gamma}(x) = \gamma + (1 - \gamma - \delta) \left(1 - 2^{-(x/a)^b}\right)$$

Each psychometric function was characterized by four parameters: γ , the proportion correct at zero tip separation; a , the tip separation at which the proportion correct was midway between that at zero tip separation and that at infinite separation; b , the

function slope; and δ , the lapse rate. The set of possible psychometric functions consisted of all possible combinations of γ (100 equally spaced values, ranging from 0.01 to 0.99), a (100 equally spaced values, ranging from 0.01 to 60 mm), and b (50 equally spaced values, ranging from 0.1 to 10); the lapse rate, δ , was set to 0.02. We applied a uniform prior probability distribution over psychometric functions, $P(\Psi_{a,b,\gamma}) = 1/500,000$.

From the participant’s set of correct and incorrect responses, $\{r_i\}$, on the 50 trials within a testing block, the algorithm calculated the posterior probability of each psychometric function, $P(\Psi_{a,b,\gamma} | \{r_i\})$, as well as marginal posterior densities and maximum *a posteriori* estimates (modes) for each of the three free parameters: γ , a , and b . To obtain finer resolution in this offline analysis, we used 100 values for each parameter, with the following ranges: a (0.01–10 mm for fingertip and finger base; 0.01–50 mm for palm and forearm), b (1–10), γ (0.01–0.97). We took the mode of each parameter’s marginal posterior density as the best-estimate for the parameter’s value.

Additionally, we calculated the probability of the participant’s data given random guessing on every trial, divided by the probability of the data given a psychometric function. We obtained the latter probability by integrating over the space of all psychometric functions, weighting the probability of the data given each function by the prior probability of that function. Thus, the formula for this ratio was:

$$BF = \frac{(0.5)^{50}}{\int \int \int P(\{r_i\} | \Psi_{a,b,\gamma}) P(\Psi_{a,b,\gamma}) da db d\gamma}$$

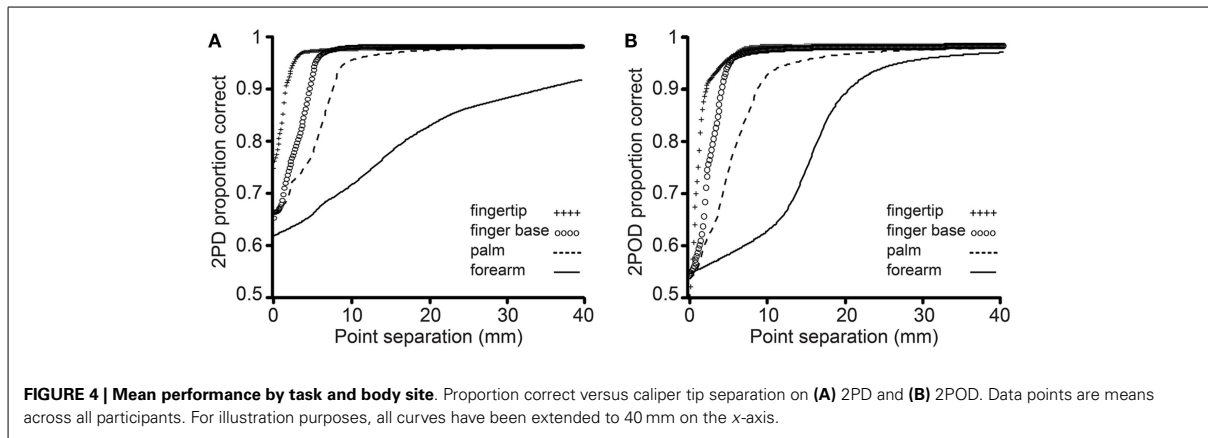
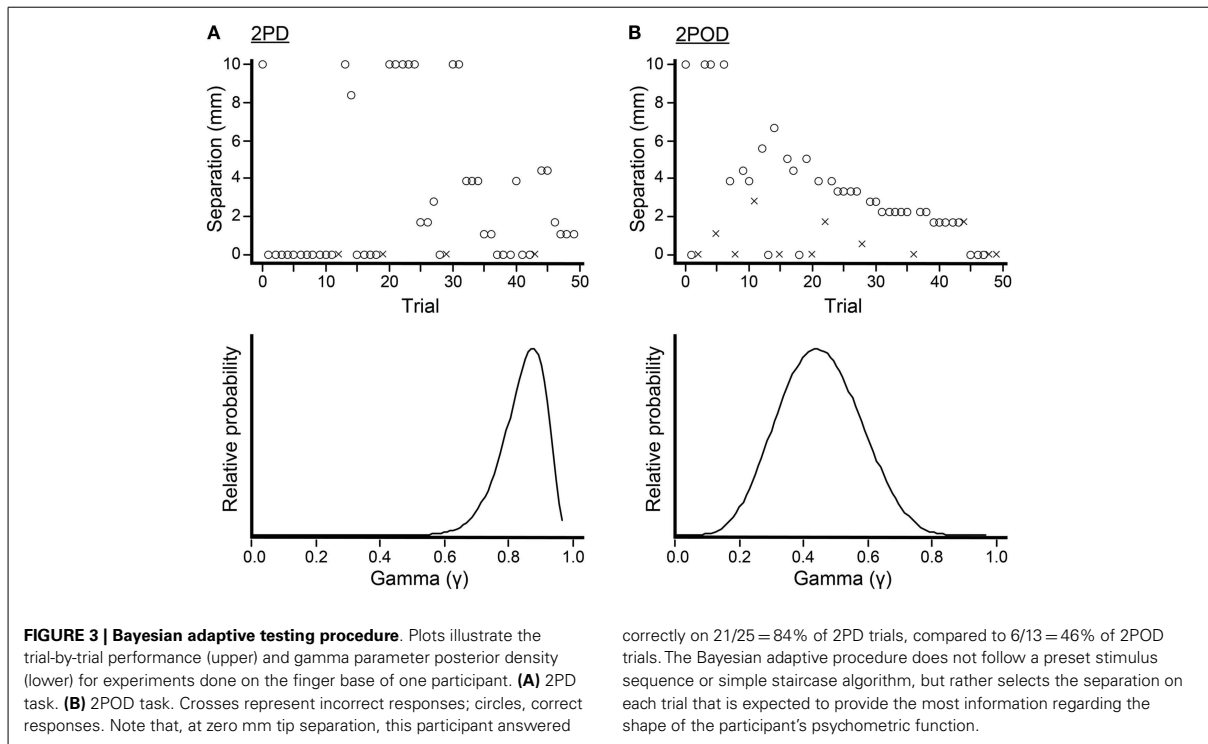
This ratio, a Bayes’ Factor (BF) for guessing, reaches 1 only if a participant’s responses are as likely to occur from pure guessing as from a psychometric function. Thus, if a participant’s BF (rounded to the nearest integer) was ≥ 1 on any testing block, we eliminated all of the participant’s data from subsequent analyses. This procedure ensured that our analyses considered data only from participants who were consistently concentrating during the sensory testing. Out of our original pool of 24 participants, 5 were eliminated on this basis.

To obtain a best-estimate of a participant’s probability of correct responding as a function of tip separation, $p_c(x)$, we integrated over the psychometric function posterior distribution the proportion correct predicted by each function:

$$p_c(x) = \int \int \int \Psi_{a,b,\gamma}(x) P(\Psi_{a,b,\gamma} | \{r_i\}) da db d\gamma$$

To obtain the mean performance across participants on each body site, we averaged $p_c(x)$ across participants.

We determined for each testing block the tip separation ($x_{95\%}$) at which the participant responded correctly with 95% probability. The probability of a particular $x_{95\%}$ value was calculated by summing the posterior probabilities of all psychometric functions that crossed 95% within ± 0.05 mm of that value. Repeating this procedure for all possible $x_{95\%}$ values, we obtained a probability distribution over $x_{95\%}$, the mode of which we report as our best-estimate of the participant’s 95%-correct threshold.



DATA ANALYSIS

Analyses of variance (ANOVA), *t*-tests, chi-square tests, and correlations were performed with SPSS v20 (IBM Corp.) for MacIntosh, using an alpha-level of 0.05. We report two-tailed *p*-values. The ANOVA model was full-factorial type III sum-of-squares.

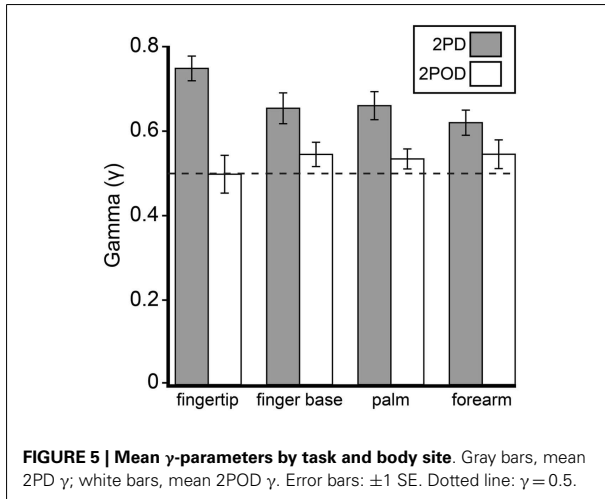
RESULTS

2POD BUT NOT 2PD APPROACHED 50%-CORRECT AT ZERO TIP SEPARATION

The mean performance for each task at each body site is shown in **Figure 4**. In accord with our prediction, the psychometric

functions for the two tasks clearly differed in their percent-correct performance at zero tip separation, with performance being close to chance (50%-correct) for the 2POD but not the 2PD task.

This observation was confirmed by an analysis of the psychometric function gamma parameter (performance at zero tip separation) (**Figure 5**). A two-way (task × body site) repeated-measures ANOVA, with γ as the dependent variable, revealed a highly significant effect of task ($F = 26.35, p < 0.001$) with no significant effect of body site ($F = 0.60, p = 0.618$) or task-by-body site interaction ($F = 2.52, p = 0.068$). Four *post hoc* one-sample *t*-tests with Bonferroni correction revealed that the mean 2PD



γ value was significantly above 0.5 on all body sites (all corrected p -values < 0.005). In stark contrast, the mean 2POD γ value did not differ significantly from 0.5 on any body site (all corrected p -values > 0.5). In contrast to the gamma parameter, the a and b -parameters did not differ significantly between tasks (separate two-way repeated-measures ANOVAs, $p = 0.063$ and 0.561 for main effects of task on a and b -parameters, respectively).

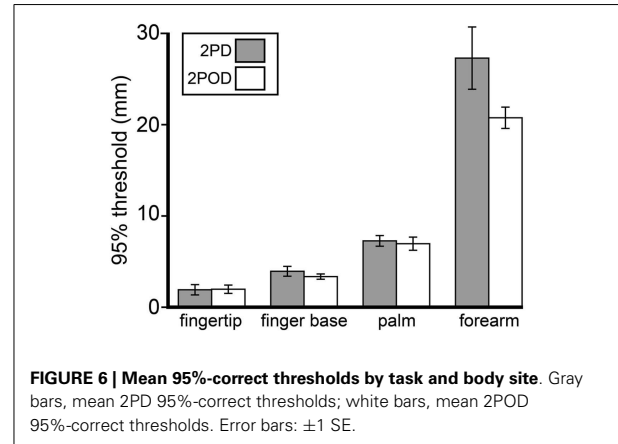
2POD BUT NOT 2PD CONSISTENTLY YIELDED A 75%-CORRECT THRESHOLD

Having found that performance at zero tip separation differed dramatically between the tasks, we next turned our attention to the participants' performance at non-zero tip separations. The 75%-correct threshold is a commonly reported psychophysical performance measure; for the experiments reported here, this threshold would be the tip separation at which a participant's psychometric function crossed the 0.75 mark. We were unable to compare the two tasks on this basis, however, because the 2PD task often failed to produce a measurable 75%-correct threshold.

Remarkably, the gamma parameter values characterizing participant performance on the 2PD task tended to be so large that only 5 of 19 participants had a measurable 75%-correct 2PD threshold (i.e., $\gamma \leq 0.75$) on all skin sites. In contrast, 15 of 19 participants had measurable 75%-correct 2POD thresholds at all skin sites. Indeed, of the 76 2PD testing blocks (19 participants \times 4 skin sites), only 53 resulted in measurable 75%-correct thresholds. In contrast, 72 of the 76 2POD testing blocks resulted in measurable 75%-correct thresholds. These differences between tasks were highly significant (participant count comparison: chi-square = 10.56, $p = 0.001$; total testing block count comparison: chi-square = 16.26, $p < 0.001$). Thus, the 2PD task, unlike the 2POD task, often failed to yield a conventional threshold measure.

2POD AND 2PD HAD SIMILAR 95%-CORRECT THRESHOLDS THAT CORRELATED WITH RECEPTOR SPACING

Because we were unable to obtain a consistent 2PD 75%-correct threshold, we chose instead to compare 95%-correct



thresholds, which were measurable on all testing blocks. Interestingly, although performance at small tip separations differed significantly between tasks, performance on the tasks converged as tip separation increased. In particular, the 95%-correct threshold did not differ significantly between tasks (Figure 6). A two-way (task \times body site) repeated-measures ANOVA, with 95%-correct threshold as the dependent variable, showed a highly significant effect of body site ($F = 106.50$, $p < 0.001$) but no significant effect of task ($F = 3.86$, $p = 0.065$).

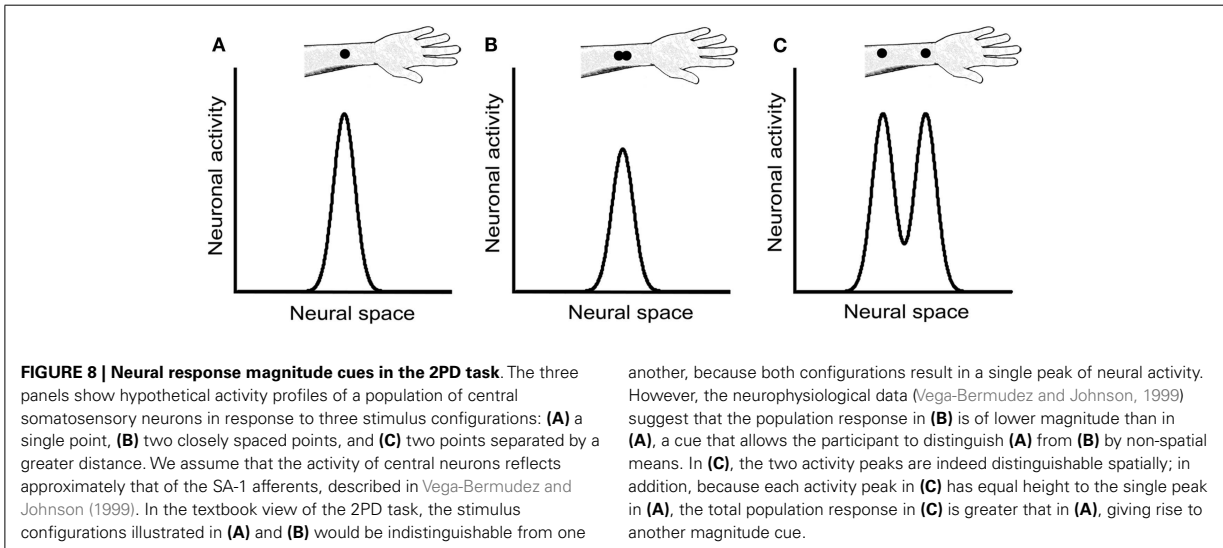
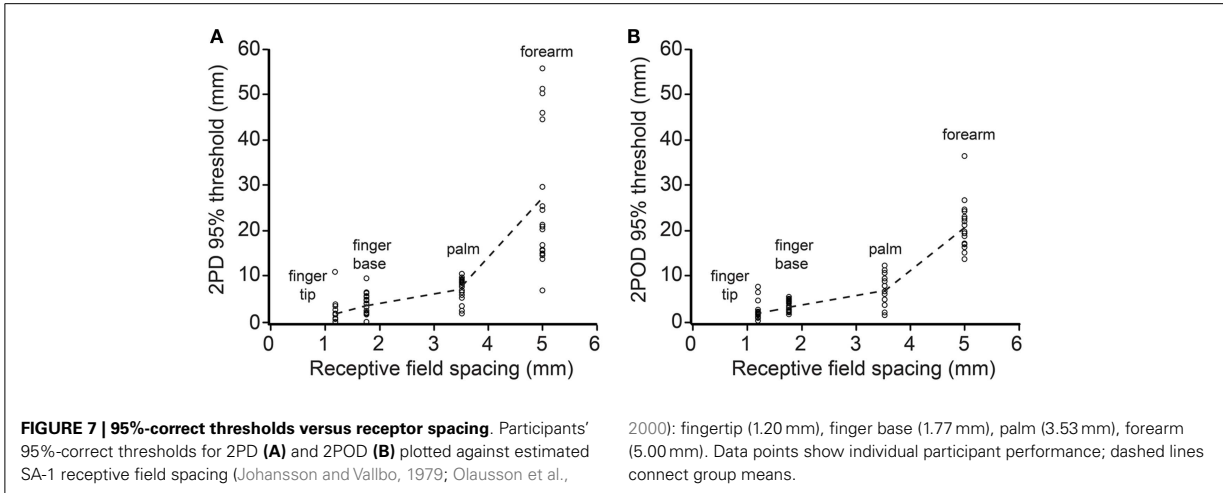
We next investigated how 2PD and 2POD 95%-correct thresholds related to the distribution of tactile receptors. For each participant, we correlated the 95%-correct thresholds with the estimated receptive field spacing of human SA-1 afferents (Johansson and Vallbo, 1979; Olausson et al., 2000). The 95%-correct performance on both tasks correlated significantly with estimated receptive field spacing (mean Pearson's r correlation coefficients: 2PD: $r = 0.906$, $p < 0.001$; 2POD: $r = 0.915$, $p < 0.001$) (Figure 7).

DISCUSSION

The 2PD task is widely used clinically (Dellon, 1981; American Society for Surgery of the Hand, 1983; Van Boven and Johnson, 1994; Lundborg and Rosen, 2004; Jerosch-Herold, 2005; Campbell et al., 2013) and has been used also in several research laboratories to characterize tactile spatial acuity in healthy populations (Godde et al., 2000; Kennett et al., 2001; Dinse et al., 2006; Boles and Givens, 2011). Nevertheless, our results confirm that the 2PD threshold is not a pure measure of spatial acuity. The data support the use of an equally convenient alternative task – 2POD. Unlike 2PD, 2POD performance approaches chance levels as tip separation approaches zero, as expected of a rigorous measure of spatial acuity.

2PD PERFORMANCE BENEFITS FROM A NON-SPATIAL CUE

Our findings support and extend upon a previous literature revealing that the 2PD task presents a non-spatial cue. Like Johnson and Phillips (1981), who conducted 2PD testing on the fingertip, we found that participants could reliably discriminate between a single point and two points at zero separation. On the fingertip, finger base, palm, and forearm, the mean 2PD γ value was significantly above 0.5, indicating that participants were able to perform



correctly even at zero tip separation. Thus, 2PD performance is starkly inconsistent with the known spatial distribution of SA-1 mechanoreceptive afferents (Johansson and Vallbo, 1979, 1980; Olausson et al., 2000). We conclude that the 2PD task presents a non-spatial cue, allowing participants to infer the presence of two points without distinctly perceiving them.

We concur with Craig and Johnson (2000) that a likely non-spatial cue in the 2PD task is a response magnitude cue: due either to skin mechanics or to neural interactions among branches of individual afferent fibers, two closely spaced stimulus points elicit fewer action potentials in the underlying afferents than does a single-point of equal indentation (Vega-Bermudez and Johnson, 1999). For instance, when a one-point stimulus over an SA-1 receptive field center is compared to a two-point stimulus consisting of that same point plus another at 1 mm distance, the two-point stimulus elicits on average about 30% fewer action potentials.

A similar effect, though weaker in magnitude, is observed when neither point overlies the center of the receptive field (Vega-Bermudez and Johnson, 1999). Thus, by merely detecting the total number of action potentials elicited in the afferent population rather than the spatial profile of neural activity, a participant could infer whether the stimulus contained one point or two (Figures 8A,B).

We note that a magnitude cue will also exist, in the opposite direction, at somewhat larger tip separations, where interactions between stimuli are not expected at the single-neuron level. For instance, a two-point stimulus at 1 cm separation should elicit about twice the number of action potentials in the afferent population as would a one-point stimulus of equal indentation, because the two-point stimulus will activate about twice as many neurons (Figures 8A,C). Therefore, the 2PD task is apparently beset with magnitude cues at all tip separations.

An additional non-spatial cue that might sometimes accompany the 2PD task is a temporal cue: if the investigator fails to apply the two points simultaneously, the participant may perceive two contacts that are distinct in time. In this case, the participant could infer that two points touched the skin, even when unable to distinguish the points spatially. A limitation of any manual stimulus application method is that exact simultaneity is not achievable. Because humans are able to distinguish temporal delays between tactile stimuli of approximately 10 ms (Gescheider, 1967; Gescheider et al., 2003), any delay of this duration or longer between the two points of contact could produce a perceptible temporal cue. We note, however, that even when the 2PD task was conducted with an automated apparatus that touched the two tips against the skin with less than 2 ms delay, performance was approximately 80%-correct at zero tip separation (Johnson and Phillips, 1981). Thus, a temporal cue, while plausibly facilitating 2PD task performance under manual stimulus delivery, is unlikely to account for the extraordinary performance of participants at zero tip separation.

An alternate explanation for above-chance 2PD performance at zero tip separation, put forth by Stevens and Patterson (1995), is that participants make use of a length cue: two apposed points might feel longer than a single point. However, we believe it unlikely that our participants could detect the 0.25 mm difference in length between our single-point stimulus and the two apposed points. In a length discrimination experiment using raised edges of either 0.5 or 5 mm baseline length, Stevens and Patterson (1995) reported that on the fingertip the average adult participant could distinguish with 71% accuracy edges that differed by 0.8–0.9 mm in length. This length discrimination threshold is consistent with the estimated SA-1 receptive field spacing on the fingertip of approximately 1 mm (Johansson and Vallbo, 1979, 1980; Olsson et al., 2000). The implication of this finding is that the 2PD task would present a perceptual length cue at zero tip separation on the fingertip whenever the individual points have a size of approximately 0.8 mm or more. This would seem to rule out a length cue in the present study, as our point stimulus had a width of approximately 0.25 mm. Furthermore, to be detectable on the finger base, palm, and forearm, which have lower receptor densities than the fingertip, the length difference would presumably need to be much larger than 0.8 mm. Nevertheless, our participants performed significantly above chance at zero tip separation on those body sites as well.

2PD PERFORMANCE REFLECTS BOTH SPATIAL AND NON-SPATIAL INFORMATION

Because it is contaminated by one or more non-spatial cues, the 2PD task is prone to yield spuriously good performance. Consequently, tactile spatial deficits – particular if not severe – may be undetected or underestimated by 2PD testing. For instance, van Nes et al. (2008) reported that 2PD testing detected mild polyneuropathy caused by diabetes mellitus, chronic inflammatory demyelinating polyneuropathy, Guillain-Barré syndrome, uremia, and other causes, with a sensitivity of only 28%. Similarly, Van Boven and Johnson (1994) found that following elective mandibular surgery that injured but did not transect the inferior alveolar nerve, 2PD on the lip returned to normal levels much earlier in the course of recovery than did grating orientation

performance, a rigorous measure of spatial acuity (see below). The authors argue that, owing to the presence of non-spatial cues, 2PD grossly overestimated the initial recovery of tactile spatial function.

Despite the presence of non-spatial cues, it would be an overly critical indictment to conclude that 2PD conveys no information regarding a patient's spatial acuity. It seems clear that spatial as well as non-spatial cues influence 2PD task performance, particularly at larger tip separations. Presumably for this reason, more severe injuries, such as nerve transections, do result in lasting elevation of 2PD thresholds despite the return of tactile sensitivity as measured by monofilament testing (Rosen et al., 2000; Jerosch-Herold, 2003). Nerve transection, unlike nerve crush, is thought to result in the misdirection of sensory axons during re-innervation; the shuffling of these axons causes severe deficits in spatial acuity (Van Boven and Johnson, 1994; Rosen et al., 2000), thereby elevating the 2PD threshold.

Among the neurologically healthy participants tested here, fewer than half had measurable 75%-correct 2PD thresholds on the four skin sites; due presumably to non-spatial cues, performance did not consistently drop below 75%-correct even at zero tip separation. Nevertheless, the 2PD performance of all participants did fall below 95%-correct at small tip separations. Analyzing participants' 95%-correct thresholds on the four body sites, we found that they correlated with mean receptive field spacing. This result is in keeping with previous reports that 2PD performance worsens on skin areas with sparser receptor distribution (Weinstein, 1968). Furthermore, the 95%-correct thresholds on the 2PD task did not differ significantly from those on the 2POD task. Presumably, at larger tip separations when distinct points are more reliably perceptible, participants do make use of the spatial pattern of the afferent population discharge.

For researchers who wish to use the 2IFC 2PD task, these results might suggest the adoption of the 95%-correct threshold as a valid performance measure. Nevertheless, we caution that the accurate estimation of a 95%-correct threshold is difficult. Conducting computer simulations of sensory tests using the method of limits, for instance, we found that the test-retest variance of the 95%-correct threshold estimate was consistently – and often considerably – greater than that of the 75%-correct threshold estimate. This difference owes to the shallower slopes of the psychometric functions (Figure 4) as they near the upper asymptote, which translates into a greater uncertainty in the x -axis value of the estimate, caused by any uncertainty in the %-correct measurement (Zuberbühler, 2002). Rather than attempting to estimate a 95%-correct threshold, we suggest that clinicians and researchers simply set aside the 2PD task and replace it with one that ensures a more purely spatial measure of acuity.

In this study, we conducted a 2IFC version of the 2PD task in order to most accurately assess the presence of non-spatial cues. In the 2IFC version, because a single-point and a two-point stimulus are presented on each trial, the participants are able to directly compare the neural responses that occur in the two configurations. Participants may therefore rather quickly become aware of non-spatial cues in this version of the task. A commonly used alternative version of the task employs single-interval trials. In each trial, the participant is stimulated just once, with either one or two-points, and asked to identify the configuration. This single-interval

version of the task, though subject to the effects of response criteria (Gescheider, 1997; MacMillan and Creelman, 2005), may in fact be preferable to the 2IFC version, because with appropriate instruction the participant can be encouraged to respond “two” only when two distinct points are clearly perceived (Kalisch et al., 2007). The single-interval task may therefore mitigate the effect of neural magnitude cues on performance, thereby yielding a more purely spatial measure of acuity. In this regard, we note that the average single-interval 2PD 50% correct threshold obtained by Kalisch et al. (2007) from the right index fingers of untrained participants was approximately 1.6 mm, a tip separation that presented in our 2IFC 2PD task would yield on average 85% correct performance (see **Figure 4A**). Based on our finding that the 2PD and 2POD tasks yield similar performance at large tip separations, we suspect that the thresholds measured by Kalisch et al. (2007) indeed reflect primarily the participant’s spatial acuity. In general, the single-interval 2PD task, combined with instructions to participants to adopt an appropriately conservative response criterion, may produce the most reliable spatial acuity data achievable with the 2PD task.

2POD IS A RIGOROUS AND CONVENIENT MEASURE OF TACTILE SPATIAL ACUITY

Unlike the 2PD task, the 2POD task involves the spatial discrimination of orientation, with two points always presented. Thus, we reasoned that the 2POD task would avoid the non-spatial cues that plague the 2PD task: the neural population response magnitude should be the same, on average, for the two orientations, and a temporal delay between the two points of contact, if present, would not compromise the task; to perform successfully, the participant would still need to discern the orientation of the points. Therefore, we predicted that 2POD performance would approach chance as the tip separation approached zero. Our results confirmed this prediction.

To our knowledge, we are the first to propose the exact version of the 2POD task described here, though Stevens and colleagues used similar tasks (Stevens and Patterson, 1995; Stevens et al., 1996) and Weber himself explored two-point perception in the horizontal compared to the vertical orientation (Weber, 1996). In Stevens and Patterson (1995), a pair of longitudinal two-point stimuli and a pair of two-point stimuli of non-matching orientations (longitudinal and transverse) were presented on every trial; the participant was asked to identify which interval had the non-matching pairs. In Stevens et al. (1996), a single two-point stimulus was given in either longitudinal or transverse orientation, and the participant was asked to identify the orientation. Some participants in Stevens and Patterson (1995) performed correctly at zero tip separation, perhaps because relatively large caliper tips (0.44 mm each) permitted the perception of orientation even when fully closed. To prevent this, we recommend that the 2POD task be performed with caliper tips of approximately 0.25 mm diameter.

The 2POD task that we have used combines the rigor of a gold standard in tactile spatial acuity testing, the grating orientation task, with the convenience of the 2PD task. In the grating orientation task, participants attempt to discern the orientation (typically, horizontal or vertical) of square-wave gratings with equal ridge and groove width. Groove width is reduced to make the task more

difficult, or increased to make it easier. Acuity is measured as the groove width whose orientation the participant can discern with a particular probability (e.g., 75%-correct). Whether a grating is applied horizontally or vertically, it is expected to elicit on average the same afferent population discharge magnitude; only the spatial structure of the population discharge varies. Therefore, to perform the task correctly the participant must discern the spatial pattern of afferent activity, rendering this a rigorous test of tactile spatial acuity (Johnson and Phillips, 1981; Gibson and Craig, 2002, 2006). The similarity to the 2POD task is clear.

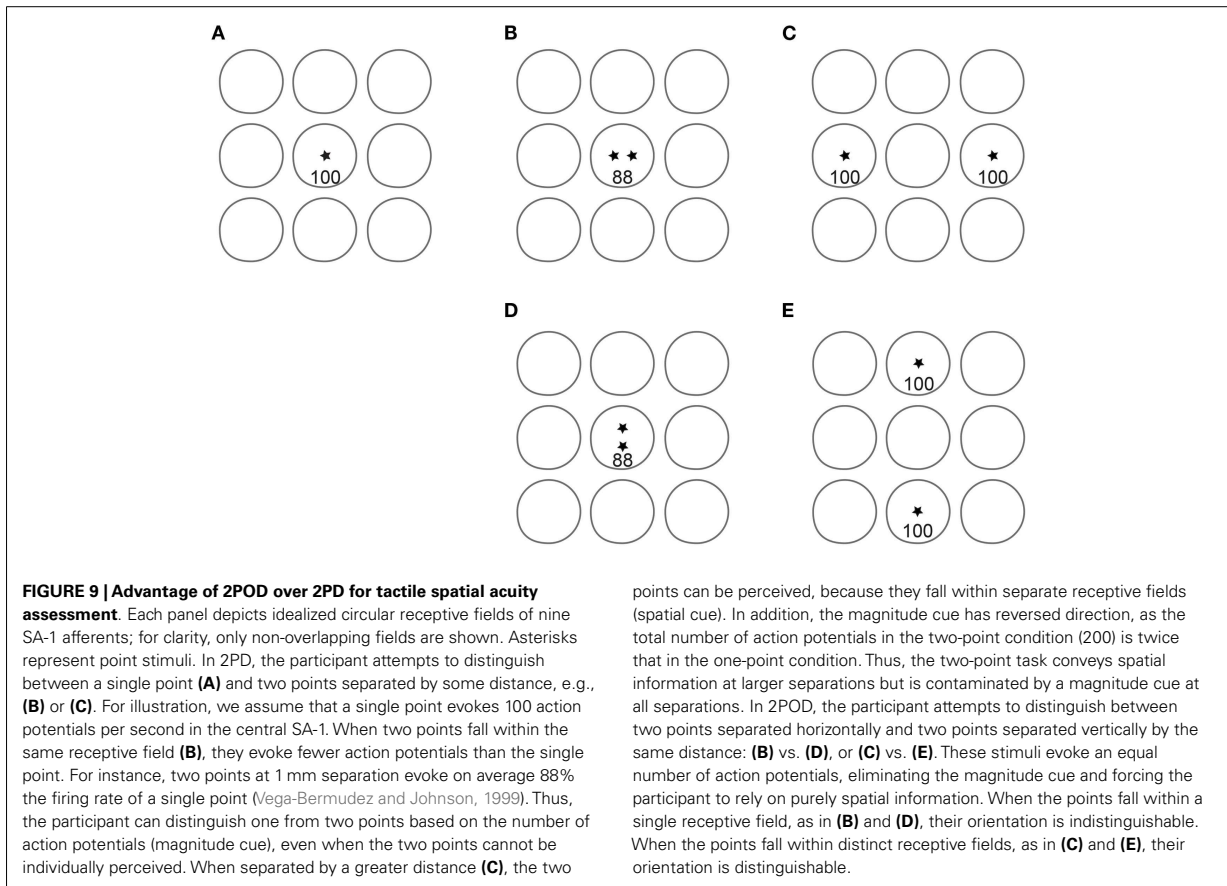
While tactile research laboratories such as ours make extensive use of the grating orientation task (Goldreich and Kanics, 2003; Goldreich et al., 2009; Peters et al., 2009; Wong et al., 2011a,b, 2013), we recognize that the task has certain practical disadvantages, particularly as concerns the clinical setting. Among these is that each grating must be prefabricated; consequently, the variable of interest, groove width, cannot be adjusted outside a predetermined range. This is particularly problematic if one wishes to test patients who may have atypical spatial acuity due to neurological damage. The 2POD task does not suffer from this practical inconvenience. Rather, like the 2PD task, the 2POD task is remarkably flexible in requiring only a single tool (calipers) that is easily adjustable during testing.

RECOMMENDATIONS FOR FUTURE STUDIES AND FOR CLINICAL PRACTICE

In conclusion, our data confirm that the 2IFC 2PD task is contaminated by one or more unintended non-spatial cues that result in inflated spatial acuity reports. An alternative task, 2POD, provides a rigorous measure of spatial acuity. The advantage of 2POD over 2PD as a measure of spatial acuity is summarized in **Figure 9**.

We have performed the 2POD task using vertically and horizontally (i.e., longitudinally and transversely) oriented stimuli. One recommendation for future studies and for clinical practice would be to use oblique (e.g., ± 45 -degree) orientations. The use of oblique stimuli would offer two practical advantages. First, it would permit greater tip separations. On the digits and limbs, the maximum tip separation in the vertical-horizontal 2POD task is limited to the width of the body part, a constraint that is overcome by the use of oblique stimuli. Second, the use of oblique stimuli would prevent magnitude cues that might arise from receptive field anisotropy. A majority of receptive fields on the fingers and palm reportedly are elongated rather than circular; furthermore, roughly two-thirds of the elongated fields are oriented longitudinally with respect to the arm (Johansson and Vallbo, 1980). Perhaps for this reason, performance anisotropy has been reported on several body areas, in a variety of tactile acuity tests (Essock et al., 1992; Stevens and Patterson, 1995; Gibson and Craig, 2005), beginning with the report by Weber himself that 2PD acuity was better when the tips were aligned transversely (Weber, 1996). The use of oblique stimuli should prevent performance anisotropy caused by alignment of the two-point configuration in parallel or orthogonal to the average receptive field orientation.

Given its evident advantages, we recommend that 2POD replace 2PD testing in the clinic and in research settings. Additional studies should be carried out to further validate the 2POD task by measuring inter-rater and test-retest reliability and by



comparing 2POD with grating orientation thresholds in neurologically healthy participants and in patients. Our laboratory has previously shown that grating orientation thresholds correlate with fingertip surface area (Peters et al., 2009), suggesting that receptive fields are more widely spaced in larger fingers. As an exploratory analysis, we checked for this effect in the current 2PD and 2POD data, but not surprisingly, we observed no significant correlations between finger size and performance on either task in our relatively small participant sample. In analogy with previous grating orientation studies, we predict that, with sufficiently large sample sizes (Peters et al., 2009) or with trained participants (Wong et al., 2013), 2POD performance will also be found to correlate with finger size.

Although we have used adaptive psychophysical data collection methods and mathematical analyses in order to evaluate the 2POD and 2PD tasks, we suggest that more practical, less elaborate procedures be used in the clinic. To facilitate the use of the task for clinical purposes, we recommend that the patient be stimulated with 10 or 20 2POD 2IFC trials at each of several tip separations. A plot could then be made of the number of correct responses at each separation. The interpolated tip separation corresponding to 75%-correct could be reported as the

patient's spatial acuity. Alternatively, for greater convenience and to reduce testing time, a single-interval 2POD task could be used, in which the participant is stimulated just once on each trial, and attempts to identify the stimulus orientation; we favor the 2IFC testing protocol, however, to prevent possible criterion effects (Gescheider, 1997). For equipment, we recommend the use of adjustable calipers with pointed tips not exceeding 0.25 mm width and 0.5 mm thickness. One such device is the Absolute Digimatic caliper (Mitutoyo Corp.) used in this study; many similar devices are available from Starrett Co., Digital Measurement Metrology, Inc., and other companies. The cost of these calipers ranges from under \$20 to over \$100, depending on their material and precision.

ACKNOWLEDGMENTS

This research was supported by an Individual Discovery Grant from the Natural Sciences and Engineering Research Council of Canada (NSERC). The authors thank Aemal Akhtar for help with preliminary experiments, Arielle Chan, Kate Feather-Adams, Luxi Li, and Faiza Shafaqat for help with preliminary analyses, Natasha Crighton for photography, and Dr. Deda Gillespie for suggestions on the manuscript.

REFERENCES

- American Society of Surgery of the Hand. (1983). *The Hand: Examination and Diagnosis*. Edinburgh, NY: Churchill Livingstone.
- Boles, D. B., and Givens, S. M. (2011). Laterality and sex differences in tactile detection and two-point thresholds modified by body surface area and body fat ratio. *Somatosens. Mot. Res.* 28, 102–109. doi:10.3109/08990220.2011.627068
- Brodal, P. (ed.). (2010). “Peripheral parts of the somatosensory system,” in *The Central Nervous System: Structure and Function*, 4th Edn. New York: Oxford University Press, 165–189.
- Campbell, W. W., Dejong, R. N., and Haerer, A. F. (2013). *DeJong's The Neurologic Examination*. Philadelphia: Wolters Kluwer/Lippincott Williams & Wilkins.
- Craig, J. C., and Johnson, K. O. (2000). The two-point threshold: not a measure of tactile spatial resolution. *Curr. Dir. Psychol. Sci.* 9, 29–32. doi:10.1111/1467-8721.00054
- Dellon, A. L. (1981). *Evaluation of Sensibility and Re-Education of Sensation in the Hand*. Baltimore: Williams & Wilkins.
- Dinse, H. R., Kleibel, N., Kalisch, T., Ragert, P., Wilimzig, C., and Tegenthoff, M. (2006). Tactile coactivation resets age-related decline of human tactile discrimination. *Ann. Neurol.* 60, 88–94. doi:10.1002/ana.20862
- Essock, E. A., Krebs, W. K., and Prather, J. R. (1992). An anisotropy of human tactile sensitivity and its relation to the visual oblique effect. *Exp. Brain Res.* 91, 520–524. doi:10.1007/BF00227848
- Gescheider, G. A. (1967). Auditory and cutaneous temporal resolution of successive brief stimuli. *J. Exp. Psychol.* 75, 570–572. doi:10.1037/h0025113
- Gescheider, G. A. (1997). *Psychophysics: The Fundamentals*. Mahwah, NJ: L. Erlbaum Associates.
- Gescheider, G. A., Bolanowski, S. J., and Chatterton, S. K. (2003). Temporal gap detection in tactile channels. *Somatosens. Mot. Res.* 20, 239–247. doi:10.1080/08990220310001622960
- Gibson, G. O., and Craig, J. C. (2002). Relative roles of spatial and intensive cues in the discrimination of spatial tactile stimuli. *Percept. Psychophys.* 64, 1095–1107. doi:10.3758/BF03194759
- Gibson, G. O., and Craig, J. C. (2005). Tactile spatial sensitivity and anisotropy. *Percept. Psychophys.* 67, 1061–1079. doi:10.3758/BF03193632
- Gibson, G. O., and Craig, J. C. (2006). The effect of force and conformance on tactile intensive and spatial sensitivity. *Exp. Brain Res.* 170, 172–181. doi:10.1007/s00221-005-0200-1
- Godde, B., Stauffenberg, B., Spengler, E., and Dinse, H. R. (2000). Tactile coactivation-induced changes in spatial discrimination performance. *J. Neurosci.* 20, 1597–1604.
- Goldreich, D., and Kanics, I. M. (2003). Tactile acuity is enhanced in blindness. *J. Neurosci.* 23, 3439–3445.
- Goldreich, D., Wong, M., Peters, R. M., and Kanics, I. M. (2009). A tactile automated passive-finger stimulator (TAPS). *J. Vis. Exp.* 28:e1374. doi:10.3791/1374
- Grant, A. C., Zangaladze, A., Thiagarajah, M. C., and Sathian, K. (1999). Tactile perception in developmental dyslexia: a psychophysical study using gratings. *Neuropsychologia* 37, 1201–1211. doi:10.1016/S0028-3932(99)00013-5
- Jerosch-Herold, C. (2003). A study of the relative responsiveness of five sensibility tests for assessment of recovery after median nerve injury and repair. *J. Hand Surg. Br.* 28, 255–260. doi:10.1016/S0266-7681(03)00017-2
- Jerosch-Herold, C. (2005). Assessment of sensibility after nerve injury and repair: a systematic review of evidence for validity, reliability and responsiveness of tests. *J. Hand Surg. Br.* 30, 252–264. doi:10.1016/j.jhsb.2004.12.006
- Johansson, R. S., and Vallbo, A. B. (1979). Detection of tactile stimuli. Thresholds of afferent units related to psychophysical thresholds in the human hand. *J. Physiol.* 297, 405–422.
- Johansson, R. S., and Vallbo, A. B. (1980). Spatial properties of the population of mechanoreceptive units in the glabrous skin of the human hand. *Brain Res.* 184, 353–366. doi:10.1016/0006-8993(80)90804-5
- Johnson, K. O. (2001). The roles and functions of cutaneous mechanoreceptors. *Curr. Opin. Neurobiol.* 11, 455–461. doi:10.1016/S0959-4388(00)00234-8
- Johnson, K. O., and Phillips, J. R. (1981). Tactile spatial resolution. I. Two-point discrimination, gap detection, grating resolution, and letter recognition. *J. Neurophysiol.* 46, 1177–1192.
- Johnson, K. O., Van Boven, R. W., and Hsiao, S. S. (1994). “The perception of two points is not the spatial resolution threshold,” in *Touch, Temperature, and Pain in Health and Disease: Mechanisms and Assessments: a Wenner-Gren Center International Symposium*, 1st Edn, eds J. Boivie, P. Hansson, and U. Lindblom (Seattle: IASP Press), 389–404.
- Kalisch, T., Tegenthoff, M., and Dinse, H. R. (2007). Differential effects of synchronous and asynchronous multifinger coactivation on human tactile performance. *BMC Neurosci.* 8:58. doi:10.1186/1471-2202-8-58
- Kennett, S., Taylor-Clarke, M., and Haggard, P. (2001). Noninformative vision improves the spatial resolution of touch in humans. *Curr. Biol.* 11, 1188–1191. doi:10.1016/S0960-9822(01)00327-X
- Klein, S. A. (2001). Measuring, estimating, and understanding the psychometric function: a commentary. *Percept. Psychophys.* 63, 1421–1455. doi:10.3758/BF03194552
- Kontsevich, L. L., and Tyler, C. W. (1999). Bayesian adaptive estimation of psychometric slope and threshold. *Vision Res.* 39, 2729–2737. doi:10.1016/S0042-6989(98)00285-5
- Lundborg, G., and Rosen, B. (2004). The two-point discrimination test – time for a re-appraisal? *J. Hand Surg. Br.* 29, 418–422. doi:10.1016/j.jhsb.2004.02.008
- MacMillan, N. A., and Creelman, C. D. (2005). *Detection Theory: A User's Guide*. Mahwah: Lawrence Erlbaum Associates.
- Mountcastle, V. B., and Bard, P. (1968). “Neural mechanisms in somesthesia,” in *Medical Physiology*, 12th Edn, ed. V. B. Mountcastle (St. Louis: Mosby), 1372–1423.
- Olausson, H., Wessberg, J., and Kakuda, N. (2000). Tactile directional sensibility: peripheral neural mechanisms in man. *Brain Res.* 866, 178–187. doi:10.1016/S0006-8993(00)02278-2
- Peters, R. M., Hackeman, E., and Goldreich, D. (2009). Diminutive digits discern delicate details: fingertip size and the sex difference in tactile spatial acuity. *J. Neurosci.* 29, 15756–15761. doi:10.1523/JNEUROSCI.3684-09.2009
- Purves, D., Augustine, G. J., Fitzpatrick, D., Hall, W. C., LaMantia, A., and White, L. E. (eds). (2012). “The somatic sensory system: touch and proprioception,” in *Neuroscience*, 5th Edn (Sunderland: Sinauer Associates), 189–208.
- Rosen, B., Dahlin, L. B., and Lundborg, G. (2000). Assessment of functional outcome after nerve repair in a longitudinal cohort. *Scand. J. Plast. Reconstr. Surg. Hand Surg.* 34, 71–78. doi:10.1080/02844310050160204
- Stevens, J. C., Foulke, E., and Patterson, M. Q. (1996). Tactile acuity, aging, and braille reading in long-term blindness. *J. Exp. Psychol. Appl.* 2, 91–106. doi:10.1037/1076-898X.2.2.91
- Stevens, J. C., and Patterson, M. Q. (1995). Dimensions of spatial acuity in the touch sense: changes over the life span. *Somatosens. Mot. Res.* 12, 29–47. doi:10.3109/08990229509063140
- Vallbo, A. B., and Johansson, R. S. (1978). “The tactile sensory innervation of the glabrous skin of the human hand,” in *Active Touch, the Mechanism of Recognition of Objects by Manipulation*, ed. G. Gordon (Oxford: Pergamon Press Ltd), 29–54.
- Van Boven, R. W., and Johnson, K. O. (1994). A psychophysical study of the mechanisms of sensory recovery following nerve injury in humans. *Brain* 117(Pt 1), 149–167. doi:10.1093/brain/117.1.149
- van Nes, S. I., Faber, C. G., Hamers, R. M., Harschnitz, O., Bakkers, M., Hermans, M. C., et al. (2008). Revisiting two-point discrimination assessment in normal aging and in patients with polyneuropathies. *J. Neurol. Neurosurg. Psychiatr.* 79, 832–834. doi:10.1136/jnnp.2007.139220
- Vega-Bermudez, F., and Johnson, K. O. (1999). Surround suppression in the responses of primate SA1 and RA mechanoreceptive afferents mapped with a probe array. *J. Neurophysiol.* 81, 2711–2719.
- Weber, E. H. (1996). *E. H. Weber on the Tactile Senses*. Hove: Erlbaum (UK) Taylor & Francis.
- Weinstein, S. (1968). “Intensive and extensive aspects of tactile sensitivity as a function of body part, sex and laterality,” in *The Skin Senses*, 1st Edn, ed. D. R. Kenshalo (Springfield, IL: Charles C. Thomas), 195–222.
- Wichmann, F. A., and Hill, N. J. (2001). The psychometric function: I. Fitting, sampling, and goodness of fit. *Percept. Psychophys.* 63, 1293–1313. doi:10.3758/BF03194544
- Wong, M., Gnanakumaran, V., and Goldreich, D. (2011a). Tactile spatial acuity enhancement in blindness: evidence for

- experience-dependent mechanisms. *J. Neurosci.* 31, 7028–7037. doi:10.1523/JNEUROSCI.6461-10.2011
- Wong, M., Hackeman, E., Hurd, C., and Goldreich, D. (2011b). Short-term visual deprivation does not enhance passive tactile spatial acuity. *PLoS ONE* 6:e25277. doi:10.1371/journal.pone.0025277
- Wong, M., Peters, R. M., and Goldreich, D. (2013). A physical constraint on perceptual learning: tactile spatial acuity improves with training to a limit set by finger size. *J. Neurosci.* 33, 9345–9352. doi:10.1523/JNEUROSCI.0514-13.2013
- Zuberbühler, H. J. (2002). *Rapid Evaluation of Perceptual Thresholds: The Best-Pest Calculator: a Web-based Application for Non-expert Users*. Zurich: Swiss Federal Institute of Technology Zurich (ETHZ), Institute for Hygiene and Applied Physiology (IHA).
- Conflict of Interest Statement:** The authors declare that the research was conducted in the absence of any commercial or financial relationships that could be construed as a potential conflict of interest.
- Received: 03 May 2013; accepted: 28 August 2013; published online: 13 September 2013.
- Citation: Tong J, Mao O and Goldreich D (2013) Two-point orientation discrimination versus the traditional two-point test for tactile spatial acuity assessment. *Front. Hum. Neurosci.* 7:579. doi: 10.3389/fnhum.2013.00579
- This article was submitted to the journal Frontiers in Human Neuroscience. Copyright © 2013 Tong, Mao and Goldreich. This is an open-access article distributed under the terms of the Creative Commons Attribution License (CC BY). The use, distribution or reproduction in other forums is permitted, provided the original author(s) or licensor are credited and that the original publication in this journal is cited, in accordance with accepted academic practice. No use, distribution or reproduction is permitted which does not comply with these terms.*

Chapter 4

4.1 Preface

In previous chapters, we have explored the effects of stimulus and peripheral factors on the perception of point stimuli. Using a computational model to decode simulated afferent activity, we demonstrated that noise in the nervous system is a major cause for variability in task performance and ultimately adds imprecision to the perceptual process (beyond what can be accounted for by receptive field properties alone). Bayesian models of perception have been proposed to overcome this type of sensorineural imprecision: prior information (based on experience and expectation) is incorporated into the inference process of decoding sensorineural information. This probabilistic process often results in perception that reflects what is statistically likely to occur in reality, therefore mitigating the random effects of noise. However, when stimuli violate what is statistically likely a priori, illusions may arise. In this chapter we explore and provide evidence for a Bayesian model of trajectory estimation for sequential point stimuli that incorporates a low-velocity prior, and replicates a famous perceptual length contraction illusion.

4.2 Abstract

Bayesian perceptual models have been proposed to explain many perceptual phenomena, including illusions. Viewing perception in a Bayesian

framework is fitting, as expectation or experience (modeled as a prior) appears to strongly influence perception. When sensorineural processes are imprecise, priors are more heavily relied upon; under these conditions, illusions may result when reality violates expectation. In this chapter we review and test a Bayesian perceptual model of trajectory estimation that replicates a famous length contraction illusion: when two taps at different locations occur in quick succession, the intervening distance is often underestimated. When spatial uncertainty is high, the model's low velocity prior has a stronger influence on perception and thus observers are predicted to experience greater length contraction. Indeed, we show that increasing an observer's spatial uncertainty by using weaker taps (sine wave rather than square wave pulses) effectively increases the magnitude of perceptual length contraction on the forearm. Furthermore, we show that our Bayesian perceptual model provides relatively good fits to the magnitude of length contraction as a function of the time between successive taps.

4.3 Introduction

In the second chapter of the thesis, we explored how input characteristics like receptor spacing and variability in firing-rate give rise to imprecision and variability in perceived stimulus location. Imprecision and variability are therefore innate characteristics of perception. However, it has been proposed that the

incorporation of prior information can mitigate perceptual imprecision, as Bayesian methods are the optimal strategy for making inferences under uncertainty (Knill, 1996). The Bayesian framework proposes that perception integrates the statistics of the environment (prior) with the sensorineural signals elicited by stimulation (likelihood). For example, by taking into account the frequency of occurrence (prior) of various stimulus trajectories, based on experience, the process of inferring the position of sequential stimuli from sensorineural data can be improved in normal conditions (Goldreich, 2007; Goldreich and Tong, 2013). Interestingly, though, this framework can also give rise to illusions: under special conditions, when prior expectations are violated, perception may reflect expectation rather than reality.

This chapter explores a Bayesian perceptual model that implements a low-speed prior to infer stimulus trajectory and, thus, explains the occurrence of a well known tactile illusion: perceptual length contraction (Goldreich 2007; Goldreich & Tong, 2013). We start by briefly introducing the model and then move on to describe a series of experiments we have carried out to test some of the model's predictions.

The Bayesian Perceptual model

We introduce a model that views perception as the result of a Bayesian operation, in which the locations of multiple tap stimuli are inferred. For the sake of simplicity and relevance we will keep the focus on sequential two-point stimuli. In the model, candidate positions for each tap are considered; each pair of positions makes up a candidate trajectory, much like in the ideal observer analysis of the sequential two-point task in Chapter 2. However, in this particular Bayesian model, a non-uniform prior distribution over trajectories is considered: specifically, the model assumes that trajectories consistent with low velocity stimuli are, a-priori, more likely than those of higher velocities, with stationary stimuli (zero velocity) being the most likely (see Fig. 1). This prior is based on the belief that stationary stimuli occur much more frequently than quick stimuli (i.e. clothing typically remains at rest on the body surface). Therefore, the prior probability distribution over velocities, $p(v)$, is modeled as a Gaussian distribution centered on zero with a standard deviation of σ_v (see Fig. 1). To translate this distribution over velocity to a distribution over possible stimulus trajectories for a pair of taps, $p(x_1, x_2|t)$, one simply divides the probability of the velocity corresponding to a pair of taps by the time required to traverse those candidate positions at that velocity (see equation 2 and figure 1).

Above, we have described how the model incorporates a low velocity prior; however, this is only one component of the Bayesian computation. The other

component of interest is the likelihood distribution over trajectories, $p(x_{1m}, x_{2m} | x_1, x_2, t)$. The likelihood of each candidate position is defined as the probability of the sensorineural input (the observer’s “internal “measurement,” x_m) given that candidate position. The distribution of likelihoods over possible positions is modeled as a Gaussian centered over the true stimulus position with a standard deviation of σ_s . It is useful to imagine the task of localizing a single point stimulus: on average, the perceived location should equal the true location; however, from trial to trial the perceived location will deviate from this true location with a standard deviation related to σ_s . Therefore, better acuity corresponds to a smaller σ_s .

According to Bayes rule, the product of likelihood and prior distributions is proportional to the posterior probability distribution (see Equation 1). The posterior distribution over trajectories (positions of taps 1 and 2) is therefore proportional to the product of the prior and likelihood distributions over trajectories (see fig. 2) The pair of tap positions with the highest posterior probability, maximum a posteriori (MAP) or mode, is taken as the perceived trajectory.

$$\text{posterior} \propto \text{likelihood} * \text{prior}$$

Eqn 1.

$$p(x_1, x_2 | x_{1m}, x_{2m}, t) \propto p(x_{1m}, x_{2m} | x_1, x_2, t) p(x_1, x_2 | t)$$

Eqn 2. **Converting a prior over velocity to a prior over trajectories**

Velocity is defined as the distance traversed over time:

$$v = \frac{x_2 - x_1}{t}$$

$$x_2 = x_1 + vt$$

Therefore, the position of tap 2, x_2 , is conditional upon the position of tap 1, x_1 , and the time between taps, t . Since tap 1 can, a priori, occur at any position with equal probability:

$$p(x_1, x_2 | t) \propto p(x_2 | x_1, t)$$

The probability of x_2 , conditional on x_1 and time, is related to the probability of velocity, v , in the following way:

$$p(x_2 | x_1, t) = \frac{p(v)}{t}$$

Therefore,

$$p(x_1, x_2 | t) \propto \frac{p(v)}{t}$$

The Bayesian operation of multiplying the non-uniform prior over trajectories with the likelihood over trajectories (Eqn. 1), may result in a MAP that is shifted away from the likelihood towards the prior (see Figure 2). This is equivalent to an underestimation in the perceived distance between stimulus positions (see Figure 7). Progressively lowering the inter-stimulus time (IST) between taps effectively shifts the perceived trajectory closer and closer to zero separation as can be seen in Fig. 2. Holding the IST constant, but changing the spatial acuity, σ_s , also has an effect on the degree of length-contraction (see Fig. 3): an observer with low spatial acuity (high uncertainty) would experience greater length contraction than one with higher spatial acuity (low uncertainty).

Testing the model's predictions

The Bayesian framework, laid out above, is described and discussed in greater detail in a previous publication (Goldreich and Tong, 2013); also covered in that article is the full derivation of the model's central formula starting from Bayes' Theorem (Eqn. 1) (see appendix of Goldreich and Tong, 2013). Here, we will focus on the central formulation relating perceived length, l^* , to the measured

length, l_m (which on average is the true length), given the inter-stimulus time, t , and the single free parameter, τ :

Eqn. 3

$$l^* = \frac{l_m}{1 + 2\left(\frac{\tau}{t}\right)^2}$$

The parameter τ is the ratio between σ_s and σ_v , or in other words, the strength of low-speed expectation over spatial acuity:

Eqn. 4

$$\tau = \frac{\sigma_s}{\sigma_v} = \frac{1/\sigma_v}{1/\sigma_s} = \frac{\text{strength of low-speed expectation}}{\text{spatial acuity}}$$

Looking at Equations 3 and 4 together, it is mathematically intuitive as to how greater spatial acuity results in less length contraction and, conversely, greater expectation for low-speeds leads to more marked length contraction. Also evident in Equation 3, is that τ is essentially a time constant: when the interstimulus time, t , is equivalent to τ , the perceived length will be 1/3 of the measured length. Therefore τ is a parameter that describes the overall magnitude of length contraction experienced by an observer under a set of stimulus conditions.

The goal of this chapter is to test some of the model's major predictions: 1) With decreasing time between a pair of sequential taps, the perceived distance between such taps should underestimate the true distance in accordance with Eqn. 3; 2) Assuming that σ_v remains constant, conditions that lead to poor spatial acuity should, in turn, result in an overall greater magnitude of length contraction (τ should be proportional to σ_s).

We test the first prediction by having participants compare two pairs of sequential taps. One pair of taps functions as a reference, and thus has a fixed separation and intervening time interval (large enough to not cause any appreciable length contraction); the other pair, which we term the comparison pair, varies in temporal and spatial separation. For a given comparison pair time interval, we estimate the spatial separation between the comparison pair necessary to evoke a perceived separation equal to that of the reference pair. This is repeated for each comparison pair time interval (progressively decreasing in time). The model predicts that the comparison separation must be larger, relative to the reference separation, to achieve this "point of subjective equality" (PSE) when the comparison time is shorter than that of the reference; as the time interval between comparison taps shrinks, the comparison length PSE should grow correspondingly. Furthermore, if the model is correct, it should also provide a

good fit to participants' comparison separation PSE as a function of the time between comparison taps.

We test the second prediction by comparing the τ parameter that gives the best fit to each human participant's data under different stimulus conditions (i.e. different stimulus waveforms and stimulation on different body-sites) that presumably result in varying spatial acuity. For example, sine-wave stimuli have a slower rise time, and thus feel weaker than square-wave stimuli, which have nearly instantaneous rise times. We predict that sine wave stimuli will be more difficult to localize, giving rise to a larger σ_s (lower spatial acuity) than for square-wave stimuli. Therefore, in the length comparison task described above, the best-fit τ for a given observer should be larger when σ_s is larger (i.e. sine-wave $\tau >$ square-wave τ). If the above predictions indeed reflect the trends found in observers, our proposed experiments will lend further credence to the concept of perception as Bayesian inference and the existence of a low-velocity prior in somatosensation.

4.4 Methods

Pulse stimuli

Each pulse stimulus consisted of a 5ms half-sinusoid or half-square wave displacement with an amplitude of 0.1mm, delivered by one of three computer-

controlled precision cylindrical motors (Tactile Stimulator MkII; Fong Engineering; Oakland, CA, USA). Attached to each motor was a probe-tip: a rounded stainless-steel pinhead, 1mm in diameter, which displaced the skin by a baseline of approximately 0.5 mm. The motion of each pulse stimulus was confined to an axis perpendicular to the skin surface. Depending on the experimental condition, either two or all three stimulators were used. Before administering each task, the experimenter, with the aid of a linear displacement display, lowered the probe tips such that the baseline indentation of each probe was 0.5 mm. From there, micro-adjustments to the displacement of each probe (in 100 μ m increments) were made such that the subjective strength of each tap felt approximately equal (reported by participant). The experimenter also had control over the x and y positions of each motor, by means of manipulators that held each motor in place, allowing for precise probe placements to achieve the necessary separations. The dorsal forearm or proximal phalanx of the index finger was marked, in advance, in 0.5 cm or 0.5 mm increments to aid the experimenter in probe placement.

Measuring spatial uncertainty (σ_s)

We measured each participant's tactile spatial uncertainty (inverse of acuity), σ_s , in localizing square-wave and sine-wave pulses. This was done by giving two taps to different locations on the tested body site (longitudinally oriented on the forearm and transversely oriented on the finger) separated by

1000ms, and subsequently having the participant identify the order of stimulation by button press (arm: was the first one closer to the wrist or elbow? finger: was the first one on the left or right?) (see figure 4A). The goal was to measure the participant's psychometric function in this task: percent correct as a function of the separation between the taps (see figure 4B). We used a Bayesian adaptive procedure (modified from Kontsevich and Tyler, 1999) to estimate the best fitting psychometric function, as well as to determine the next, most informative, separation to give. Every 10 trials the separation was adjusted accordingly, until a total of 100 trials was completed (a single block). After 50 trials, midway through a block, the participant was given a ~3 minute break. This task was done four times each with square-wave stimuli and sine-wave stimuli. For finger testing, participants started the task on the fingertip; if their performance did not max out at floor levels (the minimum separation possible is 1mm), the participant continued subsequent testing on the fingertip. However, if the participant performed perfectly at the lowest separation, the task would be moved to the finger base, where all subsequent finger experiments were carried out.

The parameter of interest, for each participant's best fitting psychometric function, was the separation at which the participant performed at 76% (the a -parameter). According to signal detection theory, the 76% threshold, for a 2 interval forced-choice task, is equivalent to the stimulus value at which d' takes

on a value of 1. d' is a measure of the signal-to-noise ratio and is defined as the difference between the means of two Gaussians divided by their shared standard deviation ($d' = (x_2 - x_1) / \sigma$). In our spatial acuity task, we assume that the mean perceived position of each tap is equal to its actual location, with some standard deviation σ . At some separation ($x_2 - x_1$), the uncertainty in the positions of each tap will cause the observer to perform at 76% accuracy, this is where d' is 1; therefore, since $\sigma = (x_2 - x_1) / d'$, this separation is equivalent to the standard deviation, which we specifically term σ_s for spatial uncertainty (see Figure 4B).

Length comparison blocks

We measured each participant's ability to compare/discriminate lengths of separation between two pairs of taps. In each trial, a pair of taps, known as the reference pair, separated by a fixed length of either 3 or 2.5 (cm on the arm, mm on the finger) was given; another pair of taps, known as the comparison pair, was separated by a varying length (see Fig. 5A). The ordering of the reference and comparison pairs was randomized in each trial and the participant was asked to identify whether the pair with the longer separation occurred first or second (see Fig. 5B). Participants responded by button press. The goal was to measure each participant's psychometric function: the proportion of times the comparison pair was judged to be longer than the reference pair, as a function of the comparison pair separation (see Fig. 5B). We used a Bayesian adaptive procedure to

estimate the participant's best fitting psychometric function, as well as to determine the next, most informative, comparison pair separation to give. Every 10 trials the separation was adjusted accordingly, until a total of 100 trials was completed (a single block) (see Fig. 6A). Midway through the block, the participant was given a ~3 minute break. The parameter of interest, for each participant's best fitting psychometric function, was the comparison pair separation that the participant reported feeling longer than the reference pair 50% of the time. This point of subjective equality (PSE) was also known as the a -parameter (see Fig. 6B).

Length comparison qualification

In order to familiarize participants with the task, and to ensure they could reliably perform it, we implemented various qualification criteria for the initial block. In these "qualification blocks", the inter-stimulus time (IST) between reference taps was equal to that of the comparison taps; the reference and comparison ISTs were both set at 1000ms. The following are the qualification criteria we implemented: 1) participants must have a Bayes factor no greater than 0.001, to ensure that participants were likely not guessing for a majority of trials and 2) participants must yield an a -PDF mode (best fit PSE), that is no greater than 1 (cm on arm, mm on finger) away from the reference pair separation of 3 (i.e. the PSE must be ≤ 4 and ≥ 2). This is to

ensure that there are no extreme, intrinsic response biases that could make subsequent interpretation of results difficult. When these two criteria were met, participants could continue length comparison testing with “length contraction” conditions. When either of the criteria were not met, participants were given a second chance (extra block) and were disqualified from the study if they again failed to meet criteria.

Length comparison blocks with “length contraction” conditions

Once participants qualified in the qualification blocks they moved on to length comparison, with a special condition to elicit length contraction. That is, participants completed length comparison blocks in which the time between comparison taps (comparison time, t_{com}) was always less than the time between reference taps. For the first length comparison block under the “length contraction” condition the comparison time was set at 200ms ($t_{com}=200ms$). For subsequent testing blocks, the comparison time was set to half the value of the previous comparison time (e.g., the next block, following the 200ms block, is $t_{com}=100ms$). However, if the previous comparison time had an a-PDF that was clipped at 10 (length contraction beyond what our set up can measure) then the next comparison time was set at 1.5X the previous one (e.g., if the 100ms block had a clipped a-PDF, the next comparison time was 150ms, rather than 50ms). This was done to maximize the chances of measuring a PSE that was not

pegged on following blocks. This procedure was repeated until a total of 5 length comparison blocks were run (including the qualification block).

The Bayesian adaptive procedure

For each of the experiments, we used a Bayesian Adaptive Procedure (BAP) to fit performance to a psychometric function and adaptively choose the next stimulus to give after every stretch of 10 trials. The specific type of function we chose to fit participant data with was the Weibull function:

For the spatial uncertainty experiment (σ_s) the Weibull function took the following form:

$$p(\text{correct}) = 0.5 + (0.5 - \delta) \left(1 - 2.0854^{-\left(\frac{x}{a}\right)^b} \right) + \frac{\delta}{2}$$

For the length comparison experiment the Weibull function took the following form:

$$p(l_{com} > l_{ref} | x) = (1 - \delta) \left(1 - 2^{-\left(\frac{x}{a}\right)^b} \right) + \frac{\delta}{2}$$

Where x is the separation between taps, a is the performance threshold, b is related to the slope of the psychometric function and δ is the lapse rate (i.e. the probability that the subject will guess on any given trial due to a lapse in

concentration). For either experiment, we considered 500 possible a values (with a range of 0.1 to 10), 50 possible b values (with a range of 0.2 to 5), and 10 possible δs (with a range of 0.01 to 0.08). As can be seen above, the Weibull function takes on the value of 0.5 as the separation approaches zero for the spatial uncertainty experiment, as participants will be guessing below their spatial resolution; however, the function takes on the value of 0 as the comparison pair separation approaches zero for the length comparison experiment, which reflects the fact that the probability that a participant will report the comparison pair as being longer will diminish to 0 as the comparison separation is well below that of the reference pair. In either experiment, the a -parameter estimate is of primary interest since it represents either σ_s (in spatial uncertainty experiments) or the comparison length resulting in the PSE (in length comparison experiments).

Order of experiments

The total series of experiments spanned 12 days of testing (non-consecutive); the first 6 days were devoted to testing on a single body site (forearm or finger) and the final 6 days for the other body site (ordering was counterbalanced). On the first day, participants underwent spatial uncertainty testing (σ_s experiment) for square and sine wave pulses (4 blocks each, order counterbalanced). On the second day of testing, participants completed 5 blocks of length comparison with a reference length 3 (cm or mm) and one of the

waveform types (counterbalanced), starting with the qualification block (com time =1000ms) and then moving on to length contraction conditions (com time < ref time) with progressively decreasing comparison times. On the third day, this was repeated with the other reference length (2.5 cm or mm). The fourth and fifth testing days followed the same procedure as days 2 and 3, with the other stimulus waveform. The sixth, and final day for a given body site, was devoted to retesting spatial uncertainty (σ_s), and followed the same procedure as day 1. The remaining six days were a repeat of the above procedure, but on the other body-site.

Additional participants

The exact methods explained above pertain to experiments run on the 4 initial participants. We decided to run an additional 4 participants for a total $n=8$; however with these additional 4 participants, the experimental design was reorganized to make data collection more efficient, cutting down the overall 12 days of experiments into 6 days. The following changes were made for the additional 4 participants: 1) Only a single spatial uncertainty block was run on the first and last days of testing. 2) Only a reference of 3 cm or mm was used on forearm or finger. 3) Finger testing was done on the finger base only, as the fingertip's resolution was often too fine for us to measure. All the results we report

include data from the full set of subjects (n=8); one subject did not qualify for finger testing, therefore for results pertaining to finger measurements only, n=7

Fitting length comparison PSE estimates with the model

We fit the comparison length PSE estimates obtained from length comparison experiments of varying comparison time, with a range of possible τ values: we considered τ ranging from 0.001s to 0.2s in 10000 equally spaced steps (2.0×10^{-5} s). The estimated PSEs under each condition (body-site and waveform combination) have a likelihood of being observed given each possible τ value ($p(\text{estimated PSEs}|\tau)$); we thus calculated the likelihood distribution over the full range of τ , and used the mode of this distribution as the best-fitting τ for a given data set. The calculation of likelihoods over τ was done in the following way: the mean perceived separation of reference and comparison pairs were considered to be equal under each PSE condition; therefore, using Equation 3 we can write the following expressions:

$$l_{ref}^* = l_{com}^*$$

$$\frac{l_{ref}}{1 + 2 \left(\frac{\tau}{t_{ref}} \right)^2} = \frac{l_{com}}{1 + 2 \left(\frac{\tau}{t_{com}} \right)^2}$$

Eqn 5

$$l_{com} = \frac{l_{ref} \left(1 + 2 \left(\frac{\tau}{t_{com}} \right)^2 \right)}{1 + 2 \left(\frac{\tau}{t_{ref}} \right)^2}$$

Given the experimental parameters $t_{ref} = 1s$,

$l_{ref} = 3$ or 2.5 cm (0.3 or 0.25 cm on the finger), and t_{com} , each candidate τ results in a predicted l_{com} given by Equation 5, above. The likelihood for a particular τ , corresponding to a predicted l_{com} , is then interpolated from the full a-PDF that was obtained in each experiment (i.e. the a-PDF is interpolated at the predicted l_{com}). This is repeated for each experiment (all comparison time blocks and both reference lengths), and each of the corresponding interpolated likelihoods is multiplied together, under the assumption that the experiments are conditionally independent. The resulting product is taken to be the overall likelihood of obtaining the participant's full set of data given a τ value. This procedure is repeated for each τ to obtain a full likelihood distribution over τ . We report the mode of this distribution as the best-fit τ .

Statistical analyses

To test whether using different stimulus waveforms would result in different measured spatial uncertainties (σ_s), we first pooled the data from all σ_s blocks, by testing day, to generate a grand σ_s distribution for testing day 1 and one for testing day 2 (this was done for each waveform condition); we then carried out a two-by-two repeated measures ANOVA with testing day and waveform as the two factors and the mode of the σ_s distributions as independent variables. This analysis also tests whether there is an effect of testing day, to rule out the possibility of practice effects (a changing σ_s over days).

Best-fit τ values were obtained computationally as described above, in the section “Fitting length comparison PSE estimates with the model”. We used Labview 2009 to carry out these computations.

To test whether the best-fit τ values differed significantly by stimulus waveform condition, we carried out paired t-tests for each body site (forearm and finger) comparing the best-fit τ measured in sine wave and square wave conditions. We used t-tests instead of a repeated measures ANOVA because one participant was unable to qualify on the finger, resulting in an unequal number of repeated measurements.

4.5 Results

The effect of stimulus waveform on spatial uncertainty (σ_s)

The two stimulus waveform types (sine and square wave pulses) gave rise to measurable differences in spatial uncertainty. A two-by-two repeated measures ANOVA carried out on the forearm experimental data, with testing day and waveform as factors and spatial uncertainty (σ_s) as the dependent measure, showed a significant effect of waveform ($F=65.91$, $p<0.0001$) with no significant effect of testing day ($F=0.0861$, $p=0.78$) or interactions ($F=1.28$, $p=0.29$). On the finger, the repeated measures ANOVA again showed a significant effect of waveform ($F=14.23$, $p=0.0093$), with no significant effect of testing day ($F=2.63$, $p=0.156$) or interactions ($F=2.75$, $p=0.15$). To summarize, there was a clear effect of stimulus waveform type on both body sites (forearm and finger), with the mean spatial uncertainty for sine wave stimuli taking on larger values than that of square wave stimuli (see Figure 8). Pooling across testing days, the average σ_s for sine wave stimuli was 2.55 times greater than that of square wave stimuli. There was no evidence of practice effects, since initial and final testing days showed similar spatial uncertainty measures.

Length contraction measured as a shift in PSE

Our length comparison results consistently exhibited the following trend: as the time between comparison taps decreases, the spatial separation between

these taps must be made progressively larger than that of the reference pair in order to achieve perceptual length equality. This shift in the point of subjective equality (PSE) as a function of the comparison time can be fit with the length-contraction equation proposed by our Bayesian model (see Fig. 9). In fact, in 26 out of 30 cases (87%), the best-fit τ parameter was greater than 0, suggesting significant length contraction across all body-sites and stimulus waveform conditions. Since we varied the τ parameter in each condition, to obtain the best fit, we were able to obtain an entire likelihood distribution over τ . In other words, we computed the probability of obtaining the data we observed (across comparison times), given each candidate τ value. The τ value with the highest likelihood was considered the best-fit τ . For the purposes of obtaining a measure for goodness of fit we normalized these likelihood distributions by the sum of likelihoods to generate a “probability distribution” over τ that integrated to 1. Across conditions, the average width of the 95% CI of this “normalized” τ likelihood distribution was 0.018s (with a standard deviation of 0.032s), demonstrating a relatively high level of confidence in the model’s ability to fit each participant’s data set (on average we were 95% confident that the best fit τ fell within a 0.018 s interval containing the mode).

A paired t-test comparing the best-fit τ between square and sine wave conditions for the forearm showed a significant effect of waveform ($p=0.029$, one-

tailed) (see Figure 10). The mean best-fit τ for square wave pulses on the forearm was 0.033s (SE 0.012s); the mean best-fit τ for sine wave pulses on the forearm was 0.059s (SE 0.02s). Therefore, on average, the best-fit τ for sine wave stimuli was almost double the best-fit τ for square wave stimuli.

A paired t-test comparing the best-fit τ between square and sine wave conditions for the finger did not show a significant effect of waveform ($p=0.23$) (see Figure 11). The mean best-fit τ for square wave pulses on the finger was 0.064s (SE 0.025s); the mean best-fit τ for sine wave pulses on the finger was 0.039s (SE 0.011s). Therefore, on average, the best-fit τ on the finger showed the opposite trend to what was predicted, although pairwise differences were not significant.

4.6 Discussion

In this chapter we have outlined and summarized our preliminary findings in testing a Bayesian model of spatiotemporal tactile perception. We demonstrated a replication of the tau effect on both finger and forearm for a majority of participants, using a length comparison task; we further demonstrated that our proposed model produces relatively good within-subject fits to the behavioural data in this task. Our results further support a central prediction of the model: weaker taps, which are more difficult to localize (high spatial uncertainty), will on average result in greater length contraction (a large τ parameter) than for

easily locatable taps. On average, spatial uncertainty (σ_s) of sine wave stimuli was greater than that of square wave stimuli by a factor of 2.55; correspondingly the best-fit τ for sine wave stimuli was almost double the best-fit τ for square wave stimuli.

Length contraction as measured by others

In this study, we have explored the most basic variant of perceptual length contraction, the tau effect, with sequential pairs of pulse stimuli. The tau effect is characterized by the underestimation of length (i.e. the separation or distance) between two points of stimulation, when the temporal separation between stimuli is sufficiently short. In general, as this temporal separation is decreased, so to is the perceived length between sequential stimuli. Length contraction, however, is also thought to underlie other, more complex, illusions like the cutaneous rabbit effect. In the cutaneous rabbit effect/illusion, multiple points are stimulated (typically 3 or more locations, each stimulated multiple times) in quick succession such that intervening areas are perceived to be stimulated; many observers liken this sensation to the feeling of a "rabbit hopping down the arm" (Geldard and Sherrick, 1972; Geldard, 1982). As we have noted in a previous publication (Goldreich and Tong, 2013), the cutaneous rabbit illusion can be viewed as a complex variant of the general length contraction phenomenon consisting of many taps: each of the taps, separated by a sufficiently short time-intervals, is perceptually pulled towards all others occurring closely in time, giving the

impression of continuous "hopping" along intervening areas. In the same publication, we have also demonstrated that our Bayesian perceptual model, replicates the cutaneous rabbit and provides a relatively good fit to the findings of Geldard's 15-tap rabbit experiment (1982). We propose that the model is capable of predicting the trajectories of any sequence of taps, of an arbitrary number, tap locations and temporal separations and need not be limited to the simple case of a single pair of taps.

It has also been demonstrated that the general length contraction illusion also need not be limited to sequential pulsatile stimuli of the type used in this study. Whitsel et. al. (1986) and Seizova-Cajic et. al. (2014) have shown that even the trajectories of continuous motion stimuli, applied by brushes, are subject to perceptual length contraction. The traversed distance of a moving brush across the arm is consistently underestimated when the brush moves at high velocities. According to the framework of our model, the low-velocity prior should also apply to this type of continuous motion stimulus just as it does to sequential pulses. Interestingly, the illusion has also been found to occur with stimuli applied to an object in contact with the body surface: vibratory stimuli applied to different locations on a bar, resting on the index fingers of each hand, are also mislocalized in such a way that mirrors the typical perceptual length contraction illusion on the skin. With this finding in mind, we postulate that the low-velocity

prior applies even to stimuli making contact with objects extending from the body (i.e. tools, prosthetics etc.).

Helson and King (1931) have carried out a similar length comparison experiment as ours, and have also demonstrated marked length contraction on the forearm.

In their experiment, the average performance across subjects for different “comparison times” was best-fit by a τ of 0.1s (Goldreich and Tong, 2013).

Although some of our best-fit τ -values reported here are comparable, we tend to find best-fit τ -values that are somewhat smaller (the average on the forearm was 0.033s for square wave stimuli and 0.059s for sine wave stimuli). Their experiments seem to produce greater length contraction, overall, compared to the length contraction reported here. These differences could arise from differences in methodology. For example, Helson and King’s pulse stimuli consisted of rods that fell to the skin by 2mm (with an average weight of 11.54g) for a duration of 100ms; these stimuli might give rise to a different σ_s , than for the stimuli we use.

The effect of spatial uncertainty on perceptual length contraction

A central prediction of the Bayesian model is that higher spatial uncertainty produces a stronger illusory length contraction effect. The model’s τ parameter should, therefore, be greater for stimulus conditions of higher spatial uncertainty.

We have shown that a practical method for manipulating spatial uncertainty,

within a given testing site, is to give pulse stimuli with different waveforms: a square wave pulse produces a sharper rise, and therefore a more intense stimulus, than a sine wave pulse. A majority of RA1 and SA1 afferents respond to increasing indentation velocity with increasing impulse rate (Knibestol, 1973; Esteky and Schwark, 1994; Pubols and Pubols, 1983). Therefore, the rapidly-rising square wave pulses presented in this study are likely to produce greater responses in afferents than to the slowly-rising sine wave pulses. This difference in evoked impulse rate may account for differences in localizability of square-wave versus sine wave pulses. Our measurements of spatial uncertainty under these two conditions indeed show that square wave stimuli are more accurately localized than sine wave stimuli. Furthermore, our length comparison data on the arm seem to suggest that there is a greater propensity for length contraction when taps are more difficult to localize, under the sine wave stimulus condition, compared with square wave stimuli. Current studies are being run to achieve higher statistical power and increase our confidence in this trend.

Another way to manipulate spatial uncertainty is through selectively focusing attention to a given location. Selective spatial attention is associated with both the recruitment and sharpening of cortical receptive fields within the attended location (Anton-Erxleben and Carrasco, 2013). As we have demonstrated in chapter 2, smaller and more densely distributed receptive fields allows for higher spatial

acuity (whether measured by sequential or simultaneous two-point discrimination, orientation discrimination or single point localization). The effect of selective spatial attention on spatial acuity has been confirmed in studies showing that the error in single-point localization decreases up to 30% when observers attend to the location of stimulation (Moore et al., 1999; O’Boyle et al., 2001). Furthermore, Kilgard and Merzenich (1995) have demonstrated that selective spatial attention results in a shift in the midpoint of the perceived trajectory towards the attended location; that is, a stimulus further away from the attended location is more perceptually pulled (mislocalized) towards a tap nearby the locus of attention. Our model can replicate this effect, if we decrease σ_s within the attended region, relative to the σ_s for the remainder of the arm. Future studies should measure the effect of spatial attention on σ_s , within subjects, and quantitatively test the shift in the trajectory midpoint predicted by our model.

The low-velocity prior (exploring stimulus statistics and neural mechanisms)

Our model makes a central assumption that observers use a low-velocity prior when inferring stimulus trajectories, and that this low-velocity prior reflects the actual stimulus statistics encountered during a lifetime of experience. We also note that our perceptual model is not the first to propose a low velocity-prior to

explain illusory phenomenon; in vision, a low-velocity prior has also been proposed (Weiss et al., 2002; Stocker and Simoncelli, 2006). Whether these assumptions are in fact true, or justified, remains to be addressed experimentally. Probing the statistics of frequently encountered stimuli could prove not only useful for confirming, or refuting, such low-velocity priors but could also inform other possible priors that may exist in sensory experience. Furthermore, because the low-velocity prior is based on experience, the question of how easily the prior can be molded by new experiences must be addressed. Are priors for trajectories highly plastic throughout life or is there a critical period for forming such priors? Can σ_v be made larger by presenting a train of high-velocity stimulus trajectories, if so what is the time course of this change? These questions should be experimentally addressed in future studies.

Although we have found a clear trend matching the prediction that greater spatial uncertainty should result in greater length contraction on the forearm, the same was not true for the finger. We note, however, that 2 out of 7 subjects performed testing on the fingertip, while the remainder performed testing on the finger base, yet in our statistical analysis we combined data obtained on the two finger sites into a single “finger condition”. It is also important to note that although we did find a significant difference between spatial uncertainty measured with sine and

square waves, this effect appeared to be weaker on the finger than on the forearm. It is also possible that a prior uncertainty over stimulus velocities (σ_v) might be more variable between subjects on the finger than on the forearm. This could imply that the fingers tend to experience a much more varied range of stimuli than on the forearm, especially between different individuals; perhaps the fingers of different individuals are exposed to different distributions of stimulus velocities (based on the daily manual activities of each individual), the distribution of velocities encountered on the arm, however, are likely more uniform across individuals. Within a subject, experience is also likely to vary greatly between body-sites; one could imagine that the fingertips in general would experience a wider variety of stimulus velocities than on the forearm, making σ_v larger on the finger. However, Goldreich (2007) shows that across studies on multiple body sites, there seems to be a linear relationship between the best-fit τ and the mean spatial uncertainty (σ_s) on these body-sites, suggesting that σ_v is on average constant across body sites and therefore may be more “hard-wired” than “plastic”. Figure 12 shows the predicted relationship between the ratio of τ s (for sine and square wave stimuli) and σ_s s (for sine and square wave stimuli) if σ_v is constant between sine and square wave conditions: these two ratios should be equal, since a fractional change in σ_s should result in an equal fractional change in τ . Our preliminary data appear to roughly follow this trend (see figure 12), however, further testing must be carried out to see whether this relationship holds true; with

the levels of measurement variability shown in this study, our current data set is likely too small to confidently address this question.

If the brain does in fact use a low-velocity prior, how does it do so? Addressing this question would not only provide a neural mechanism for our proposed model, but also give insight into nature of priors in the nervous system and how networks of neurons encode experiences and subsequently use them during decoding. One obvious question to start probing is how neurons, specifically those in the somatosensory system, encode stimulus velocity. Whitsel et. al. (1999) have found that S1 neural responses in macaque, on average, monotonically increase with the velocity of a continuous brush stimulus from 1cm/s up to 100cm/s. It is unknown, however, whether this monotonic relationship continues indefinitely with higher velocities (until the absolute limit of spiking) or whether saturation occurs earlier at specific velocity values. A full characterization of velocity tuning in the somatosensory neurons may elucidate the limits of velocity encoding and thus provide a neural based interpretation for our proposed low-velocity prior. A network model proposed by Wiemer et al (2000) does not take into account velocity encoding, yet nevertheless seems to predict length contraction. The authors attribute the illusion to the cortical spread of activity triggered by the first stimulus pulse, which pulls the peak of activity generated by the second stimulus pulse towards it by virtue of superposition. However, we argue that such a model

can only explain the mislocalization of the second tap towards the first and not vice versa. Furthermore, under certain conditions (at large inter-stimulus times), this model would predict length expansion, which has not been found to occur.

Conclusion

We conclude that our Bayesian perceptual model for trajectory estimation of touch stimuli not only explains perceptual length contraction, but also provides a relatively good fit to human data in this study and others (Goldreich, 2007; Goldreich and Tong, 2013). Furthermore, we have shown in this study that poorer spatial acuity does indeed seem to result in a stronger length contraction illusion on the forearm, a major prediction that comes from our Bayesian perceptual model. Further work needs to be done to confirm the presence of a low-velocity prior in the somatosensory system.

4.7 Figures

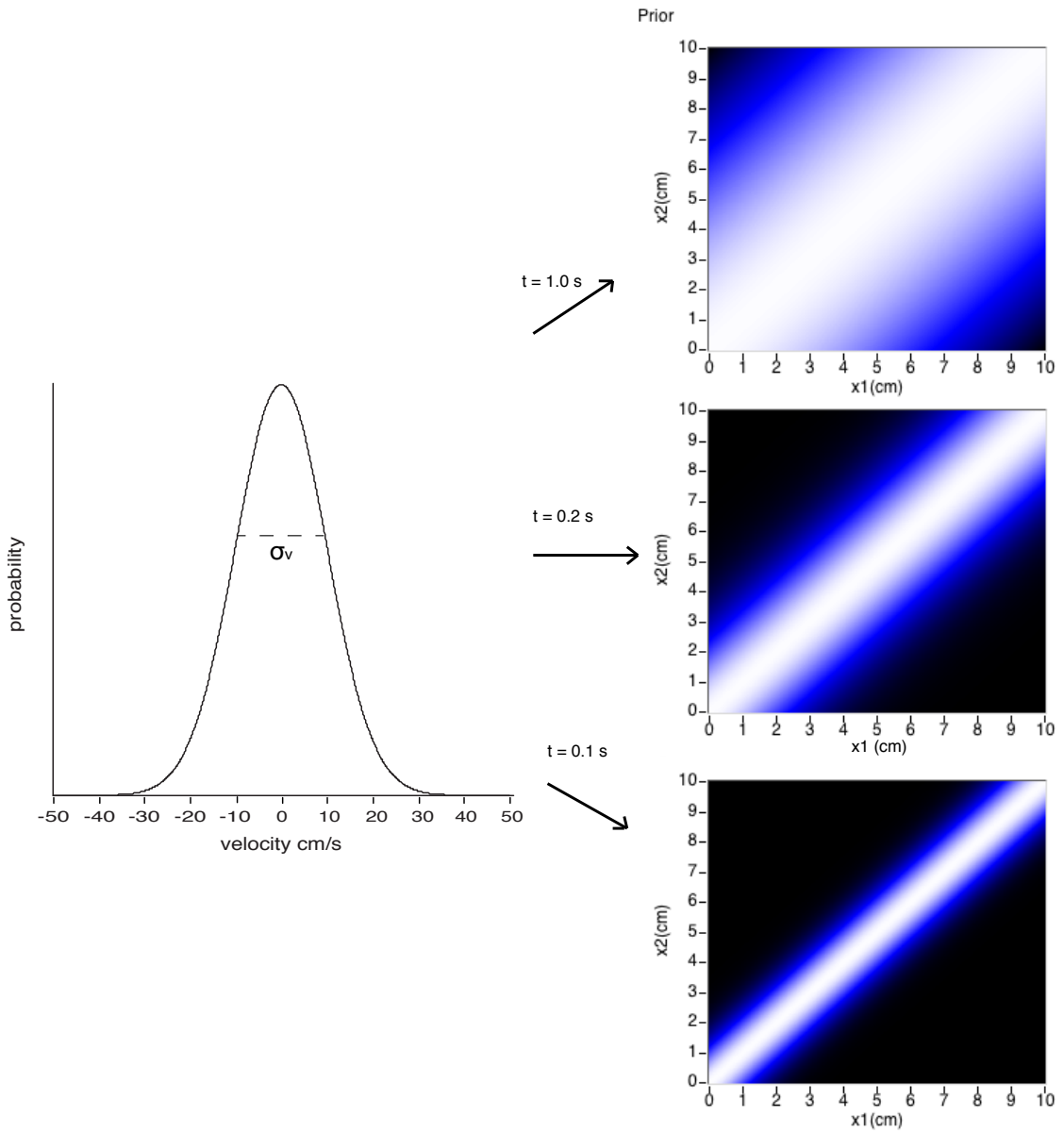


Figure 1: The low-velocity prior: A low-velocity expectation sets up a non-uniform prior over trajectories. The graph on the left shows the low-velocity prior, a probability distribution centered on zero velocity with a standard deviation of σ_v (in this case, $\sigma_v=10$ cm/s). This low-velocity prior gives rise to different probability distributions over trajectories (positions of a pair of taps), corresponding to different-ISTs. Note that as IST decreases the “width” of the distribution over trajectories shrinks; in other words, greater ISTs result in larger perceptually allowable differences between tap positions. This equates to a prior for small separations, that becomes stronger with smaller IST.

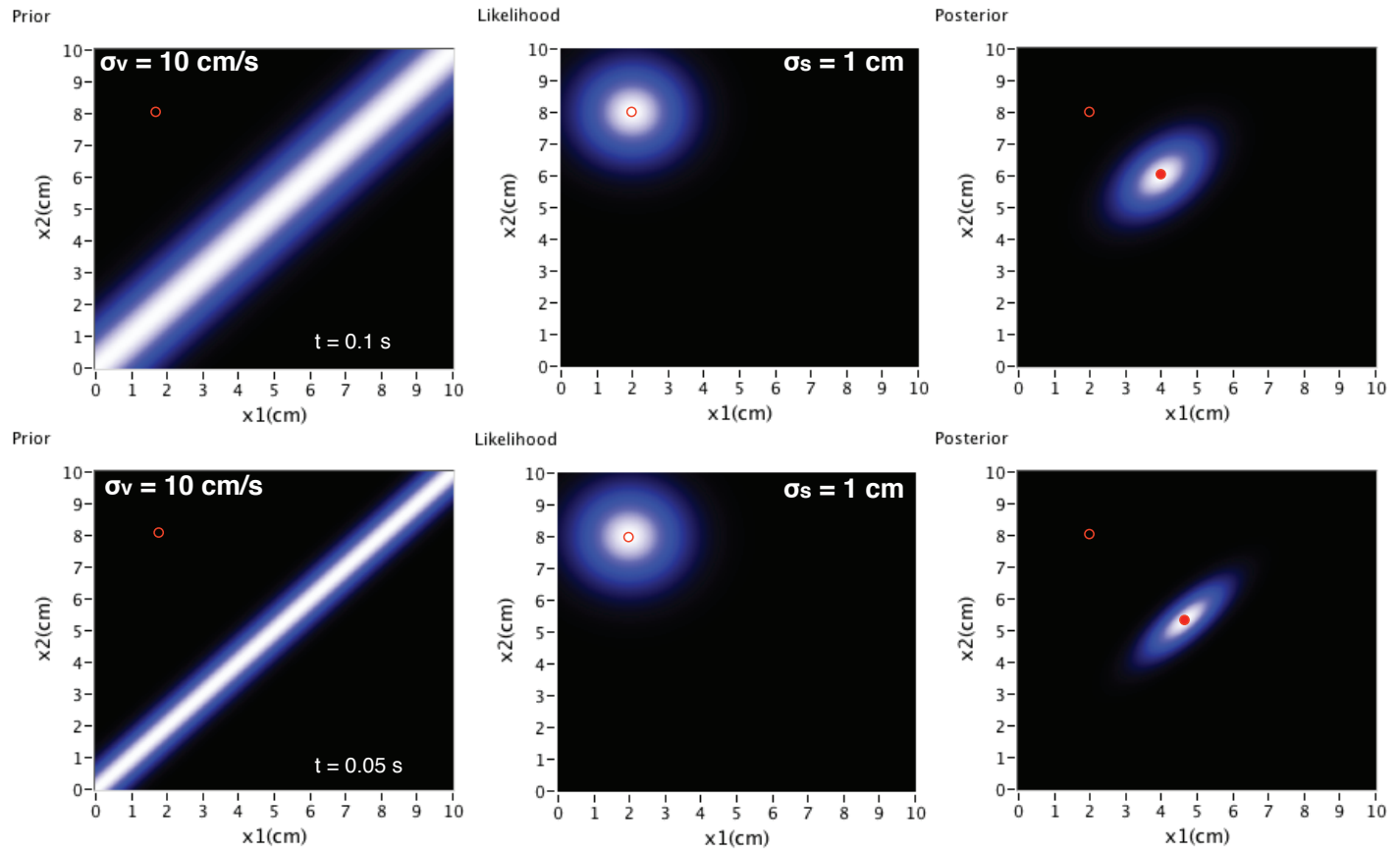


Figure 2: Prediction 1: The effect of interstimulus time (IST) on the extent of length contraction. Each row illustrates the process of combining prior and likelihood distributions to acquire a posterior distribution over possible stimulus locations for taps 1 and 2. The true tap locations, signified by the open circle, are $x_1 = 2$ cm, $x_2 = 8$ cm (an intervening distance of 6 cm). In the top row, a spatial acuity of 1 cm and interstimulus time of 0.1s results in length contraction such that the perceived tap locations are $x_1 = 4$ cm, $x_2 = 6$ cm (an intervening distance of 2 cm). With a smaller ISI ($t = 0.05$), as illustrated in the bottom row, there is a greater extent of length contraction such that the perceived positions of taps are

$x_1 = 4.66$ cm, $x_2 = 5.33$ cm (an intervening distance of 0.67 cm). Note that a smaller ISI further limits the prior probability of non-zero distances between taps 1 and 2 (the width of prior over possible trajectories becomes narrower).

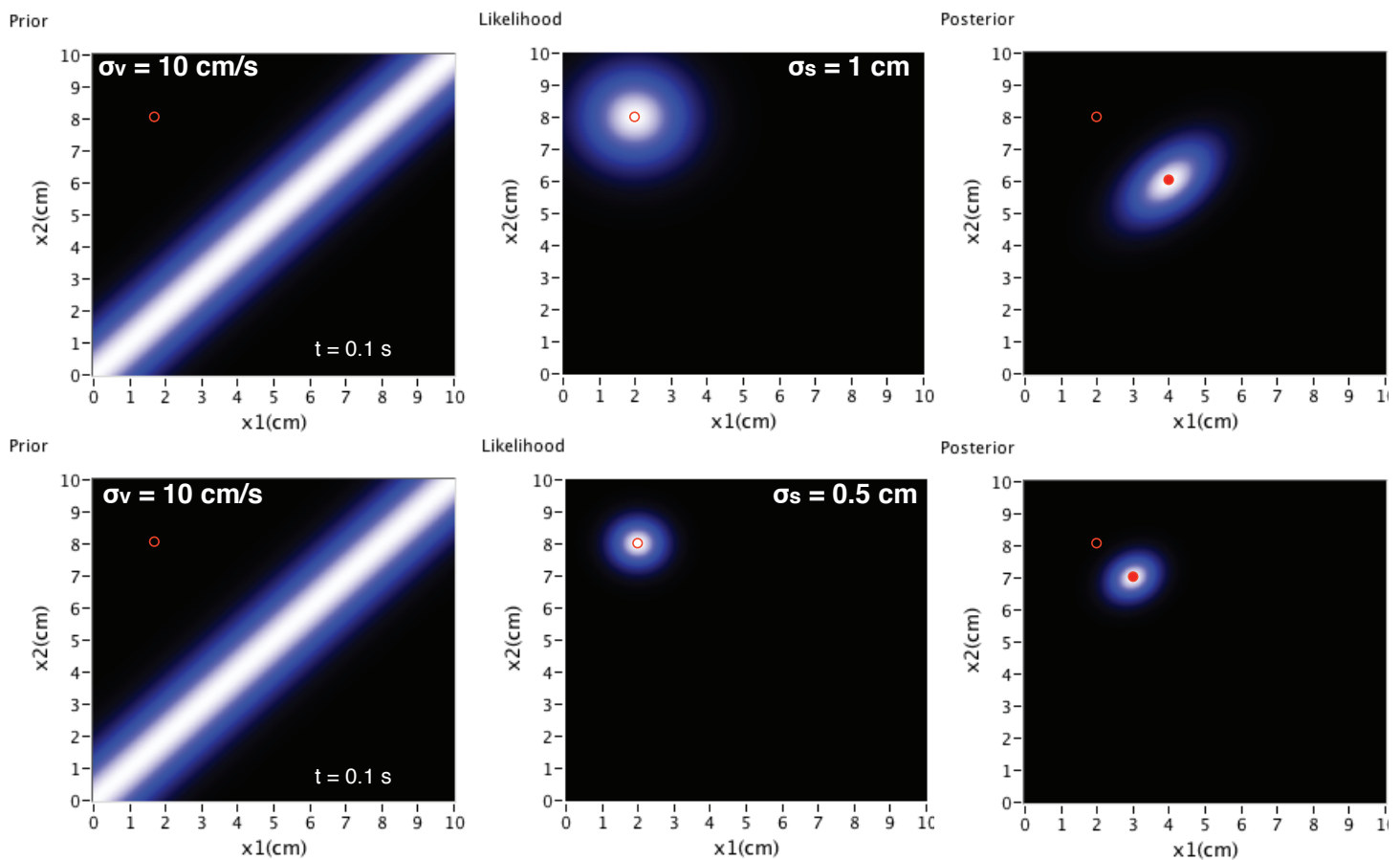


Figure 3: Prediction 2: The effect of spatial acuity on the extent of length contraction. Each row illustrates the process of combining prior and likelihood distributions to acquire a posterior distribution over possible stimulus locations for

taps 1 and 2. The true tap locations, signified by the open circle, are $x_1 = 2$ cm, $x_2 = 8$ cm (an intervening distance of 6 cm). In the top row (reproduced from Fig. 2), a spatial acuity of 1 cm and interstimulus time of 0.1 s results in length contraction such that the perceived tap locations are $x_1 = 4$ cm, $x_2 = 6$ cm (an intervening distance of 2 cm). With greater spatial acuity ($\sigma_s = 0.5$ cm) as illustrated in the bottom row, there is less length contraction such that the perceived positions of taps are $x_1 = 3$ cm, $x_2 = 7$ cm (an intervening distance of 4 cm).

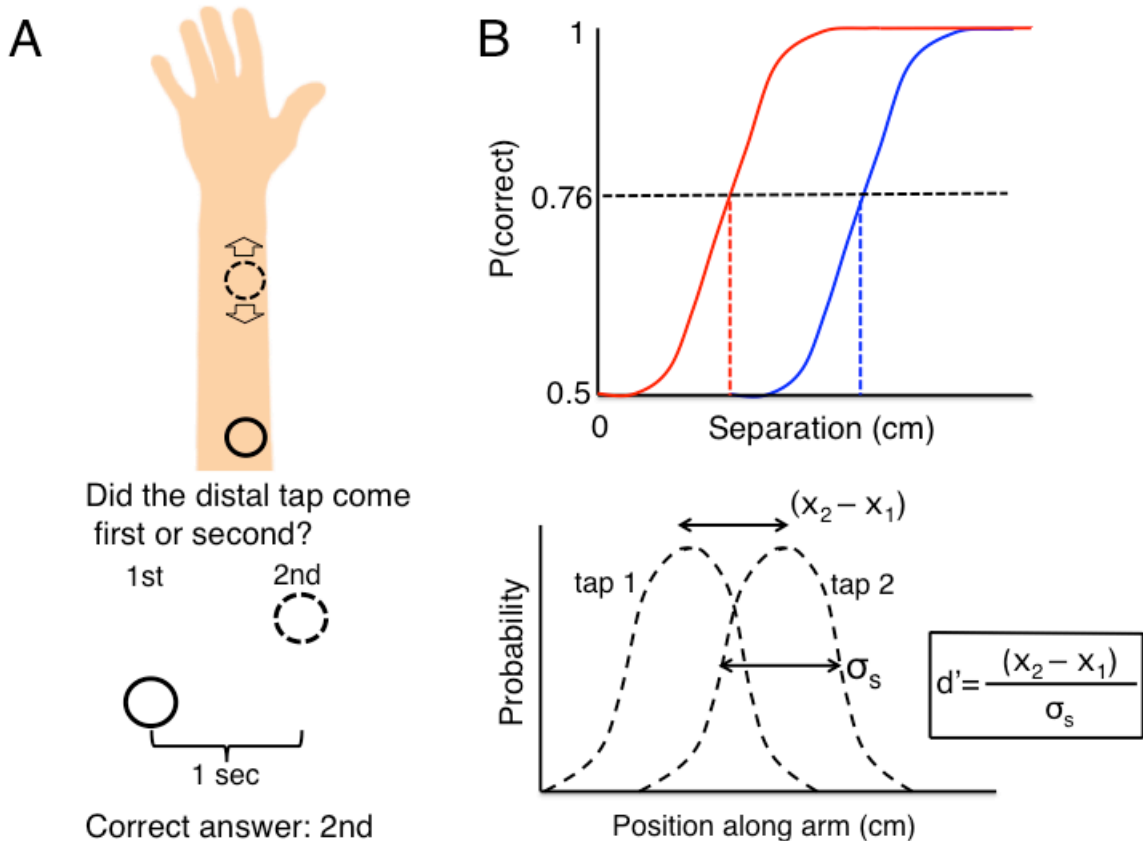


Figure 4 Measuring spatial uncertainty: A. Participants are asked to identify the order of two taps, one more distal than the other. The separation between taps varies. B. Upper panel: predicted performance on the task as a function of separation between taps; the red plot corresponds to a condition with stronger taps (i.e. square wave), the blue plot corresponds to a condition with weaker taps (i.e. sine wave). As separation approaches zero, participants are unable to discern the tap locations and are forced to guess; as the separation increases, the tap locations become more easily discernable and accuracy increases. Lower panel: according to signal detection theory, the 76% threshold in this task is equivalent to σ_s . For a 2 interval forced choice task, at the 76% threshold, $d'=1$. Assuming that the taps are on average perceived at their true locations with the same standard deviation, d' is defined as the difference between mean positions (the true separation) over the shared standard deviation (σ_s); when $d'=1$, at the 76% threshold, the true separation is equal to σ_s .

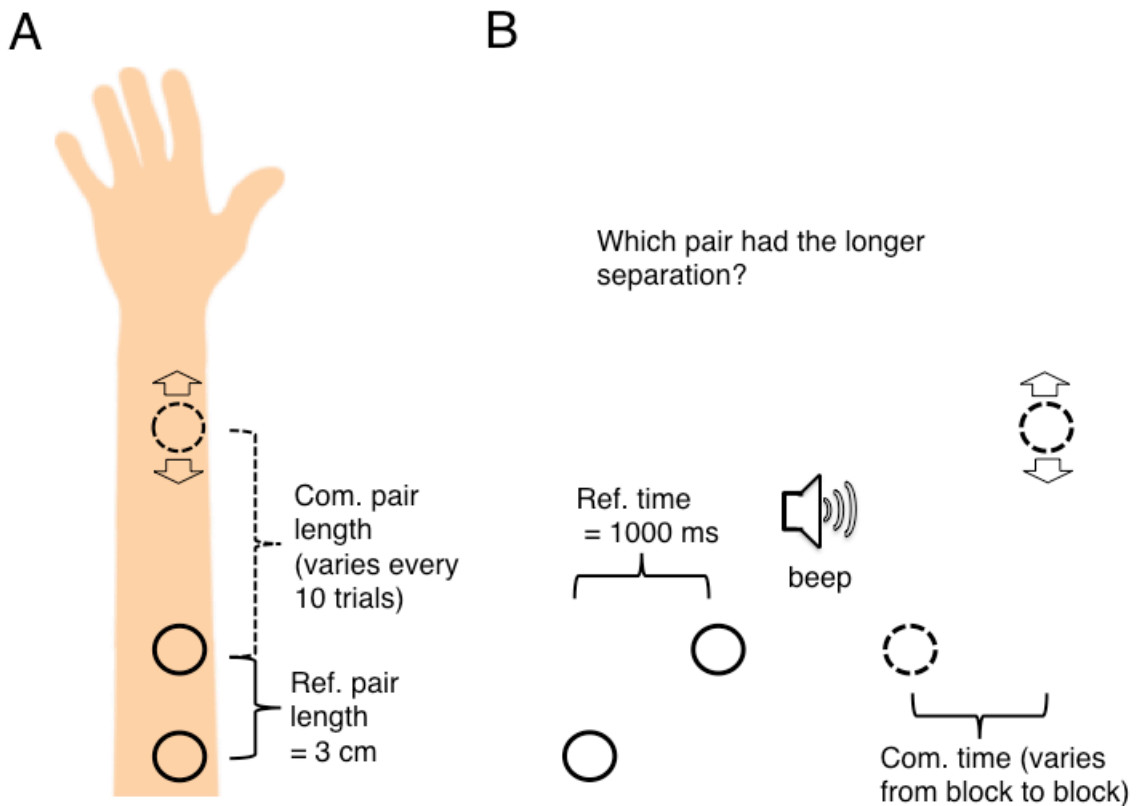


Figure 5: Length contraction experiment: A) The relative probe placements on the forearm: the reference pair is comprised of the proximal and medial probes while the comparison pair is comprised of the medial and distal probes. The distal probe is moved along the arm to vary the comparison pair length (which changes every 10 trials); the reference pair length is fixed at 3cm (or 2.5 cm).

B) On each trial, after receiving both pairs (order randomized), the participant answers the question “which pair had the longer separation (first or second)?”

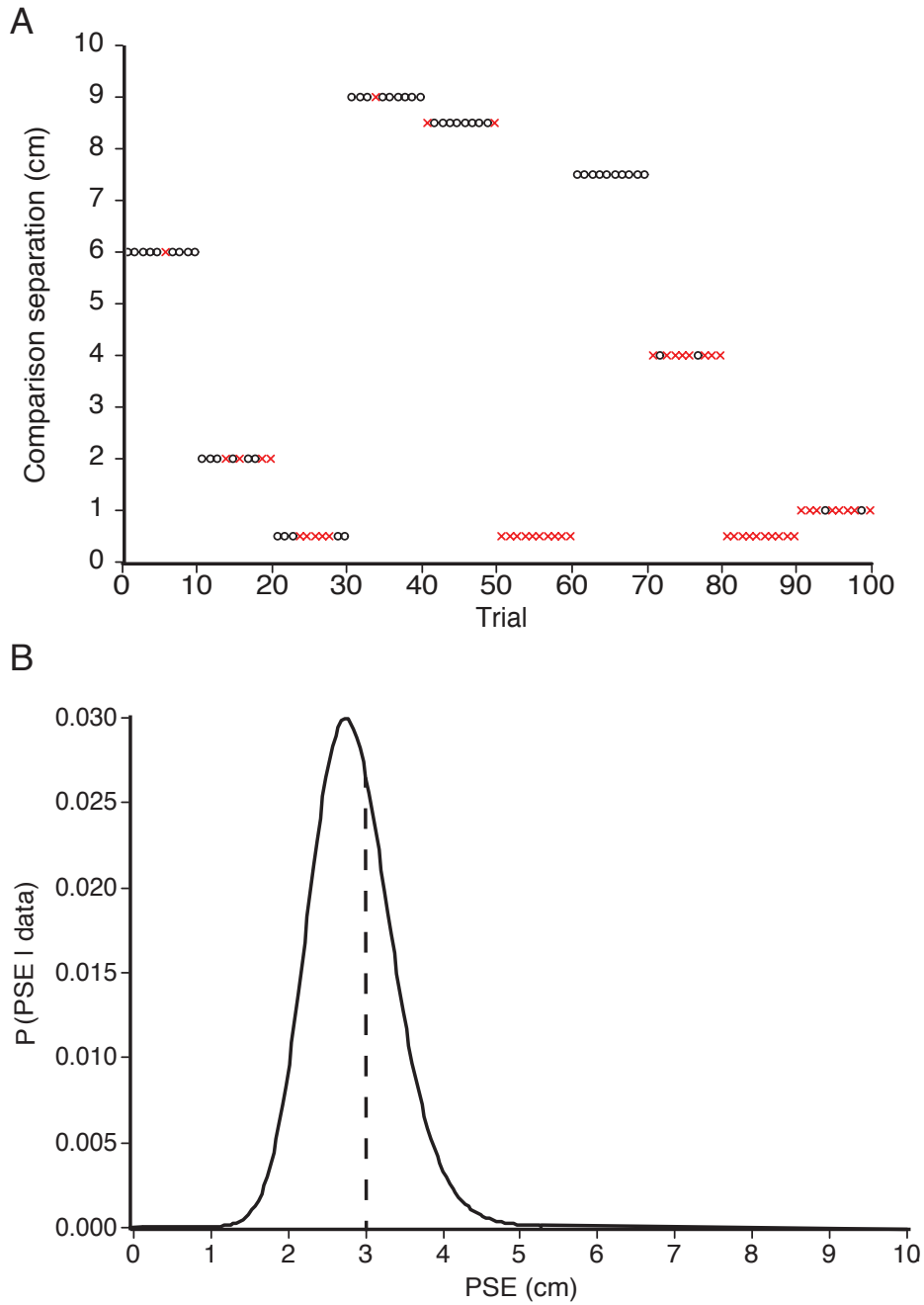


Figure 6: Performance on length comparison: A) A performance plot of a typical length comparison experiment; black circles represent trials in which the participant judged the comparison pair to be longer than the reference, red crosses represent those trials in which the comparison pair was judged to be

shorter than the reference (in this experiment the comparison time was 1s). The BAP chose the next most informative comparison separation to give after every 10 trials.

B) The PDF of the a -parameter in the Weibull function (i.e., the PSE) corresponding to the performance plot in (A). The mode of the distribution is very close to 3cm, the reference length; for this set of data, the most likely comparison separation to give rise to perceptual length equality was approximately 2.7cm (the 95% confidence interval was between 1.77 and 3.89cm). The predicted PSE for this specific experimental condition (comparison time = 1s), for any given τ , is 3cm (see Equation 5). In the example shown, this predicted PSE has a likelihood of approximately 0.025 (see dotted line).

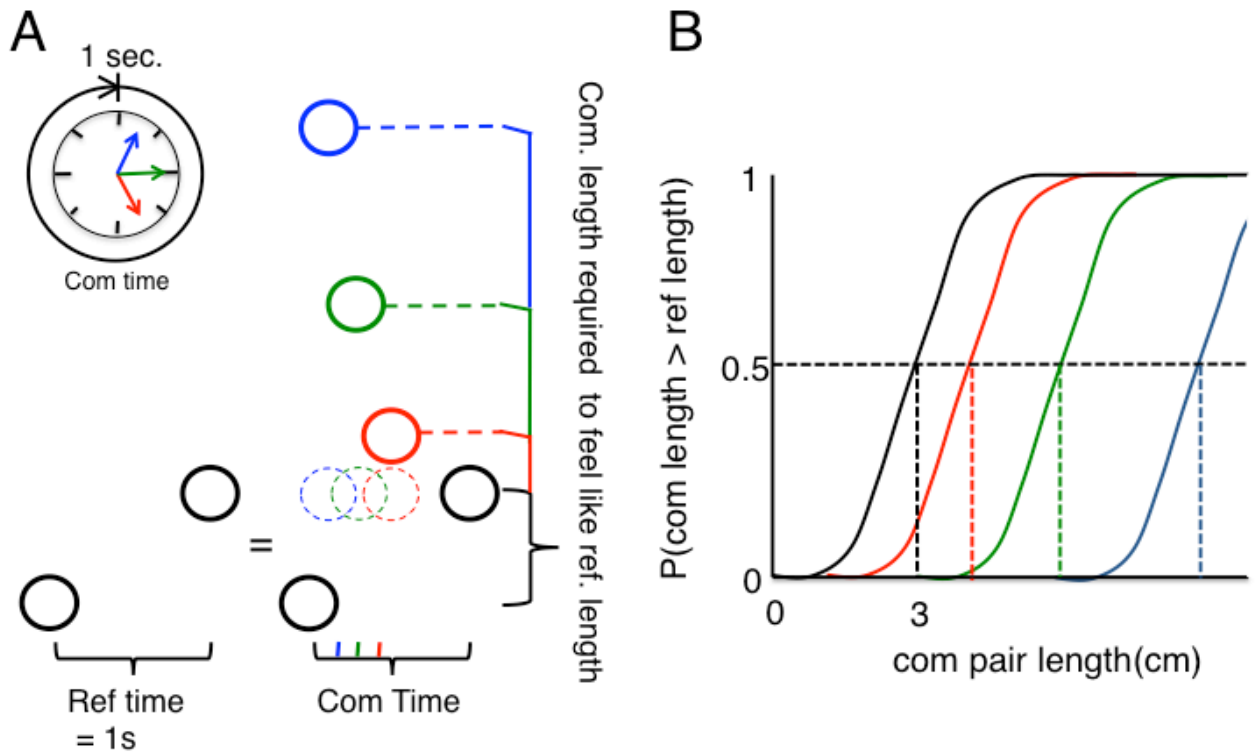


Figure 7: Predicted behavior in length contraction experiments: A) When reference time and comparison time are equal (both 1 s), the comparison length required to achieve perceptual equality (PSE) should equal the reference length (black condition). As the comparison time is decreased relative to reference time, however, the comparison pair length must correspondingly be made larger than the reference length in order to feel equal (see red, green, and blue conditions). B) The PSE is determined as the point at which the participant reports that the comparison length feels longer than the reference length 50% of the time (dotted vertical lines). As shown in (A), the PSE shifts to higher values as the time

separating comparison taps is decreased (red, green and blue once again denote progressively decreasing time intervals).

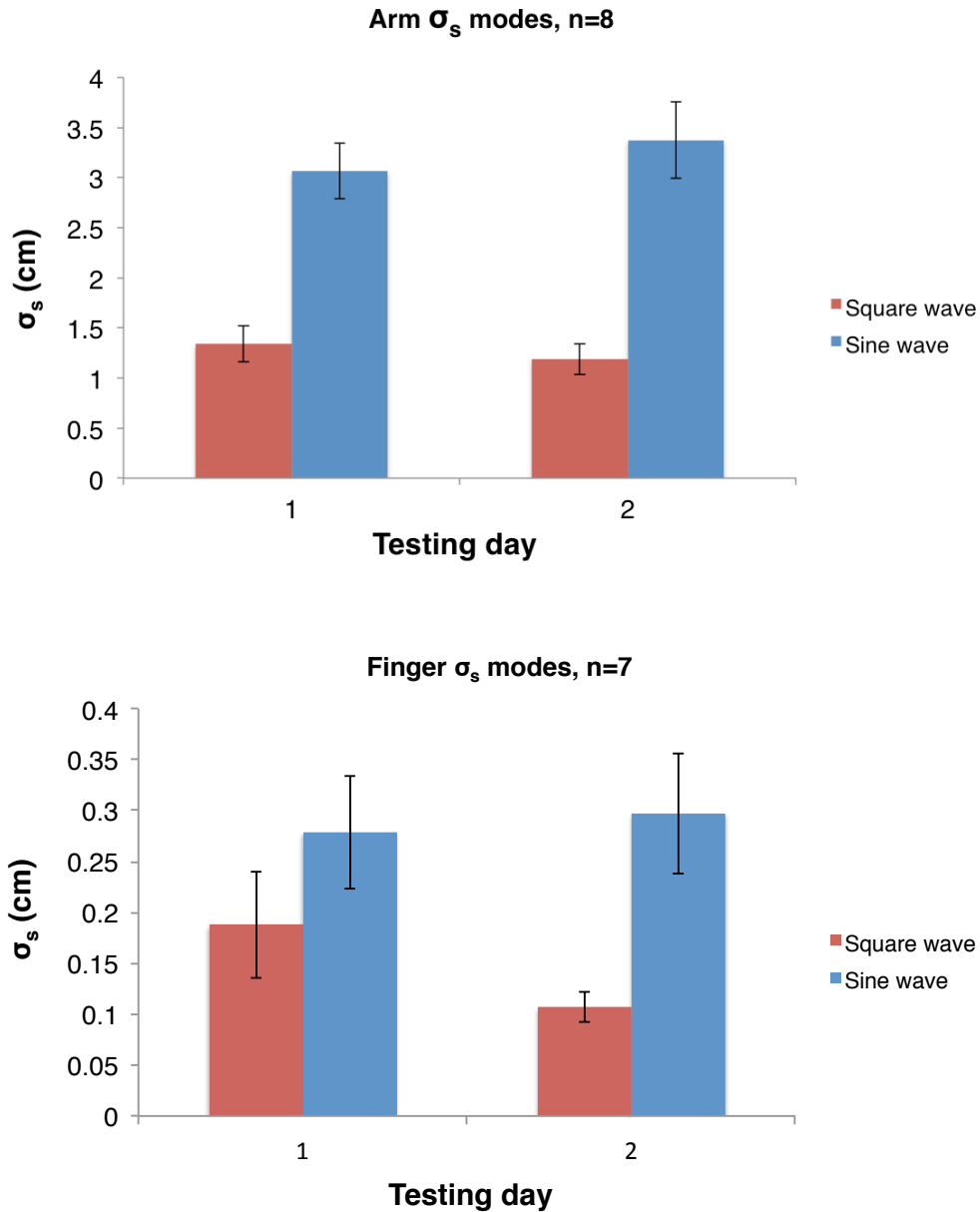


Figure 8 Mean σ_s : Mean square wave and sine wave σ_s , across days, for forearm, (upper panel) and finger (lower panel).

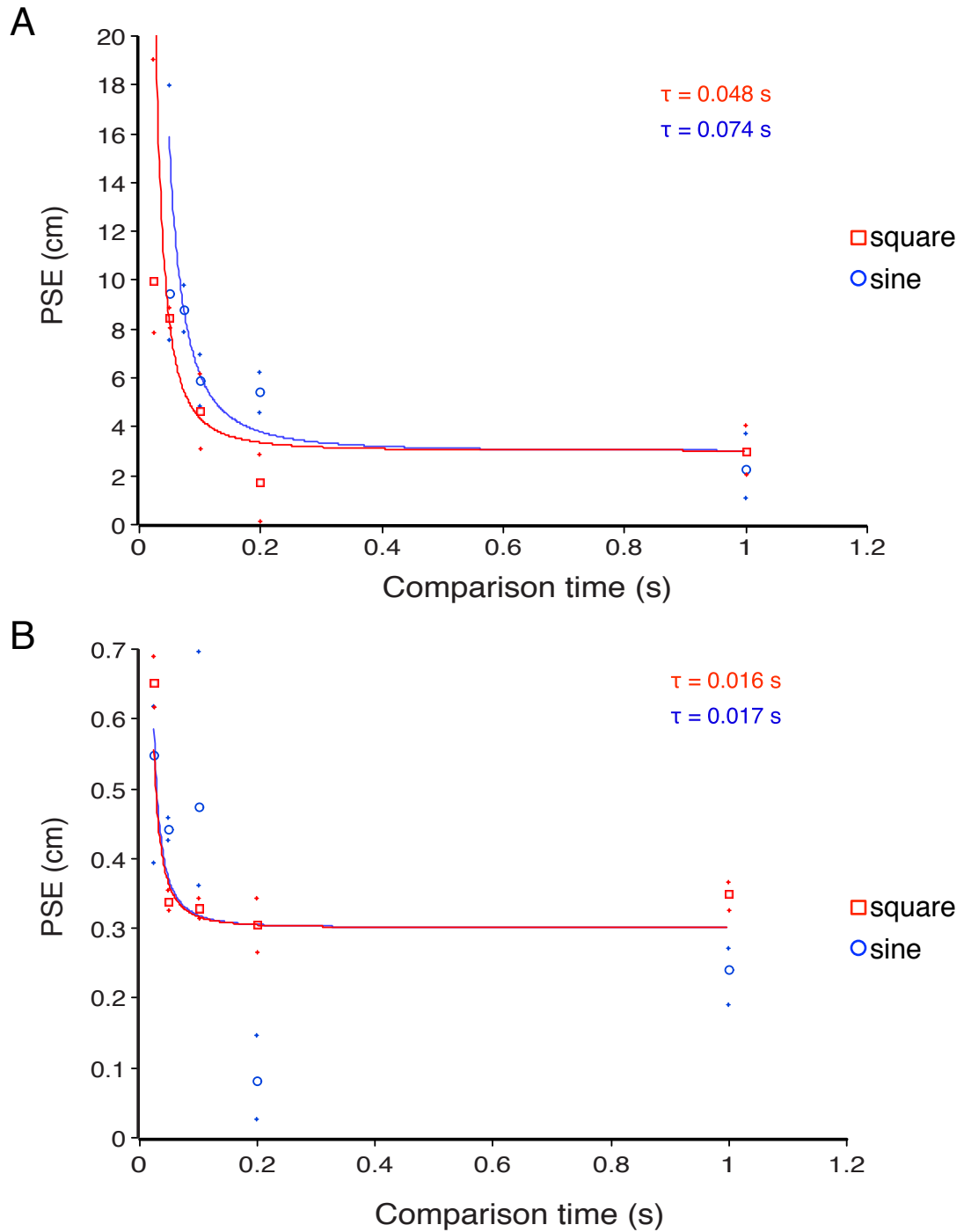


Figure 9 Length comparison PSEs as a function of comparison time: The mode of the PSE (open data points), and corresponding 95% confidence intervals

(small crosshairs), obtained for each length comparison experiment is plotted against the comparison time. Solid curves represent the best fit. Data for square wave stimulus conditions are in red (modes are shown as squares) and data for sine wave stimulus conditions are in blue (modes are shown as circles). Plot A shows forearm data from a representative participant; plot B shows finger base data from the same participant. In each plot the corresponding best-fit τ is shown for sine wave and square wave conditions.

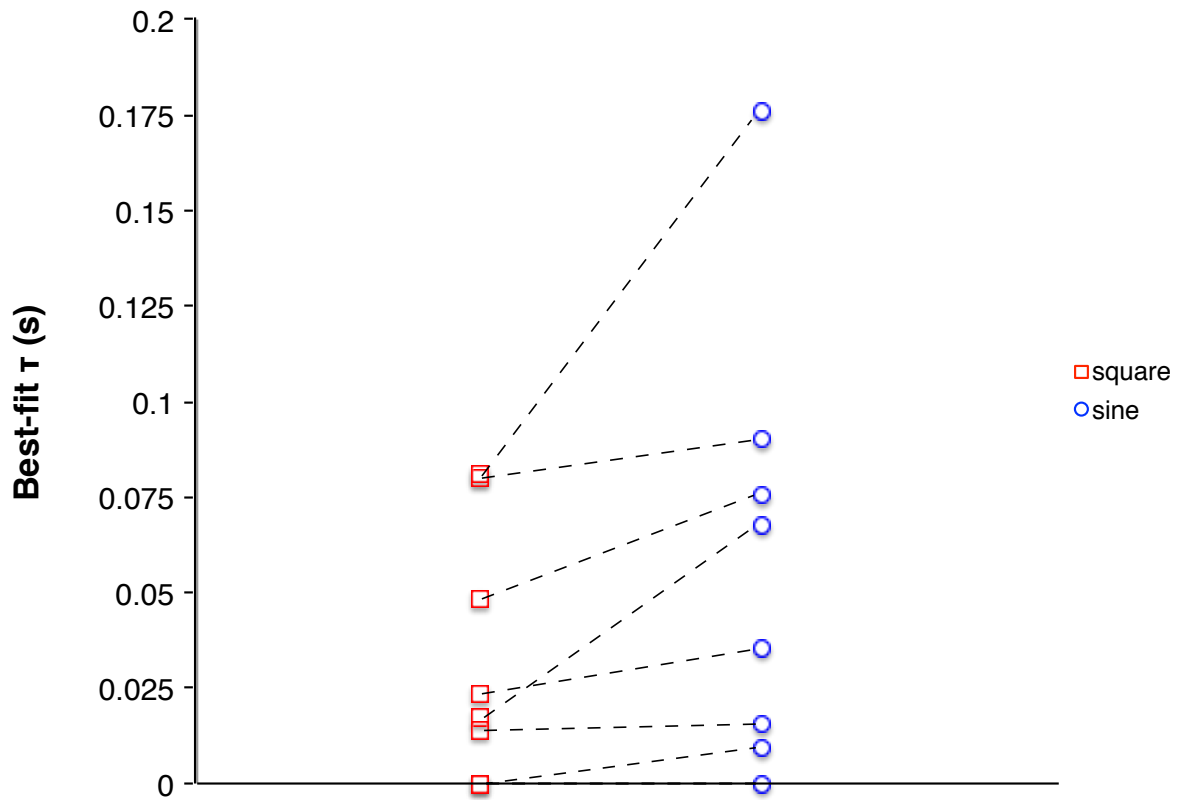


Figure 10: Forearm best-fit τ : A plot of the forearm best-fit τ for sine and square wave conditions for each subject ($n=8$). The best-fit τ for sine wave (blue circles) is typically greater than that for square wave (red squares).

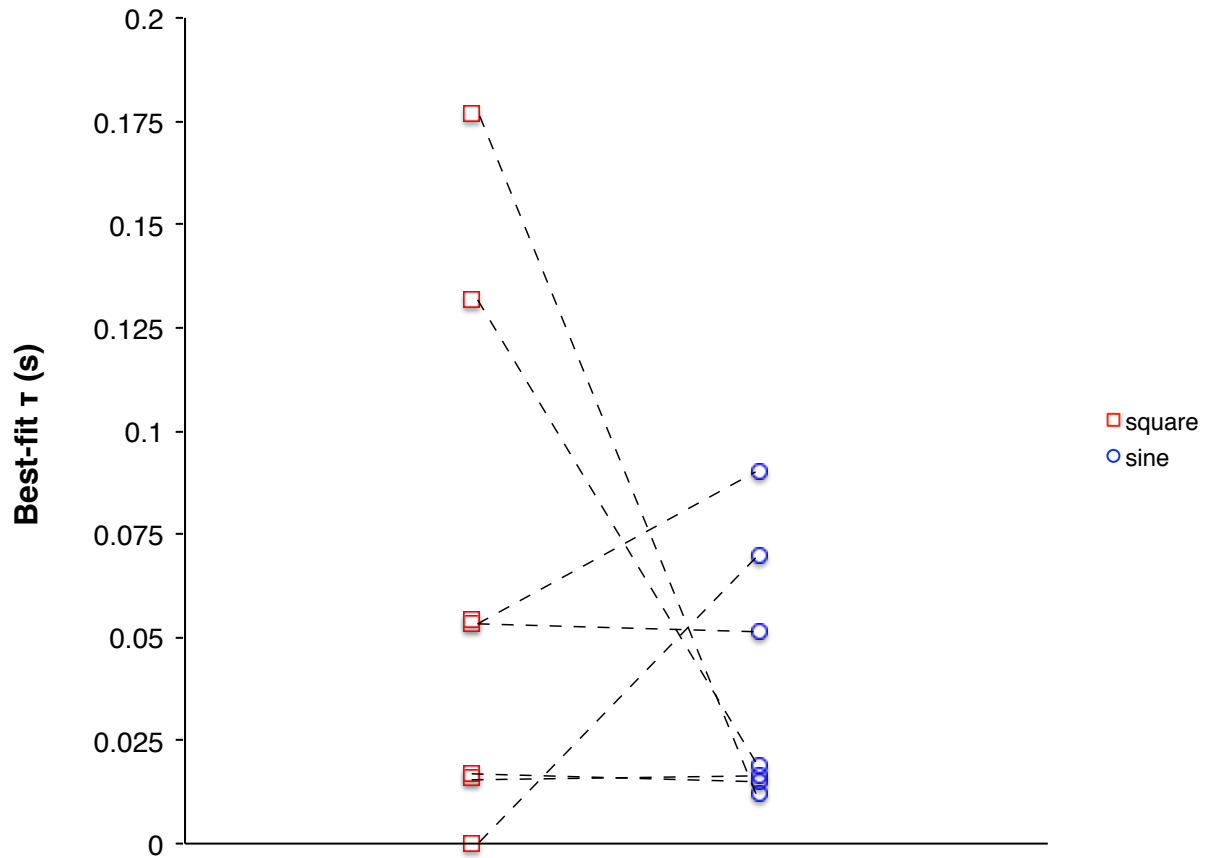


Figure 11: Finger best-fit τ : A plot of the finger best-fit τ for sine and square wave conditions for each subject (n=7).

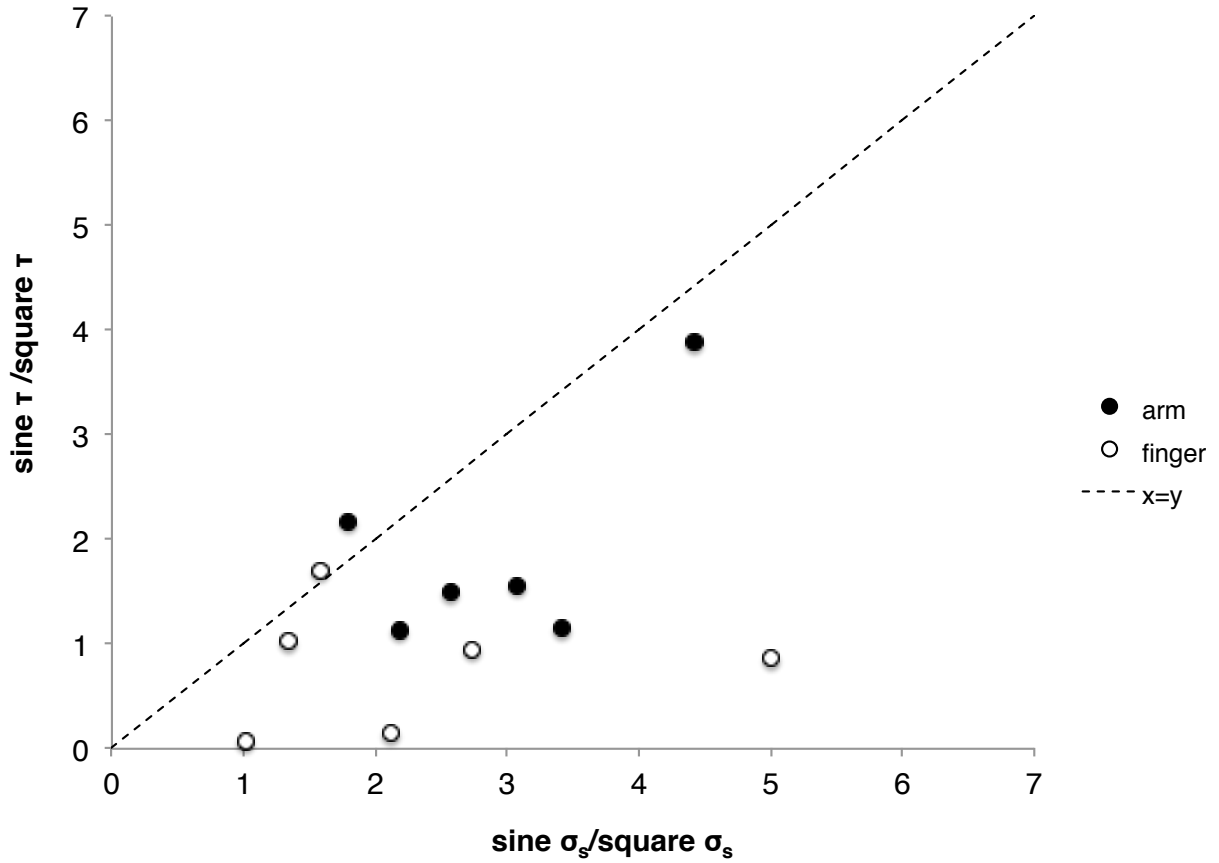


Figure 12: Ratio of best-fit tau for sine and square wave stimuli plotted against the ratio of σ_s for sine and square wave stimuli for each subject (best-fit taus of zero are omitted; solid points indicate arm data, open points indicate finger data). The equality line ($x=y$) illustrates the predicted relationship when σ_v is constant.

4.8 References

- Anton-Erxleben, K., and Carrasco, M. (2013). Attentional enhancement of spatial resolution: linking behavioural and neurophysiological evidence. *Nat. Rev. Neurosci.* 14, 188–200.
- Esteky, H. O. S. S. E. I. N., & Schwark, H. D. (1994). Responses of rapidly adapting neurons in cat primary somatosensory cortex to constant-velocity mechanical stimulation. *Journal of neurophysiology*, 72(5), 2269-2279.
- Geldard, F. A., & Sherrick, C. E. (1972). The cutaneous "rabbit": a perceptual illusion. *Science*, 178(4057), 178-179.
- Geldard, F. A. (1982). Saltation in somesthesia. *Psychological Bulletin*, 92(1), 136.
- Goldreich, D. (2007). A Bayesian perceptual model replicates the cutaneous rabbit and other tactile spatiotemporal illusions. *PLoS One*, 2(3), e333.
- Goldreich, D., & Tong, J. (2013). Prediction, postdiction, and perceptual length contraction: a Bayesian low-speed prior captures the cutaneous rabbit and related illusions. *Frontiers in psychology*, 4.
- Helson, H., & King, S. M. (1931). The tau effect: an example of psychological relativity. *Journal of Experimental Psychology*, 14(3), 202.
- Héritier, A., Knill, C., & Mingers, S. (1996). Ringing the changes in Europe: Regulatory competition and the transformation of the state. Britain, France, Germany (Vol. 74). Walter de Gruyter.
- Kilgard, M. P., and Merzenich, M. M. (1995). Anticipated stimuli across skin. *Nature* 373, 663.
- Knibestöl, M. (1973). Stimulus—response functions of rapidly adapting mechanoreceptors in the human glabrous skin area. *The Journal of physiology*, 232(3), 427-452.
- Miyazaki, M., Hirashima, M., and Nozaki, D. (2010). The “cutaneous rabbit

” hopping out of the body. *J. Neurosci.* 30, 1856–1860.

- Moore, C. E., Partner, A., and Sedgwick, E. M. (1999). Cortical focusing is an alternative explanation for improved sensory acuity on an amputation stump. *Neurosci. Lett.* 270, 185–187.
- O’Boyle, D. J., Moore, C. E., Poliakoff, E., Butterworth, R., Sutton, A., and Cody, F. W. (2001). Human locognosic acuity on the arm varies with explicit and implicit manipulations of attention: implications for interpreting elevated tactile acuity on an amputation stump. *Neurosci. Lett.* 305, 37–40.
- Pubols, B.H., Pubols, L.M. (1976). Coding of mechanical stimulus velocity and indentation depth by squirrel monkey and raccoon glabrous skin mechanics. *J Neurophysiol.* 1976 Jul;39(4):773-87.
- Seizova-Cajic, T., and Taylor, J.L. (2013). Somatosensory Space Abridged: Rapid Change in Tactile Localization Using a Motion Stimulus. *PloS one*, 9(3), e090892
- Stocker, A. A., and Simoncelli, E. P. (2006). Noise characteristics and prior expectations in human visual speed perception. *Nat. Neurosci.* 9, 578–585.
- Weiss, Y., Simoncelli, E. P., and Adelson, E. H. (2002). Motion illusions as optimal percepts. *Nat. Neurosci.* 5, 598–604.
- Whitsel, B. L., Franzen, O., Dreyer, D. A., Hollins, M., Young, M., Essick, G. K., & Wong, C. (1986). Dependence of subjective traverse length on velocity of moving tactile stimuli. *Somatosensory & Motor Research*, 3(3), 185-196.
- Whitsel, B. L., Favorov, O., Delemos, K. A., Lee, C. J., Tommerdahl, M., Essick, G. K., & Nakhle, B. (1999). SI neuron response variability is stimulus tuned and NMDA receptor dependent. *Journal of neurophysiology*, 81(6), 2988-3006.
- Wiemer, J., Spengler, F., Joublin, F., Stagge, P., and Wacquant, S. (2000). Learning cortical topography from spatiotemporal stimuli. *Biol. Cybern.* 82, 173–187.

Chapter 5

General Discussion

5.1 Summary of studies

Early pioneering studies in the sense of touch characterized the limits of spatial acuity throughout the body surface (Weber, 1834; Weinstein, 1968). Many investigators used point stimuli to map spatial acuity in tasks such as two-point discrimination or single point localization, attributing the limits of acuity to the relative density of innervation (Schady et al., 1983; Weinstein, 1993). Further studies, incorporating neurophysiology and anatomy, have confirmed the correlation between spatial acuity and innervation density as demonstrated by the size and density of receptive fields on different body sites (Johansson and Vallbo, 1983). Other properties of primary afferents and their receptive fields have been studied in greater detail, revealing many characteristics that were previously overlooked. For example, receptive fields in the arms and hands of humans tend to be elongated and oriented with the longitudinal axis (Johansson and Vallbo, 1980), and multiple point stimuli may interact, producing suppressed responses compared to that of a single point stimulus (Vega-Bermudez and Johnson, 1999). These more recently discovered properties have introduced a need to revisit the relationship between peripheral neural responses and spatial acuity, as they may explain such phenomena as anisotropy or the presence of magnitude cues in two-point discrimination. It was therefore a major goal of this thesis to investigate

how these properties, among others, can give rise to known trends in spatial acuity. In the three studies detailed in this thesis, we have used computational and empirical methods to explore many of the factors that determine or affect punctate tactile spatial acuity.

In the second chapter we implemented an ideal observer analysis on the responses of primary afferents, simulating a variety of tasks used to measure spatial acuity with point stimuli. We modeled many of the properties of peripheral afferents involved in extracting spatial details, known as Slowly Adapting type 1 afferents (SA1). For example, we used realistic receptive field size and spacing, as measured by Johansson and Vallbo (1979, 1980), as well as special characteristics such as elliptical receptive fields with uniform orientation or surround suppression between two-point stimuli (Vega-Bermudez and Johnson 1999). These properties informed the responses of a modeled population of SA1 afferents (with added noise) to a particular stimulus, which we then optimally decoded using a Bayesian ideal observer. Our simulations demonstrated that humans perform these tasks far from optimally, given the afferent population response and noise (either peripheral or cortical-like). Nevertheless, our analysis provided a strong computational and theoretical explanation for a number of well-documented trends in human performance, including sequential two-point thresholds being significantly lower than simultaneous two-point thresholds,

anisotropy of two-point discrimination thresholds, the correlation between receptive field size and localization error, and the presence (absence) of magnitude cues in two-point discrimination (two-point orientation discrimination).

In the third chapter, we report an empirical study we carried out to further investigate the issue of magnitude cues contaminating the two-point discrimination task and proposed a new task for measuring spatial acuity involving orientation discrimination of two-point stimuli. In this study, participants performed two-interval versions of two-point discrimination (2PD) and two-point orientation discrimination (2POD), with manually applied stimuli (as would be done in a clinical setting). We found evidence supporting a magnitude cue in two-point discrimination but not in two-point orientation discrimination: at zero separation between two points (well below receptor spacing), participants were able to identify the two-point stimulus with well above chance probability; however, they were unable to tell the orientation of two-point stimuli. This finding has the potential to improve clinical practice, as we propose that 2POD replace 2PD in the neurological exam and other clinical settings.

Finally, in the fourth chapter, we explored the spatiotemporal illusion known as the tau effect, or perceptual length contraction, and tested a Bayesian model of how this effect could arise from a combination of poor spatial acuity and

expectation. We measured participant's spatial acuity on a variation of the sequential two-point discrimination task, using stronger and weaker taps (square and sine waveforms). Sine wave stimuli tended to be more difficult to localize than square wave stimuli. Furthermore, we tested participants' ability to discriminate differences in separations between pairs of taps and measured the point of subjective equality. By decreasing the temporal separation between one of the pairs of taps, we found that the PSE correspondingly shifted to higher values; that is, the pair with a shorter temporal interval had to be made longer than the reference pair to feel equal in length. Using this method to measure length contraction, with both sine and square wave stimuli, we found preliminary evidence supporting the model's prediction that greater spatial uncertainty tends to give rise to greater length contraction.

5.2 Other channels involved in the processing of tactile information

Four distinct mechanoreceptor channels, or classes of somatosensory primary afferents, have been described in the glabrous skin. Rapidly Adapting type afferents, which account for almost half of all cutaneous afferents (56%) in the hand, are characterized by a transient burst of spiking at stimulus onset, and they subsequently adapt quickly during the static phase of the stimulus (Johansson and Vallbo, 1983). Because of their brief transient responses, RA fibers are ideal for conveying frequency information of vibratory stimuli, as they

can typically phase lock with great precision to each cycle of a vibration. The RA type afferents are further divided into two subcategories: RA1s are associated with superficial receptor cells known as Meissner corpuscles and are most sensitive to vibrations of 10-100Hz; RA2s are associated with large receptors, found deep in the tissue, known as Pacinian corpuscles and are most sensitive to vibrations of 40-800 Hz (Bolanowski et al. 1988). Slowly adapting afferents, on the other hand, have a characteristic sustained response during the static phase of a stimulus (Johnson and Lamb, 1981). These afferent types are also further broken down into two subclasses: Slowly adapting type 1 (SA1) and type 2 (SA2). SA2 afferents, which are absent in non-human primates, are associated with elongated and bulbous receptor cells known as Ruffini corpuscles. They have large receptive fields and are thought to mainly detect lateral stretch and tension deep within skin (Torebjork and Ochoa, 1980). SA1s, on the other hand, have small receptive fields and are associated with superficial Merkel cells that are responsible for their sustained responses (Maricich et. al., 2009). For these reasons, SA1s are ideal for encoding the static stress and strain profile of the skin.

When a spatial pattern is pressed against the skin, each point of contact experiences stress and strain, which is, in turn, transduced by SA fibers into spike trains (Johnson and Lamb, 1981; Phillips & Johnson, 1981b; Sripati et al., 2006a). According to continuum mechanics, stress is defined as a quantitative

measure of the internal forces that adjacent units of a continuous medium exert on one another. Strain characterizes the extent of deformation of a continuous medium when forces are applied (Phillips & Johnson, 1981b; Sripati et. al., 2006a). Because SA1s have a static response phase to the stresses and strains resulting from indentations and edges, they provide the clearest “picture” of fine spatial detail; using a rotating drum with embossed dot patterns (much like Braille) to stimulate the fingertips of macaque monkeys, Johnson and Lamb (1981) demonstrated that the spatiotemporal output of stimulated SA1 fibers had the highest correlation with the stimulus pattern, compared to the rapidly adapting type afferents. The authors concluded that SA1s are the ideal candidate for encoding fine spatial details, including Braille-like patterns. Therefore, the SA1 channel is regarded as the primary system for conveying spatial information of statically indented points, which is why we focus primarily on these afferent types. In chapter 4 however, we implement rapid pulse stimuli that are likely to equally activate RA and SA afferents (either channel type would fire similar numbers of impulses); whether both, or only one, channel type is involved in encoding the position of pulses remains to be addressed.

5.3 Central mechanisms of tactile spatial acuity

This thesis has focused mainly on the peripheral features that affect tactile spatial acuity; we consider many well-characterized properties of SA1 neurons

while treating central mechanisms as an unspecified “black box” that carries out bottom-up processing of these inputs (chapter 2) and top-down processes reflecting expectations based on stimulus statistics (chapter 4). However, central processing plays a pivotal role in transforming, integrating and interpreting the signals conveyed by primary afferents to form a percept. Therefore, it is worth considering how these processes may shape tactile perception. Here, we will speculate on some of the central mechanisms involved in the tactile perception of point stimuli.

The four channel types mentioned in the previous section, relay touch information in a parallel fashion: RAs and SAs converge onto distinct post-synaptic targets in the brainstem, conserving the respective properties associated with the specialization of encoding either vibrotactile stimuli or fine spatial patterns. These distinct properties are retained even in the next stage of processing, in the Ventral Posterior nucleus (VPN) of the thalamus neurons fall within rapidly or slowly adapting classes. However, evidence of convergence between RA and SA class neurons first appears in primary somatosensory cortex (S1), where thalamic inputs drive neurons in sub-regions 3b and 1 (Sripati et. al. 2006b). A proportion of neurons in these areas respond with a combination of SA and RA-like responses (with both sustained and phasic properties). Whether this type of convergence is helpful or detrimental to either vibrotactile or spatial

discrimination has yet to be understood. Interestingly, even with this evidence of convergence, neurons in area 3b and 1 have receptive field sizes that are comparable to those of primary afferents; the mean excitatory surface area of 3b and 1 receptive fields is 19.7 and 18.2 mm², for primary afferents, the mean receptive field area is 10 mm² (Sripati et al 2006b). Because RF size does not appear to increase greatly from primary afferent to S1, convergence alone is unlikely to cause much loss of spatial information. It is more likely that the accumulation of noise decreases the fidelity of spatial information up to S1, a property that we have briefly addressed in Chapter Two. In secondary somatosensory cortex (S2), which receives inputs from S1 (3b and 1), receptive fields have been observed to span multiple digits and grow immensely in size (sometimes covering an entire digit pad) relative to those of afferents or S1 neurons, suggesting much convergence of receptive fields within and between body sites (Fitzgerald et al 2006a,b). Therefore, it is highly unlikely that S2 neurons specialize in encoding the types of fine and isolated spatial details covered in this thesis; S2 neurons may play a larger role in preliminary identification of objects that make contact with multiple digits (e.g. Identifying a baseball by gripping it between the fingers).

Although interactions between stimuli are known to occur on the skin surface (i.e. surround suppression, additive responses, etc.), these effects

originate solely from the skin mechanics (stress and strain profiles) and not by interactions between afferent fibers (Vega-Bermudez and Johnson, 1999a). In fact afferent activity is independent between primary afferents, as interneuronal signaling is absent at this level; such is not the case in cortical somatosensory neurons, however, as neurons may receive common inputs (convergence) and many interneuronal interactions have been identified (both inhibitory and excitatory horizontal connections are present) (von Békésy, 1967). In fact, some investigators have posited that lateral inhibition among cortical neurons may aid in the discrimination of point stimuli; the inhibition of neurons with receptive fields in the intervening skin areas would theoretically enhance the resolution of the activity profile such that separate peaks are more easily distinguishable (Mountcastle and Bard, 1968). Whether this mechanism is truly involved in two-point discrimination has yet to be addressed. We argue, however, that the information present at the peripheral afferent population sets the theoretical limit for resolution, as information is only lost (corrupted) as signals ascend the somatosensory pathway due to the accumulation of noise (Geisler, 1984). Therefore, we believe that the optimal performance demonstrated by our ideal observer (in Chapter 2) truly reflects the absolute limits of acuity along the somatosensory pathway, and that human observers are unable to access all the information at the periphery. Hence, as we have demonstrated, there is a great discrepancy between human and ideal performance.

In Chapter 4, we introduced the concept of the brain using a prior over stimulus velocities to infer trajectories, leading to the perception of illusory length contraction (tau effect). Although such a prior explains the tau effect (and related cutaneous rabbit illusion) in an elegant Bayesian framework, and our preliminary behavioural findings seem to support such a model, evidence for its neural implementation in the central nervous system is yet to be found. S1 neural responses in macaque have been shown, on average, to monotonically increase with the velocity of a continuous brush stimulus from 1cm/s up to 100cm/s (Whitsel et al. 1999). Whether these neurons are able to encode higher velocities remains to be investigated; perhaps the limited range of velocities encoded by the population of S1 neurons may reflect our proposed low-velocity prior. The tuning of these neurons to the velocity of sequential pulse stimuli, like the ones used in our experiments, has not been characterized; however, length contraction has been demonstrated with brushing stimuli (Whitsel et al., 1986; Seizova-Cajic et al., 2014) similar to that used by Whitsel et al (1999). Other central mechanisms have been proposed to explain the tau effect, including a network model that attributes the illusion to the cortical spread of activity triggered by stimulus pulses (Wiemer et al, 2000); however, we note that such a model also predicts cortical length expansion under certain conditions, which has not been reported in the literature.

5.4 Future directions

This thesis has only begun to explore the intricacies of the peripheral somatosensory system and their consequences on the brain's ability to extract spatial information. It is a logical next step to include newly discovered peripheral properties into our existing models as they become characterized in greater detail. Furthermore, as the properties of central somatosensory neurons are elucidated, they should also be implemented in models of perceptual processing. In Chapter 4, we introduced the concept of incorporating stimulus statistics in perceptual processing; particularly we proposed a low-velocity prior for objects contacting the skin. Such a prior must be confirmed by identifying the true distributions of velocities encountered on the body surface during daily experience. Furthermore, models of how the brain would implement a low-velocity prior should be proposed and explored. Finally, future efforts should be made to explore how active touch and more complex stimuli, such as edges and textures are affected by peripheral properties.

5.5 Conclusion

In conclusion, this thesis has explored stimulus and peripheral factors affecting the perception of static tactile point stimuli. We have provided an ideal observer analysis of performance on a number of well-known discrimination tasks by optimally decoding the simulated responses of SA1 afferents. By doing so, we

have quantitatively predicted many performance trends attributed to SA1 receptive field anatomy and response properties, including anisotropy and non-spatial intensity cues in two-point discrimination. Experimentally, we have provided further evidence for the contamination of two-point discrimination by non-spatial cues and have demonstrated that an alternative task involving orientation discrimination avoids these cues. We recommend that clinicians and tactile researchers, with limited access to sophisticated equipment, use this orientation discrimination task in place of two-point discrimination. Finally, we have provided preliminary evidence supporting a Bayesian model of multi-point tactile perception that replicates a famous length contraction illusion. Altogether, this thesis has computationally and experimentally addressed many theories and speculations on basic touch sensation, developed over the past century by classical researchers like Weber, Weinstein and more modern pioneers in the field of touch research, Johansson, Vallbo, and Johnson. Furthermore, it has explored some contemporary ideas including Bayesian theories of perception. Much more work is to be done to further elucidate the often overlooked and under-explored sense of touch.

5.6 References

- Bolanowski Jr, S. J., Gescheider, G. A., Verrillo, R. T., & Checkosky, C. M. (1988). Four channels mediate the mechanical aspects of touch. *The Journal of the Acoustical society of America*, 84(5), 1680-1694.
- Fitzgerald PJ, Lane JW, Thakur PH & Hsiao SS (2006a). Receptive field properties of the macaque second somatosensory cortex: representation of orientation on different finger pads. *The Journal of Neuroscience*. 26(24): 6473–6484.
- Fitzgerald PJ, Lane JW, Thakur PH & Hsiao S (2006b). Receptive field (RF) properties of the macaque second somatosensory cortex: RF size, shape and somatotopic organization. *The Journal of Neuroscience*. 26(24): 6485– 6495.
- Geisler WS (1984). Physical limits of acuity and hyperacuity. *Journal of the Optical Society of America*. A(1): 775–782.
- Johansson RS & Vallbo ÅB (1979). Tactile sensibility in the human hand: relative and absolute densities of the four types of mechanoreceptive units in glabrous skin. *Journal of Physiology*. 286: 283–300.
- Johansson RS, Vallbo ÅB & Westling G (1980). Thresholds of mechanosensitive afferents in the human hand as measured with Von Frey hairs. *Brain Research*. 184: 343–351.
- Johansson, R. S., & Vallbo, Å. B. (1983). Tactile sensory coding in the glabrous skin of the human hand. *Trends in Neurosciences*, 6, 27-32.
- Johnson, K. O., & Lamb, G. D. (1981). Neural mechanisms of spatial tactile discrimination: neural patterns evoked by braille-like dot patterns in the monkey. *The Journal of physiology*, 310(1), 117-144.

- Maricich, S. M., Wellnitz, S. A., Nelson, A. M., Lesniak, D. R., Gerling, G. J., Lumpkin, E. A., & Zoghbi, H. Y. (2009). Merkel cells are essential for light-touch responses. *Science*, *324*(5934), 1580-1582
- Mountcastle, V. B., and Bard, P. (1968). "Neural mechanisms in somesthesia," in *Medical Physiology*, 12th Edn, ed. V. B. Mountcastle (St. Louis: Mosby), 1372–1423.
- Phillips JR & Johnson KO (1981). Tactile spatial resolution. III. A continuum mechanics model of skin predicting mechanoreceptor responses to bars, edges, and gratings. *Journal of Neurophysiology*. *46*: 1204-1225.
- Schady, W. J. L., Torebjörk, H. E., & Ochoa, J. L. (1983). Cerebral localisation function from the input of single mechanoreceptive units in man. *Acta physiologica scandinavica*, *119*(3), 277-285.
- Seizova-Cajic, T., & Taylor, J. L. (2014). Somatosensory Space Abridged: Rapid Change in Tactile Localization Using a Motion Stimulus. *PloS one*, *9*(3), e90892.
- Sripathi, A. P., Bensmaia, S. J., & Johnson, K. O. (2006). A continuum mechanical model of mechanoreceptive afferent responses to indented spatial patterns. *Journal of neurophysiology*, *95*(6), 3852-3864.
- Sripathi AP, Yoshioka T, Denchev P, Hsiao SS & Johnson KO (2006). Spatiotemporal receptive fields of peripheral afferents and cortical area 3b and 1 neurons in the primate somatosensory system. *The Journal of Neuroscience*. *27*(7): 2101–2114.
- Torebjörk, H., & OCHOA, J. L. (1980). Specific sensations evoked by activity in single identified sensory units in man. *Acta Physiologica Scandinavica*, *110*(4), 445-447.
- Weber, E. H. (1834). *De tactu*. Koehler, Leipzig.

- Weinstein, S. (1968). Intensive and extensive aspects of tactile sensitivity as a function of body part, sex and laterality. In *the First Int'l symp. on the Skin Senses, 1968*.
- Weinstein, S. (1993). Fifty years of somatosensory research: from the Semmes-Weinstein monofilaments to the Weinstein Enhanced Sensory Test. *Journal of Hand therapy, 6(1)*, 11-22.
- Whitsel, B. L., Franzen, O., Dreyer, D. A., Hollins, M., Young, M., Essick, G. K., & Wong, C. (1986). Dependence of subjective traverse length on velocity of moving tactile stimuli. *Somatosensory & Motor Research, 3(3)*, 185-196.
- Whitsel, B. L., Favorov, O., Delemos, K. A., Lee, C. J., Tommerdahl, M., Essick, G. K., & Nakhle, B. (1999). SI neuron response variability is stimulus tuned and NMDA receptor dependent. *Journal of neurophysiology, 81(6)*, 2988-3006.
- Wiemer, J., Spengler, F., Joublin, F., Stagge, P., and Wacquant, S. (2000). Learning cortical topography from spatiotemporal stimuli. *Biol. Cybern. 82*, 173–187.
- Vega-Bermudez, F., and Johnson, K. O. (1999). Surround suppression in the responses of primate SA1 and RA mechanoreceptive afferents mapped with a probe array. *J. Neurophysiol. 81*, 2711–2719.
- von Békésy G. Sensory inhibition. Princeton, NJ: Princeton Univ. Press; 1967.